Dissertation

THE ROLE OF REGULATOR OF G PROTEIN SIGNALING 5 (RGS5) IN LUNGS

Submitted by

Neha SHARMA

for the Academic Degree of

Doctor of Philosophy (PhD)

at the

Medical University of Graz

Department of Anesthesiology and Intensive Care Medicine

Ludwig Boltzmann Institute for Lung Vascular Research

under the Supervision of

Prof. Dr. Andrea OLSCHEWSKI

2021

Statutory Declaration

I hereby declare that this dissertation is my own original work and that I have fully acknowledged by name all of those individuals and organizations that have contributed to the research for this dissertation. Due acknowledgment has been made in the text to all other material used. Throughout this dissertation and in all related publications I followed the "Standards of Good Scientific Practice and Ombuds Committee at the Medical University of Graz".

Neha Sharma
Date: 5th September 2021
Graz, Austria

Disclosures

Most data presented in this thesis have been previously published as peer-reviewed original article.

Int. J. Mol. Sci. 2021, 22, 9342. https://doi.org/10.3390/ijms22179342

"RGS5 Determines Neutrophil Migration in the Acute Inflammatory Phase of Bleomycin-Induced Lung Injury (1)"

Neha Sharma [1,2], Chandran Nagaraj [1], Bence M. Nagy [1], Leigh M. Marsh [1], Natalie Bordag[1,3], Diana Zabini [1,4], Malgorzata Wygrecka [5], Walter Klepetko [6], Elisabeth Gschwandtner [6], Guillem Genové [7], Akos Heinemann [8], E Kenneth Weir [9], Grazyna Kwapiszewska [1,4], Horst Olschewski [1,10] and Andrea Olschewski [1,2,*]

[1] Ludwig Boltzmann Institute for Lung Vascular Research, Graz 8010, Austria

[2] Experimental Anaesthesiology, Department of Anaesthesiology and Intensive Care Medicine, Medical University of Graz, Graz 8036, Austria

[3] Department of Dermatology and Venereology, Medical University of Graz, Graz 8036, Austria

[4] Otto Loewi Research Center, Medical University of Graz, Graz 8010, Austria

[5] Center for Infection and Genomics of the Lung (Member of the German Center for Lung Research), University of Giessen, Giessen 35392, Germany

[6] Department of Thoracic Surgery, Medical University of Vienna, Vienna 1090, Austria

[7] Integrated CardioMetabolic Centre (ICMC), Department of Medicine, Karolinska Institute

[8] Otto Loewi Research Center for Vascular Biology, Immunology and Inflammation, Division of Pharmacology, Medical University of Graz, Graz 8010, Austria

[9] Department of Medicine, University of Minnesota, Minneapolis, MN 55455, USA

[10] Department of Internal Medicine, Division of Pulmonology, Medical University of Graz, Graz 8036, Austria

All co-authors, who actively contributed to the research in this thesis agreed to the use of their data.

Presentations

Neutrophil recruitment in the acute inflammatory phase of interstitial lung disease is determined by RGS5
Neha Sharma, Chandran Nagaraj, Bence M. Nagy, Leigh M. Marsh, Natalie Bordag, Diana Zabini, Malgorzata Wygrecka, Walter Klepetko, Elisabeth Gschwandtner, Guillem Genové, Akos Heinemann, E Kenneth Weir, Grazyna Kwapiszewska, Horst Olschewski, Andrea Olschewski
(Die Österreichische Gesellschaft für Pneumologie (ÖGP), virtual conference, 2020)

Poster Presentations

Neutrophil recruitment in the acute inflammatory phase of interstitial lung disease is determined by RGS5
Neha Sharma, Chandran Nagaraj, Bence M. Nagy, Leigh M. Marsh, Natalie Bordag, Diana Zabini, Malgorzata Wygrecka, Walter Klepetko, Elisabeth Gschwandtner, Guillem Genové, Akos Heinemann, E Kenneth Weir, Grazyna Kwapiszewska, Horst Olschewski, Andrea Olschewski

(Die Österreichische Gesellschaft für Pneumologie (ÖGP), virtual conference, 2020)

Impact of Regulator of G protein signaling 5 in pulmonary circulation
Neha Sharma, Chandran Nagaraj, Bence Nagy Miklos, Davor Skofic-Maurer, Grazyna Kwapiszewska, Andrea Olschewski, Horst Olschewski

(Die Österreichische Gesellschaft für Pneumologie (ÖGP), Linz, Austria, 2018)

Role of RGS5 in pulmonary vascular homeostasis
Neha Sharma, Chandran Nagaraj, Bence Nagy Miklos, Davor Skofic-Maurer, Grazyna Kwapiszewska, Andrea Olschewski, Horst Olschewski

(International Vascular Biology Meeting, Helsinki, Finland 2018)

Foreword

First and foremost, I would like to thank my supervisor Prof. Andrea Olschewski for her continuous support, encouragement, critical scientific inputs, and unreserved time. Thank you for accepting me as part of your scientific group and providing me with the opportunity to pursue my doctoral project. I owe the deepest gratitude to Dr. Chandran Nagaraj and Dr. Bence M. Nagy for their valuable scientific inputs, patience, and motivating me every day throughout these years.

I would always be grateful to my advisor committee involving Prof. Horst Olschewski, Prof. Akos Heinemann, Prof. Gunther Marsche, Dr. Chandran Nagaraj, and Prof. Andrea Olschewski for their providing scientific input, interesting discussions, and very helpful explanations. I would like to thank Dr. Grazyna Kwapiszewska and Dr. Leigh M. Marsh for your scientific advice and assistance throughout these years.

I owe a debt of gratitude to Elisabeth Blanz and Sabine Halsegger for their technical assistance and for amazing working atmosphere. Thanks to Natalie Bordag for helping me with R programming and for beautiful heatmaps. A big thank to Davor Skofic-Maurer, Diana Zabini, Helene Thekekkara Puthenparampil, Valentina Biasin, Anna Birnhuber, and Ceren Mutgan for all the fun and support. I would like to thank all my colleagues in the Ludwig Boltzmann Institute for Lung Vascular Research and Medical University of Graz for their assistance and scientific inputs. I want to thank all collaborators from diverse institutes for their invaluable contributions to this study.

Last but not least, I am thankful to my family for their love, patience and support. A very special thanks to Madhu who was always there supporting and encouraging me through difficult times.

Acknowledgments

This work was conducted at the Ludwig Boltzmann Institute for Lung Vascular Research and the Center for Medical Research (ZMF I and II) of the Medical University of Graz. The Ph.D. study was supported by the Medical University of Graz, Graz, Austria through Ph.D. Program Molecular Medicine (MolMed).

Neutrophil migration assay and calcium measurements were carried out in collaboration with Prof. Akos Heinemann at the Division of Pharmacology, Medical University of Graz, Graz, Austria.

RGS5 staining on ARDS lung tissue was performed in collaboration with Prof. Malgorzata Wygrecka at the Center of Infection and Genomics of the Lung, University of Giessen, Giessen, Germany.

RGS5-/- mice were received in collaboration with Prof. Guillem Genové from Karolinska Institute, Stockholm, Sweden

I would like to thank Elisabeth Blanz, Thomas Fuchs, Eva Grasmann, Sabine Halsegger, Lisa Oberreiter, Iris Red, and Nina Treitler for their excellent technical assistance.

Table of Contents

Abbreviations and Definitions

A	Estimation of inspiratory capacity
AECs	Alveolar epithelial cells
AHR	Airway hyperresponsivenss
ALI	Acute lung injury
AlvMp	Alveolar macrophages
ASM	Arterial smooth muscle
ARDS	Acute respiratory distress syndrome
B2M	Beta-2 microglobulin
BALF	Bronchoalveolar lavage fluid
bFGF	Basic fibroblast growth factor
Cdc42	Cell division control protein 42
CCl4	Carbon tetrachloride
Ca^{2+}	Calcium
Crs	Compliance
CXCL1 and 2	The chemokine (C-X-C motif) ligand 1 and 2
ECM	Extra cellular matrix
EMT	Epithelial–mesenchymal transition
ERK1/2	Extracellular-signal-regulated kinase
ER	Endoplasmic reticulum
Ers	Elastance
FMT	Fibroblast–myo-fibroblast transition
fMLP	Formyl-Methionyl-Leucyl-Phenylalanine
G	Tissue dampening
GAP	GTPase-activating proteins
G-CSF	Granulocyte colony-stimulating factor
GDP	Guanosine diphosphate
GPCRs	G protein coupled receptors
GTP	Guanosine-5'-triphosphate
H	Tissue elastance
5-HT	5-hydroxytryptamine or serotonin

HDM	House dust mite
IAV	influenza A virus
ICAM-1	Intercellular adhesion molecule 1
IHC	Immunohistochemical
IL	Interleukin
ILD	Interstitial lung disease
IM	Interstitial macrophage
i.n.	Intranasal
IFNγ	Interferon γ
IPF	Idiopathic pulmonary fibrosis
IP3	Inositol 1,4,5-trisphosphate
i.t.	Intra tracheal
KCl	Potassium chloride
KO	Knockout (-/-)
LFA-1	Lymphocyte function-associated antigen 1
LPS	Lipopolysaccharide
LTB4	Leukotriene B4
MEK	Mitogen-activated protein kinase
MPO	Myeloperoxidase
MVE	Micro vascular epithelium
NE	Neutrophil Elastase
NET	Neutrophil extracellular trap
NF-κB	Nuclear factor 'kappa-light-chain-enhancer' of activated B-cells
PA	Pulmonary Artery
PDE2A	Phosphodiesterase 2A
PDGF	Platelet-derived growth factor
PE	Phenylephrine
PGE_2	Prostaglandin E_2
PIP3	Phosphatidylinositol-3,4,5-tris-phosphate
PLCβ	Phospholipase Cβ
PMN	Polymorphonuclear
PSGL-1	P-selectin glycoprotein ligand-1

PTEN	Phosphatase and tensin homolog
RGS	Regulator of G protein signaling
RhoA	Ras homolog family member A
ROCK	Rho-associated kinase
ROS	Reactive oxidative species
RTK	Receptor tyrosine kinase
Rrs	Resistance
RVSP	Right ventricular systolic pressure
TGF-β	Transforming growth factor-β
TH2	T helper
TNF-α	Tumor necrosis factor-α
U46619	Thromboxane A2
VEGF	Vascular endothelial growth factor
WASp	The Wiskott–Aldrich Syndrome protein
WT	Wildtype

Zusammenfassung

Entzündungen spielen eine wichtige Rolle bei der Initiierung und dem Fortschreiten akuter Lungenverletzungen und fibrosierenden interstitiellen Lungenerkrankungen (ILD). Der Regulator der G-Protein-Signalgebung (RGS) repräsentiert ein breit gefächertes Kontrollsystem zellulärer Reaktionen. Die Aktivitäten der R4-Unterfamilie von RGS wurden in den letzten Jahren bei allergischen Lungenerkrankungen aufgeklärt. Allerdings ist die R4-Signalgebung bei anderen entzündlichen Lungenerkrankungen, die eine starke zelluläre Immunantwort hervorrufen begrenzt. Daher zielte unsere Studie darauf ab die funktionelle Relevanz des R4-Familienmitglieds RGS5 als potenzielles Kontrollelement in diesem Zusammenhang aufzuklären. Die Genprofiling der R4-Unterfamilie zeigte eine stark erhöhte RGS5-Expression in Proben von humanen fibrosierenden Lungenerkrankungen. In Übereinstimmung mit den Patientendaten war die RGS5-Expression in murinen Lungen bei Bleomycin-induzierten Verletzungen deutlich erhöht. In der akuten Phase der Lungenfibrose blieb bei RGS-Knock-out-Mäusen (RGS-/-) die Lungenfunktion erhalten, während Kontrollmäuse im Vergleich dazu mit Kochsalzlösung behandelt drei Tage nach der Verabreichung von Bleomycin signifikant kombinierte Atmungsstörungen aufwiesen. Die Analyse spezifischer Immunzell-Subpopulationen in bronchoalveolärer Lavageflüssigkeit (BALF) und Lungengewebe zeigte eine signifikante Verringerung von Neutrophilen im BALF von RGS5-/-Tieren und eine abgeschwächte enzymatische Aktivität der Myeloperoxidase (MPO) im Lungengewebe. Im Gegensatz dazu waren die Langzeitwirkungen von Bleomycin bei RGS5-/- Mäusen nicht signifikant verändert. Im LPS-Lungenverletzungsmodell konnte RGS5 -/- auch keine Neutrophilen in die Lunge rekrutieren, wodurch nach 24 Stunden Begleiterscheiungen von verringerten Myeloperoxidase-Spiegeln im Gewebe auftraten. Unsere In-vitro-Assays zeigten trotz erhaltener Ca2+-Signalgebung eine beeinträchtigte Migration von RGS5-/- Neutrophilen zu Chemokinen. Wichtig ist, dass RGS5-/- Neutrophile eine verzögerte ERK-Dephosphorylierung und eine erhöhte RhoA-Aktivierung zeigten, welches in unserem Modell eine Rolle bei der reduzierten Neutrophilenmigration spielen könnte. Zusammenfassend lässt sich sagen, dass der Verlust von RGS5 die Lungenfunktion bewahrt und die Entzündung in der akuten Phase von Bleomycin-induzierter Lungenfibrose und LPS-induzierter Lungenschädigung abschwächt. Der gezielte Einsatz von RGS5, einem potentiellen Kontrollelement, könnte die Schwere von Exazerbationen bei interstitiellen Lungenerkrankungen lindern.

Abstract in English

Inflammation plays an important role in the initiation and progression of acute lung injury and fibrosing interstitial lung diseases (ILD). The regulator of G protein signaling (RGS) represents a widespread system of controllers of cellular responses. The activities of the R4 subfamily of RGS have been elucidated in allergic pulmonary diseases over the past years. However, the R4 signaling involved in other inflammatory lung diseases with a strong cellular immune response is limited. Thus, our study aimed to enlighten the functional relevance of the R4 family member, RGS5, as a potential control element in this context. Gene profiling of the R4 subfamily showed strongly increased RGS5 expression in human fibrosing lung disease samples. In line with the patient's data, RGS5 expression was markedly increased in murine lungs following bleomycin injury. In the acute phase of pulmonary fibrosis, RGS knock-out mice (RGS-/-) had preserved lung function while control mice showed significant combined ventilatory disorders three days after bleomycin application as compared to saline-treated mice. Analysis of specific immune cell subpopulations in bronchoalveolar lavage fluid (BALF) and lung tissue showed a significant attenuation of neutrophils in the BALF of RGS5-/- animals, and lowered myeloperoxidase (MPO) enzymatic activity in lung tissue. In contrast, the long-term effects of bleomycin were not significantly changed in RGS5-/- mice. In the LPS lung injury model, RGS5-/- also failed to recruit neutrophils into the lung, which was accompanied by reduced tissue myeloperoxidase levels after 24 hours. Our *in-vitro* assays showed impaired migration of RGS5-/- neutrophils towards chemokines despite preserved Ca^{2+} signaling. Importantly, RGS5-/- neutrophils showed delayed ERK dephosphorylation and increased RhoA activation which might play a role in reduced neutrophil migration in our model. In a conclusion, loss of RGS5 preserves lung function and attenuates inflammation in the acute phase of bleomycin-induced pulmonary fibrosis and LPS-induced lung injury. Targeting RGS5, a potential control element, might alleviate the severity of exacerbations in interstitial lung diseases.

1 Introduction

1.1 Idiopathic pulmonary fibrosis (IPF)

1.1.1 Pathogenesis of IPF

Idiopathic pulmonary fibrosis (IPF) is one of the most common types of interstitial lung diseases (ILDs) (2). IPF has an incidence rate of 7-16 cases per 100.000/year with poor prognosis (3) and it is the most common in elderly males above 50 years of age with a short median survival of 1.5 - 4 years from diagnosis (4–6). It's a heterogeneous, progressive, and degenerative lung disease with unclear aetiological origin. Factors e.g. Age, sex, smoking, and air pollution have been proposed to play an important role in the development of the disease. IPF clinical manifestations involve a dry cough, decline in lung function, and progressive dyspnea (7,8).

Histological evaluation of IPF lung shows alternating regions of normal and fibrotic tissue as well as lung regions with interstitial inflammation. Basal/sub-pleural parts of lung appear as honeycombed structures in IPF. Accumulation of excessive extracellular matrix proteins and tissue remodeling is believed to be caused by repetitive micro-injuries leading to inflammation and fibrotic lung fibrosis. The aberrant lung remodeling leads to reduced oxygen diffusion through the alveolar-capillary barrier, resulting in dyspnea and reduced total lung capacity (7,9). Until now, there are no therapies available that can stop or reverse the disease progression and thus, improve the life quality of IPF patients. The rising number of cases each year with high unmet medical needs represents an alarming situation.

IPF pathogenesis is complex due to the involvement of multiple factors. The classical paradigm of IPF proposes injury to alveolar epithelial cells (AECs) releasing proinflammatory cytokines and recruit inflammatory cells. Fibroblasts interact with injured AECs to prevent further damage to the lungs and heal the tissue. In the response, activated fibroblasts excessively proliferate and migrate to the site of injury and release extracellular matrix (ECM) proteins. Interstitial fibroblasts transformation to synthetic/contractile myofibroblasts phenotype which releases more ECM, promoting irreversible tissue stiffening and formation of fibrotic foci (10,11).

1.1.2 Inflammation in IPF

Inflammation seems to play an important role in the initiation and progression of lung fibrosis (10,12), dependent on acute exacerbations and progression of fibrosis. However, classical anti-inflammatory therapies in IPF failed to meet relevant clinical endpoints (13–16). The role of inflammation in the development of fibrosis and immune cells involved in disease progression is still not fully discovered. It is accepted, that upon damage to alveolar epithelium there is a release of pro-inflammatory cytokines such as interleukin 8 (IL-8), tumor necrosis factor (TNFα), transforming growth factor (TGFβ), and T helper (TH2) cytokines for the migration and recruitment of inflammatory cells to the site of damaged tissue (17). This can further initiate detrimental cross-talks between damaged epithelium, inflammatory cells, and fibroblasts for the production of ECM and lung remodeling.

Neutrophils are considered to be the second responder of the immune system upon lung tissue injury after alveolar macrophages (AlvMp). Neutrophils present in alveolar spaces can induce abnormal tissue repair upon injury and an increased influx of neutrophils can cause additional damage due to the release of reactive oxidative species (ROS), proteases, and other pro-inflammatory cytokines (18,19). Different studies have shown an increased number of neutrophils and associated cytokines e.g. IL-8 and Granulocyte colony-stimulating factor (G-CSF) in the sputum and broncho lavage fluid (BALF) of IPF patients, which correlates with reduced lung function and prognosis (20–23). Microarray analysis of BALF cells isolated from IPF patients showed increased mRNA expression of genes related to neutrophil dysfunction (24). Neutrophil elastase (NE), a neutral serine protease is localized to the azurophilic or primary granules in neutrophils. NE plays an important role in host defense, is a boost for tissue remodeling and fibrosis (19,25) as preclinical mouse models of pulmonary fibrosis have reported that NE can activate fibroblast proliferation and promote differentiation to myofibroblasts independent to TGF-β (26)(27). NE knockout (KO) mice displayed reduced fibroblast and myofibroblast content in the lungs (28)

Macrophages also play a critical role in lung fibrosis and associated acute exacerbations depending on the type of the macrophages and the cytokine environment of the tissue. There are two types of macrophages identified in the lungs, M1 and M2. M1 can differentiate into M2 and also change its function. Both can be activated and differentiated by different cytokines and involved in inflammatory, anti-inflammatory, and pro-fibrotic functions (29). In addition, macrophages are also an important source for cytokines release which is

eventually responsible for neutrophil migration and recruitment in the lungs upon injury. These findings indicate that the involvement of inflammatory cells and cytokines in the complex pathogenesis of IPF can't be neglected and more importantly, they might represent potential targets for further therapeutic interventions.

1.1.3 Treatments for the disease

After three decades from the first trial, several underlying molecular mechanisms have been investigated to foster the development of new therapies. As it is widely accepted that inflammation is an important trigger for fibrogenesis, IPF patients have been treated with corticosteroids and immunosuppressants till a few years back (14,30). However, clinical studies have also shown that unspecific immune-modulatory compounds led to an increased rate of hospitalization *via* boosting disease progression (15,31). Targeting a wide population of immune cells without understanding their function in lung fibrosis might be one of the reasons for failing. In addition, variability of inflammation in IPF patients can also explain the lack of positive effects.

Pirfenidone and nintedanib represent the current therapeutic options (32). Pirfenidone is an anti-inflammatory and anti-fibrotic orally administrable pyridine compound. The exact mechanism of its action is still unknown. In *in vitro* and *in vivo* preclinical models inhibition of fibroblast proliferation and reduced over production of collagen has been observed (33). Tested in the clinical trial ASCEND, pirfenidone showed a trend toward halting disease progression with some side effects e.g. nausea, indigestion, skin rashes, and photosensitivity. The other currently available therapeutic option is nintedanib, a multiple tyrosin kinase receptor inhibitor. The INPULSIS clinical trial showed reduced lung function loss over time with gastrointestinal side effects e.g. nausea and diarrhea (33,34). The lack of a breakthrough in pharmacotherapy for IPF patients highlights the need for novel therapeutic targets to reverse or stop the fibrotic process with an acceptable safety profile.

1.2 Acute Lung Injury (ALI)

Despite extensive research to understand the pathophysiology, acute lung injury (ALI) remains at a mortality rate of 30-40% from the past two decades (35–38). ALI is a clinical syndrome, diagnosed with severe hypoxemia, bilateral pulmonary infiltrations, and a significant decrease in lung compliance. ALI progresses into acute respiratory distress

syndrome (ARDS) with the risk of multiple organ failure in extreme cases. ALI can be a direct or indirect injury to the lungs which leads to inflammatory responses. Few common causes of ALI are pneumonia, sepsis, trauma, aspiration, and drug toxicity. The pathophysiological investigations have shown imbalance in barrier of endothelial and epithelial cells in the initial stages of ALI, and flooding of the alveolar sac with protein-rich fluid, inflammatory cells, and fibroblasts, contributing to impaired blood gas exchange barrier in the lungs (36,38). The importance of inflammation in ALI pathogenesis is well supported by clinical and preclinical studies. An increased influx of neutrophils in BALF and lung tissue correlates with mortality of ALI patients. Neutrophils adhere to the endothelium and migrate through the interstitium into the air space. The severity and progression of ALI are highly dependent on neutrophil migration into the lungs in response to AM (39,40). Locally, AlvMp releases chemokine which further activates neutrophils to migrate and produce proteases, ROS, and other pro-inflammatory molecules. Although neutrophil activation is important for the host defense, hyper infiltration and consistently elevated inflammatory mediators in the lungs impede the resolution of injury which can lead to fibroproliferative stage involving interstitial lung fibrosis (39,41).

Various injury-inducing agents has been employed to reproduce human-like acute lung injury pathophysiology in animals models (42). However, it has been difficult to show all features in one single animal model. Most of the animal models either depleting neutrophils or blocking neutrophil-specific chemokine and receptors have shown a protective phenotype upon acute lung injury (43). This indicates the crucial role neutrophils play in lung damage and resolution. Up to now, there is no drug therapy has been emerged for ALI due to very heterogeneous underlying causes. The supportive treatments are given to ALI/ARDS patients. Treatment of underlying disease, accurate mechanical ventilation, and specific treatment of secondary pulmonary pathologies are the most important strategies to manage the disease severity (38). The ideal therapeutic target should be able to balance neutrophils recruitment in the lungs where host defense from infections should not be compromised.

1.3 The Regulator of G protein signaling (RGS) family

1.3.1 Structure and Regulation

The Regulator of G protein signaling (RGS) proteins was discovered more than two decades ago. They are ubiquitously expressed in our body with specificity to tissue type for maintaining normal physiological functions. Up to date more than 30 members of RGS proteins has been discovered which are further divided into subfamilies depending on their primary sequence homology and the presence of additional signaling domains (44)(45).

RGS are localized in different compartments of the cell for e.g cytoplasm and nucleus. RGS accelerate GTP hydrolysis and selectively inhibits the magnitude and duration of G protein-coupled receptors (GPCRs) induced downstream signaling complex. RGS directly interact with the Gα subunit to speed up the hydrolysis of GTP and stabilized *via* forming a GDP-bound stable inactive heterotrimeric (αβγ) (44). RGS target Gα subunits, and mutation of Gα subunit specific to amino acids (Gly183—Ser183), makes RGS resistant to interacting with Gα. Studies have shown that Gai2 (G184S) mutation in Gα subunit leads to a global loss of RGS interaction with Gα subunits in mice. The mutation does not affect Gα binding to the receptor and other subunits (46,47) Additional domains present in RGS other than the RGS domain indicate GAP independent function of RGS (45). RGS non-GAP function has been shown *via* interaction with receptor tyrosine kinase (RTK) and nuclear activity. Studies have documented that RGS is specific to the different Gα subunits including Gi/o and Gq with exception of Gs. Also, indirect interaction with the Gs subunit has been reported *via* interaction with adenyl cyclase subtypes (48–50). Regulation of RGS protein is independent of ligand, unlike GPCR. The concentration, localization, and stability are very important factors for modulating RGS activity.

1.3.2 RGS in the lung and inflammation

Various studies have elucidated the functional relevance of different RGS of the R4 subfamily in lung diseases and inflammatory cells (51). The proteins in the R4 subfamily (RGS 1-5, 8, 13, 16, 18, and 21) are small with only minimal C- and N- terminal extensions flanking the RGS domain and 20-25 kDa size except for RGS3. One of the primary receptors on inflammatory cells responsible for sensing injury-induced chemokine is GPCRs. They help in the polarization, migration, and recruitment of inflammatory cells. A continuous

GPCR activation and failed desensitization lead to excessive inflammatory cell influx which can generate persistent tissue injury in the lung. The balance of GPCR activation and desensitization is extremely important to mitigate hyper immune response where RGS can play an important role.

RGS1 is present in multiple immune cells including macrophages, monocytes, dendritic cells, B and T lymphocytes. B cells exhibited increased response for chemotaxis and prolonged elevation of intracellular Ca^{2+} levels upon CXCL12 ligand activation from RGS1 KO mice (52,53). RGS2 is present in various organs including lungs in human and murine bronchial epithelium and arterial smooth muscle (ASM). RGS2 KO mice showed spontaneous development of airway hyperresponsiveness (AHR) and augmented Ca^{2+} mobilization and contraction of ASM cells (54). Loss of RGS2 led to increased AHR and decreased compliance of the lungs with acute neutrophilic inflammation in the lipopolysaccharide (LPS) mouse model (55). Similar results have been found in the house dust mite (HDM) mouse model. RGS2 deficient mice exhibited increased inflammation of neutrophils and eosinophils with increased AHR (56). RGS3 is a unique member of the R4 family with additional interaction domains in their structure. Loss of RGS3 has been shown to increase T cell migration in the HDM mouse model and demonstrated a redistribution of T cells from the draining lymph nodes to the lungs (57).

RGS4 remains unexplored in inflammatory cells. However, few studies are indicating its protective role in the lungs. RGS4 attenuated the overproduction of mucin in the airway *via* suppressing Prostaglandin E_2 (PGE_2)-induced Gαs-mediated signaling *in vitro* and *in vivo* by enhancing GTPase acceleration (58). Another study showed increased expression of RGS4 in ASM cells from advanced asthma patients which were correlated with disease severity (59). Overexpression of RGS4 in mice showed a protective phenotype *via* reducing the airway contraction and alteration in cytokine production upon allergen treatment (60). Contrary to the previous study, it was recently shown that RGS4 deficient mice were protected from AHR upon allergen or allergen plus aspirin challenge *via* modulated allergen-induced PGE_2 secretion. The discrepancy indicates the dynamic role of RGS4 in the lung depending on the allergen and degree of disease development (61). RGS13 function is highly restrictive to germinal center B cells and mast cells. It's highly expressed in immune cells for e.g B and T cells, mast cells (62,63). RGS13 is connected to non-allergic asthma in children, where RGS13 expression was increased in T regulatory cells from blood (64)

RGS13 KO mice exhibited enlarged germinal center in the spleen with better antibody response (65).

RGS16 is involved in T cell trafficking in the lungs. RGS16 T cell-specific transgenic mice showed decreased migration in a model of allergic airway inflammation and increased TH2 cells in lymphoid organs (66). Allergen challenged RGS16 KO mice to contain more TH2, suggesting its role in lung inflammation and T cell trafficking in the tissue (67). RGS18 is highly expressed in bone marrow cells and platelets and it seems to play an important role in the hemostatic functions of mature platelets. RGS18 KO mice showincreased numbers of platelet which result in coagulation and thrombus formation *in vivo* (68,69). Finally, RGS21 is expressed in airway epithelium and multiple tissues including the spleen, thymus, peripheral blood leukocytes, and gastrointestinal tract (70). Although our knowledge about the different RGSs in the lung has impressively increased during the two decades, further studies are required to understand their physiological and pathophysiological relevance and their regulations in different processes as well as in diseases.

1.3.3 RGS5 in the lung and inflammation

RGS5 is expressed in human and mouse lungs with a 90% homology (71). RGS5 has been localized in smooth muscle and epithelial cells in the lung tissue. In recent years, multiple studies have addressed the functional relevance of RGS5 in asthma and AHR. RGS5 has been shown to negatively regulate bronchial smooth muscle cell contraction. Isoproterenol, the non-selective β adrenoreceptor agonist decreased RGS5 expression and increased intracellular calcium on human precision lung slices. The study suggested that the use of β adrenoreceptor agonist can lead to a reduction in broncho protection and sensitize the excitation-contraction signaling pathways in asthma (72). On contrary, RGS5 basal expression was increased in bronchial tissue and cultured ASM isolated from asthmatic patients with decreased response to the Ca^{2+} eliciting agonist histamine. This was further confirmed in a mouse model where mice were challenged with allergen-inducing AHR (73). RGS5 KO mice exhibited spontaneous AHR with augmented GPCR-triggered Ca^{2+}-signaling but unaltered BALF immune cell profile, mucin production, and ASM mass, indicating the relevance of RGS5 in the pathophysiology of chronic asthma (73). Increased expression of RGS5 can result in hypo-contraction and fixed airway in patients suffering from asthma due to decreased myocyte shortening (74).

Furthermore, overexpression of RGS5 is a favorable prognostic factor in non-small cell lung cancer patients. It led to lower adhesion and migration of lung cancer cells with reduced proliferation and more apoptosis. Furthermore, RGS5 enhanced the cytotoxic effect of radiation in human lung cancer cells (75). The function of RGS5 in inflammatory cells is still limited. It has been shown in a mouse model that RGS5 is present in neutrophils and negatively regulates their chemotaxis and adhesion for the efficient mobilization to inflamed lung, also supported with *in vitro* migration assay (76). RGS5 is also expressed in macrophages and regulates atherosclerotic plaque formation. RGS5−/−ApoE−/− mice showed an increased percentage of apoptotic macrophages in atherosclerosis plaque with phosphorylated extracellular-signal-regulated kinase (ERK1/2), phospho-p65, IκBα, and cleaved caspase 3 in the macrophage, indicating that RGS5 inhibited atherosclerosis, at least partly, by inhibiting Mitogen-activated protein kinase MEK-ERK1/2 and NF-κB signaling (77).

1.3.4 RGS in organ fibrosis

Only a few studies in cardiac, kidney and lung fibrosis explored the role of RGS in pathogenesis. RGS2 expression was shown to be increased in the heart tissue obtained from rats treated with carbon tetrachloride (CCl4) to induce experimental liver cirrhosis. In this setting, RGS2 was claimed to downregulate the β-adrenergic signaling pathway together with $G\alpha_{i2}$ and phosphodiesterase 2A (PDE2A) (78). Another study reported RGS2 as a negative regulator of Angiotensin II (ANG II)-induced cardiac fibrotic responses and fibrosis development (79). RGS2 has been also shown to protect against kidney fibrosis induced by a unilateral ureteral obstruction in mice. RGS2 acted here as an inhibitor of AngII/AT1R signaling and protected the kidneys from injury (80). In the lung, RGS2 deficient mice exhibited increased peribronchial fibrosis in an acute mouse model of asthma induced by administration of intranasal interleukin (81). RGS2 expression increased upon pirfenidone treatment in fibroblasts obtained from donor and IPF, indicates that RGS2 upregulation is induced by pirfenidone independent to the disease, a significant contributor protecting from pulmonary fibrosis. WT mice lungs, treated with pirfenidone, were protected from fibrosis upon bleomycin treatment, however knockdown of RGS2 *in vivo* did not show positive effects in the mouse model (82).

RGS3 overexpression in mice led to reduced cardiac hypertrophy and fibrosis in the aortic banding model *via* inhibiting MEK-ERK signaling (83). Cardiac-specific RGS5 transgenic mice showed blunted hypertrophy, chamber dilation, and fibrosis *via* disruption of MEK-ERK1/2 signaling. In contrast, RGS5 global KO mice exhibited an exaggerated response of pathological cardiac remodeling and fibrosis (84). Mouse model of liver fibrosis induced by CCl4 developed increased expression of RGS5 in acute and chronic liver injury. Conversely, RGS5 KO mice presented increased hepatocyte damage and fibrosis upon challenge (85). RGS16 deficient mice challenged with S. mansoni eggs resulted in increased granulomatous lung fibrosis with increased eosinophil influx, anomalous localization of T cells, and increased cytokine production (67). These studies show the multifaceted and often contradictory role of RGS in organ fibrosis.

1.3.5 RGS5 in vasculature

RGS5 has been extensively explored in systemic vasculature and emerged as an important regulator of vascular pathologies (86). RGS5 is present in pericytes, endothelial and smooth muscles cells in systemic vessels. It controls cellular differentiation, migration, and contraction to assist in cardiac function, blood pressure regulation, and neovascularization such as arteriogenesis and angiogenesis (84,87–89). RGS5-deficient mice have repeatedly been reported to be hypotensive (90)(91) or hypertensive (88). The discrepancies in these findings were likely to be based on the use of different techniques (i.e. tail-cuff versus telemetric measurement), genetic backgrounds, and stress levels (increased cardiac output/systolic blood pressure), which was further clarified simply by measuring mean arterial pressure values over several days, no overt differences in blood pressure were observed between WT and RGS5-/- mice (92). An increase in pulmonary pressure is an important complication of several ILDs, particularly in IPF, and can adversely affect patient outcomes. The increase in pressure can differ between patients depending on the stage of fibrosis and can significantly affect the median survival (93). Therefore, we could provide valuable insight into the functional relevance of RGS5 in pulmonary arteries and further emphasizing RGS5 importance in pulmonary pressure homeostasis.

1.4 Neutrophil migration

1.4.1 Neutrophil migration in the lung

Neutrophils are one of the most abundant circulating cells in the blood, also called the first line of defense in the immune system. They have a condensed and multi-lobular nucleus with a large number of granules and vesicles. Neutrophils are produced from their precursor's myeloid lineage progenitor cells (common myeloid progenitors) in bone marrow and matured in the bone marrow and extramedullary tissues, including the spleen and terminally differentiated to mature neutrophils. With short life time (5-6 days) after release from bone marrow, they undergo programmed apoptosis and followed by removal by macrophages. The programmed apoptosis of neutrophils can get delayed depending on the pro-inflammatory environment and severity of the injury which leads to involvement of other cell death pathways e.g. necrosis. Necrotic neutrophils produce proteolytic and oxidant-generating enzymes which further induce unexpected severe tissue injury, therefore their removal is very important (94,95).

Neutrophil recruitment is very specific to the tissue type due to presence of small differences in cell surface marker (96,97). Balanced numbers of neutrophils are always present in the pulmonary circulation. They patrol and eliminate bacteria and toxins. AlvMp, in concert with injured epithelium and endothelium release chemokine, is responsible for the neutrophil recruitment during inflammation. Neutrophil recruitment is divided into several steps: capture, rolling, arrest, adhesion, crawling, and transendothelial migration. In the lung, upon injury and release of inflammation mediators, the circulating neutrophils contact the activated/inflamed endothelium and become primed. During first step of neutrophil priming is important as they are usually resting in the circulating blood. Endothelium expresses P and E selectins to bind with neutrophil cell surface antigens e.g. L-selectin, CD44, and P-selectin glycoprotein ligand-1(PSGL-1). This is the capture stage of the neutrophil recruitment process. Next, neutrophils express lymphocyte function-associated antigen 1 (LFA-1) and Mac-1 and bind to chemokine present on the endothelium and beta integrin, leading to the rolling stage of neutrophils. The crucial step for neutrophils is to arrest the endothelium before they transmigrate to the interstitium. During this step, LFA-1 undergo conformational changes and interact with Intercellular Adhesion Molecule 1(ICAM-1) expressed on endothelium surface. Once neutrophils are in the arrest stage, they change their cytoskeleton to reduce their surface area and start crawling toward the chemokine gradients

(e.g. fMLP1, C3a, C5a CXCL8, CXCL1, CXCL2, and LTB4). The crawling phase involves again Mac-1 and adhesion receptors expressed on the neutrophils. Finally, they transmigrate through the endothelium, leading to increase vascular permeability (96,98).

1.4.2 Neutrophil Intracellular signaling: the role of Ca^{2+} flux, ERK and small GTPase

Neutrophils express several classes of different receptors (GPCR, Fc receptor, cytokine receptor, adhesion receptors, and innate immune receptors) on their surface. GPCR is mainly responsible for the polarization and migration of neutrophils toward chemoattractants (99). Ligand activation of GPCR leads to dissociation of G complex subunits and diffuse to regulate the activation of subsequent enzymes (adenylate cyclases, phospholipase C isoforms, phosphatidylinositol (PtdIns) 3-kinases (PI3-kinases or PI3K), Ca^{2+}, Mitogen-activated protein kinases (MAPK), and ion channels). They are responsible for their activation, chemotactic migration, adhesion, chemokine release, phagocytosis, and ROS (100). Calcium represents an important second messenger in neutrophils. In the resting state, neutrophils contain 10,000-fold lower cytosolic Ca^{2+} concentration compared to their extracellular environment. Upon ligand activation of GPCR, both subunits activate phospholipase Cβ (PLCβ) enzymes lead to the generation of IP3 and concomitant release of Ca^{2+} from intracellular stores as well as to influx from extracellular sources. Studies have shown that Ca^{2+} is important for ROS production, degranulation, and cytoskeleton rearrangements during the polarization and migration of neutrophils (101). RGS controls mostly the cytosolic Ca^{2+} changes *via* regulating downstream signaling of GPCR. RGS5 overexpression in 293T cells has been reported to results in angiotensin and endothelin receptors induced cytosolic Ca^{2+} response (102). RGS5 deficient ASM, neutrophils, and other cell types exhibited a higher magnitude of GPCR induced Ca^{2+} response compared to their controls (73)(76).

MAPKs, including ERK, Jnk, and p38, are involved in the migration of neutrophils. ERK has been implicated to be the main regulator of neutrophil migration. However, reports suggest both, positive or negative regulation of neutrophil migration by ERK. The inhibition of ERK activity showed increased and directed migration of neutrophils toward different concentrations of chemokine (103). In contrast, transgenic mice expressing functional Förster resonance energy transfer biosensors for ERK showed that increased ERK activity correlates with migration velocity in the neutrophils to inflamed subcutaneous tissue (104).

As the studies, were performed in different systems and involve multiple factors, it's difficult to draw a convincing conclusion.

Rho family small GTPases are also players in the cytoskeleton rearrangement of neutrophils and they are required for polarization, migration, and adhesion (105,106). The Rho family constitutes three major proteins RhoA, RAC, and Cdc42 with few additional minor proteins. The activation of these proteins depends on the cycle between a GDP- and a GTP-bound form. RhoA is a small protein of 21kDa, localized in the leading and trailing edges of the cells, responsible for actin arrangement during cell migration. In neutrophil cell lines (HL-60 and PLB-985), RhoA is localized in the trailing edge and helps to reorganize the actin filament and the formation of contractile actin cables (stress fibers) and thus, regulates tail retraction and migration (107). The downstream effectors of RhoA are mDia and LIMK. mDia act on profilin for actin polymerization, where LIMK inhibits cofilin, responsible for actin turnover. Activation of MLCP through ROCK1/2 promotes actomyosin assembly through MLC. The role of RhoA in cell migration remains contradictory. Most of the studies use *in vitro* models of specific cell lines to investigate the functional relevance of RhoA since RhoA KO mice are embryonic lethal (108,109).

In a recent study, Rho-deficient neutrophils exhibited increased neutrophil integrin activation characterized by increased random and directional migration *in vitro* and enhanced recruitment to inflammatory sites *in vivo*. This study indicates that RhoA acts as a negative regulator of neutrophil migration and activation (110). The interaction between RGS5 and RhoA has been mostly studied in systemic vasculature. Loss of RGS5 led here to increased proliferation and migration of smooth muscle cells in *in vitro* and *in vivo* models *via* activating Rho kinase signaling (88). Another study, using RGS5 deficient vascular smooth muscle cells (SMCs) showed impaired activation of RhoA upon stretch stimuli. They claim that RGS5 promotes a sustained RhoA activity by shifting Gaq/11 to Ga12/13 signaling and present RhoA signaling as an essential step for the proliferation of smooth muscle cells during arteriogenesis (87). In a hypertension mouse model, RGS5 deletion led to impaired activation of RhoA and stress fiber formation in vascular SMCs and turned out to be a rate-limiting determinant of hypertension-induced arterial remodeling with elevated protein levels of the intracellular RhoA inhibitors, p190RhoGAP and RhoGDIa (92). These findings suggest that activation of RhoA is context-dependent.

The two other major proteins Rac and Cdc42 are present in the leading edge of neutrophils. Rac GTPase is responsible for the polarity and formation of F-actin in the leading edge (111). The process is complex involving several tightly regulated and coordinated steps. Rac 1 and 2 null neutrophils exhibited impaired migration toward chemokines, formation of actin assembly, and inflammatory recruitment *in vivo*. In contrast, other functions, like the production of superoxide remained unchanged unlike Rac2 (112,113). Rac undergoes a positive feedback loop that amplifies the gradient of internal signal: PtdIns(3,4,5)P3 located at the leading edge stimulates its accumulation by inducing activation of Rac (114,115). In addition, Rac stimulates PI3P accumulation, at least in part, *via* the actin polymers that are generated in response to activated Rac (116).

Cdc42 regulates polarity, directionality, and formation of a single leading edge and acts as a compass during chemotaxis (117,118). Cdc42 regulates neutrophil polarity *via* the effector WASp which is important for the F-actin polymerization at the leading edge (119). ROCK activation leads to phosphorylation of the Rac1-specific FilGAP, binds filamin A, and inhibits Rac, presenting a cross-talk between RhoA and Rac (120). At the posterior end of the neutrophils, the Cdc42 and RhoA regulated phosphatase and tensin homolog PTEN dephosphorylates phosphatidylinositol-3,4,5-trisphosphate (PIP3) and inhibits PI3K signaling (121). This mutual regulation between the leading edge and trailing edge involving Small GTPase activation and deactivation is important to maintain the polarity and directionality of neutrophils.

2 Hypothesis and Aims

2.1 Hypothesis

RGS5 is present in the lung and typically regulates GPCR downstream signaling. Loss of RGS5 might interfere with the development and progression of interstitial lung diseases as well as play a role in related neutrophilic inflammation in the lungs of patients.

2.2 Specific Aims

1. To profile the R4 RGS subfamily expression in human and mouse lungs.
2. To localize the RGS5 in human and mouse lung tissue.
3. To decipher the functional relevance of RGS5 in animal models of acute inflammatory lung diseases.
4. To elucidate the effect of RGS5 loss in an animal model of chronic pulmonary fibrosis.
5. To investigate the impact of RGS5 loss on pulmonary vasculature using *ex vivo* and *in vivo* models.

3 Methods

3.1 Human lung tissue samples

Between 2017 and 2020, we collected lung samples from ILD patients undergoing lung transplantation. The transplantations were carried out at the Division of Thoracic Surgery, Medical University of Vienna, Austria. The ARDS patients samples we received from the Department of Internal Medicine at the Justus-Liebig-University (JLU) Giessen, Germany. The institutional ethics committees of both universities approved the tissue donation study protocols. The protocol from the JLU has the following approval number IRB approval No 29/01. The approval number of the Medical University of Vienna is no. 976/2010. All approvals are per national law and the Good Clinical Practice/International Conference on Harmonization guidelines. Donor lungs that had to be taken apart were used as the control group. All study participants or their next-of-kin gave the consent for sample collection. All patients with ARDS met clinical American-European Consensus Conference criteria and died early, with a mean mechanical breathing duration of 92 hours. All lungs has been reviewed and diagnosis is confirmed by pneumologists and pathologists. Donor and patients clinical parameters and usage are given in **Table 1** and **Table 2**

3.2 Lung injury animal models

RGS5 knockout (RGS5-/-) mice were previously created at the Karolinska Institute Stockholm, Sweden (Division of Matrix Biology, Department of Medical Biochemistry and Biophysics) (90). The mice from age of 12-16 weeks were used in our acute and chronic treatment conditions. Accordingly, total number of animals required for the complete study is between 150-160 mice. Experimental animals were kept under controlled temperature and 12 hours dark-light cycle with water and chow diet. The treatments were performed as described previously (122,123). All the experimental procedures described further were performed under anesthesia using a continuous flow of isoflurane (2%). At the end of treatment, hemodynamic measurements and lung function testing were performed. Mice were sacrificed for further sample collection, immune cell evaluations *via* flow-cytometry analysis of BALF, and lung tissue. Molecular experiments such as gene expression analysis and western blotting were performed on the isolated lung tissue sample. Single intra-tracheal (i.t.) application of bleomycin sulfate (Sigma Aldrich, Vienna, Austria) was performed by using a microsprayer® Aerosoliser (Penn-Century. Inc. Wyndmoor, PA, USA) which takes

~5 seconds and results in a uniform distribution of aerosol throughout the lung. Local authorities approved all studies on animals. This was per national legislation (Austrian Ministry of Education, Science, and Culture (BMWF-66.010/0049-WF/V/3b/2017, BMWF-66.010/0142-V/3b/2019)).

Chronic treatment: wildtype (WT) littermate controls and RGS5-/- were treated with bleomycin sulphate (0.7 units/kg)/saline (i.t.) at day 0. The mice were kept under observation and were weighed every second day for the following 21 days until the end of the experiment.

Acute treatments: WT and RGS5-/- mice were challenged with bleomycin sulfate (1 unit/kg)/saline (i.t.) at day 0 and analyzed at day 3. In separate animal experiments, mice were given intra-nasally (i.n.) 1 mg/kg of Lipopolysaccharide (LPS) (0111 Serra, Sigma Aldrich, Vienna, Austria) in saline or saline only. After 24 hours of treatment, further physiological measurements were performed.

3.3 Measurements of hemodynamic parameters

Previous study describes the procedure of hemodynamic measurements (1). WT and RGS5-/- mice underwent cardiac catheterization under constant anesthesia using isoflurane (2%) for the ventricular pressure measurements. The SPR-671 1.4 F catheters (Millar Instruments Inc., Houston, USA) were linked to a Millar PCU-2000 pressure control unit, with a sampling rate of 1 kHz. For data acquisition, PowerLab 8/30 system (AD Instruments, Spechbach, Germany) was employed to constantly gather information on mice's body temperature, heartbeat, and ventricular pressure.Following an incision in the neck, the catheter was inserted into the right jugular vein and directed to the right ventricle to measure right ventricular systolic pressure (RVSP). Collected data were analyzed through Powerlab pro software. At the end of measurements, the mice were anesthetized intra-peritoneally (i.p.) with a mixture of Ketanest (150 mg/kg ketamine, Parke-Davis, Germany) and Rompun (20 mg/kg xylazine, Bayer, Germany) (ratio of 1:1.) before being transferred for lung function measurements. After all the measurements were performed, the Heart was isolated for the calculation of the right ventricle hypertrophy *via* Fulton index. The right ventricle was carefully dissected from the left ventricle and septum using a pair of fine scissors. Fulton index was calculated by dividing the weight of the right ventricle with the left ventricle and septum (RV/(LV+S)).

3.4 Measurement of lung function

The Flexi Vent system (SCIREQ Inc, Montreal, Canada) was used to measure the lung function of the mice, as described in the previous studies (1,123). To connect the mice trachea to the animal ventilator tube, a tracheostomy was performed. To expose the trachea, a small incision was made with the help of surgical scissors on the skin near the throat area. The trachea was exposed *via* separating muscles and sub-maxillary glands. Gently, the trachea was lifted using forceps, and suture thread passed underneath. A thin cut was made in the trachea without sectioning it. A calibrated cannula was passed through the cut and pushed gently inside the trachea. The cannula was firmly placed inside the trachea using a suture. The mice were connected to the ventilator *via* a fitting cannula with Y-tubing. The ventilation pattern was started to set the basal respiratory mechanics. Lung function parameters were obtained from pressure-volume signals generated in response to perturbations. Single compartment model, constant phase model, and pressure-volume curve were used to calculate multiple functional parameters such as compliance (Crs), resistance (Rrs), elastance (Ers), tissue elastance (H), tissue damping (G), estimation of inspiratory capacity (A) and area. After the measurements, sample collection was performed.

3.5 Wiremyograph - *ex vivo* vascular tension measurement

WT and RGS5-/- male mice (10-14 week-old) were sacrificed by cervical dislocation and lungs extracted along with intact airway for intra pulmonary artery (PA) isolation. Using a stereo zoom microscope SZX7 (Olympus, Japan), secondary order PAs were identified. The tissue surrounding the PA was cleared out using fine pair of scissors. They were also split into equal segments and tungsten wires were used to attach them to the wire myography system (Danish Myo Technology 620M, Hinnerup, Denmark). For isometric measurements, the myography chambers were coupled to force transducer units (PowerLab, ADInstruments, Oxford, UK). For 30 minutes after mounting, PAs were equilibrated in physiological salt solution (PSS; pH 7.4, 100% O_2, 37°C) with continuous aeration of 5% CO_2 in a balanced mixture of 20.9% O_2 and 74% N_2. The vitality of PAs was examined using KPSS (PSS with 120 mM KCl; isotonic substitution of NaCl by KCl) for three successive phases of depolarization, each lasting 15 minutes at 37°C, followed by an increase in basal tension to 2 mN and stability for another 30 minutes. Mean KPSS response greater than 1 mN was the cut-off to choose PA for further investigation. **Table 6** and **Table 7** contain

detailed information on solutions and materials, respectively. By directly injecting vasoactive drugs into the chamber, the effect of the agents (high potassium chloride, thromboxane analog U44619 (300 nM) was investigated. Local authorities approved all animal research under national legislation (Austrian Ministry of Education, Science, and Culture (BMWF-66.010/0049-WF/V/3b/2017)).

3.6 Sample collection and preparations

BALF was collected twice 1ml and 4ml using BAL buffer. BAL buffer was prepared with PBS containing protease inhibitor cocktail (Thermo Fischer, USA) and 1 mM EDTA. Single cells pellet was obtained after BALF spin-down (300 g at 4°C for 8 mins). The supernatant from 1 mL BALF was saved for total protein and chemokine analysis. Single cells obtained from spin down of BALF were used for further analysis for flowcytometry. Separately, Lung tissue (Lower right lobes) from mice were chopped into small pieces. The tissue digestion was performed using 0.7 mg/ml Collagenase and 30 g/ml DNAse for 40 minutes at 37°C. To obtain a single-cell solution, the digested tissue was filtered through a 100 µm cell strainer. The homogenized lung tissues were used to make single cell suspensions as previously described (1,124) and used for immune cells analysis using LSRII flow-cytometry.

3.7 Flow cytometry measurements

Single cells obtained from BALF and lung tissue were stained with the myeloid and lymphoid anti-body kits described in **Table 3**. Cells were subdivided in the following cell types/groups—myeloid: PMN (neutrophils) (CD11b+, Gr-1+, siglecF+/−), PMN imma-ture (immature neutrophils) (CD11b+, Gr-1+), PMN siglec F+ (siglec F+ neutrophils) (CD11b+, Gr-1+, siglecF+), alveolar macrophages (AlvMp) (CD11b+/−, CD11c+, siglecF+, CD64+), intersititial macrophages (IM) (CD11b+/−, CD11c-, siglecF-, MHC-II+, CD64+), monocyte macrophages Gr+ (MoMp) (CD11b+, CD64+, Gr+), monocyte macrophages Gr+ (MoMp) (CD11b+, Gr−), monocyte-derived macrophages (MoAM) (CD11b+/−, CD11c+, Siglec FLow, CD64+), eosinophils (EOS) (CD11b+, CD11c-, Siglec F+) and dendritic cells (DC) (CD11b+, Gr-1-, MHC-IIHigh). Lymphyoid: non-class T cells (CD3+), T helper cells (CD3+, CD4+), cytotoxic T cells (CD3+, CD8+), γδ T cells (CD3+, CD4+, γδTCR+), B cells (CD19+), natural killer T cells (NKT) (CD3+, NK1.1+) and natural killer (NK) (CD3-, NK1.1+) (1). The stained cells were counted with an LSRII flow cytometer (BD, Biosciences, Vienna, Austria) and cytoFLEX-SII (Beckman Coulter, Vienna, Austria) and analyzed with FACSDiva software (BD, Biosciences, Vienna, Austria) and Flowjo v10 (LLC, Ashland, Oregon, USA) (125). A

description of our scientific work includes the distribution of myeloid and lymphoid cells from the wild-type animals used in the previous investigation (126).

3.8 Myeloperoxidase activity measurements

The Myeloperoxidase activity measurements were carried out according to the protocol described previously (1,127). The snap-frozen lung tissue of mice was weighed and homogenized in phosphate buffer (pH 6.0) with 0.5% hexadecyl trimethyl ammonium bromide (Sigma Aldrich, Saint Louis, MO, USA) using ceramic beads and MagNA Lyser Rotor (Roche, Vienna, Austria). 10 µl of supernatant was added into the 96 well plates in triplicates. 200 µl of O-dianisidine buffer—50 mM potassium phosphate buffer (pH 6.0) containing 0.167 mg/ml of O dianisidine hydrochloride (Sigma Aldrich, Saint Louis, MO, USA) and 0.5 µl of 1% H_2O_2/ml— were added in each sample and measured at 460 nm using a micro-plate reader (BMG, Vienna, Austria).

3.9 Neutrophils isolation from mice

The Ly6G positive selection (Miltenyi Biotec, Bergisch Gladbach, Germany) was performed to obtain neutrophils from the bone marrow of WT and RGS5-/- mice (1). After euthanizing the mice, hind limb bones were dissected, and bone marrow was collected by flushing each bone with 1 ml of RPMI media. Collected bone marrow was spinned down (1100 rpm at room temperature (RT) for 7 mins). The obtained cell pellet was further incubated with 5 ml erythrolysis buffer for 5 mins on a rotor. The pellet was washed with 15 ml of RPMI media, spun down and the supernatant was discarded to stop the erythrolysis reaction and to obtain an erythrocyte-free cell pellet. The next steps for neutrophils isolation were performed according to the manufacturer's instructions using the anti-Ly6G positive selection kit and MACs buffer. In brief, Ly6G beads were mixed and incubated with the cell pellet at 4°C for 10 mins and further washed and spun down (300 g at RT for 7 mins). The pellet was resuspended and passed through the LS column attached to the magnet stand. The purified neutrophils were collected and counted on Neubauer chamber using trypan blue dye.

3.10 Neutrophil trans-well migration assay

Corning Trans-well plates (5µm pore size) were used for the neutrophil chemotaxis experiment. The trans-wells were pre-incubated for 30 minutes at 37°C with 1 % BSA in PBS. After 30 minutes, the trans-wells were rinsed with assay buffer. Following the positive selection of neutrophils with anti-Ly6G beads, neutrophils (20.000 cells in 100 µl) were added in the upper compartment of the trans-wells. Then they were allowed to migrate toward different chemoattractants placed in the lower compartment of the trans-well for 60 minutes at 37°C. Three different chemoattractants were used for the assay fMLP (F3506, Sigma Aldrich, Saint Louis, MO, USA), CXCL1 (250-11, Pepprotech, Cranbury, NJ, USA), and CXCL2 (250-15, Pepprotech, Cranbury, NJ, USA). From the lower compartment, neutrophils were taken out and suspended in 150 µl of fixative solution. After fixation of the neutrophils, cell counting was performed using flow cytometry (1).

3.11 Intracellular calcium flux assay

Purification of neutrophils was performed as described previously. Neutrophils were kept for 1 hour in dark at RT after resuspending in mix of 2 µM fluo-3-acetoxymethyl ester (Ca^{2+}-sensitive dye) (Thermo Fischer, Waltham, MA, USA) and 0.02 percent Pluronic F-127 (Thermo Fischer, Waltham, MA, USA. Prior to the addition of any agonist, the baseline was measured for 60 seconds. Chemoattractants fMLP, CXCL1, and CXCL2 were used as the agonist to elicit the Ca^{2+} response in neutrophils. A FACSCalibur flow cytometer was used to measure intracellular Ca^{2+} levels in fluo-3 positive cells in the FL1- channel (BD, Franklin Lakes, NJ, USA). Each agonist's Ca^{2+} response was adjusted to its baseline (1).

3.12 CXCL1 and CXCL2 ELISA

CXCl1 and CXCl2 were measured following the manufacturer's ELISA kit (DY453-05 and DY452-05; R&D Systems, USA). In Brief, the ELISA plates were coated with 100 µl capture antibody diluted in PBS overnight at RT. The wells were washed three times with wash buffer before each step otherwise mentioned. The next day, the plates were blocked with 300 µl of reagent diluent for 1 hour at RT. Next, 100 µl of samples were added into the wells for a total of 2 hours at RT. For CXCl1 samples were diluted to 1:2 and for CXCl2 Undiluted samples were used. Detection antibodies were added and incubated for another 2 hours at RT. For the next 20 min, the streptavidin was applied to the wells. A 1:1 mix of color reagent A and B substrate was used for the final reaction. In the end, 50 µl of stop solution was added and measurements were performed using a micro-plate reader at a wavelength of

450nm and 570nm. All the unknown chemokine concentrations (ng/ml) were calculated using an equation derived from standard curves. The standards and samples were corrected for blank and OD values obtained at 570 nm.

3.13 RhoA and Cdc42 G-LISA

The RhoA and Cdc42 G-LISA activation assays were performed according to the manufacturer's instructions (BK124 and BK127; cytoskeleton Inc., Denver, CO, USA). Neutrophils were treated for 5 minutes with fMLP (1 µm), CXCL1 (100 ng/ml), and CXCL2 (100 ng/ml) before being collected in lysis buffer given by the kits. As previously explained, neutrophils were extracted from the WT and RGS5-/- mice bone marrow (1). To obtain enough protein for the RhoA and Cdc42 measurements, 3 million neutrophils were used per condition. Neutrophils for each experiment were pooled from 6-7 mice for each genotype. End point measurements were performed using a micro-plate reader at absorbance wavelength 450 nm.

3.14 Neutrophil analysis from WT and RGS5-/- mice

Neutrophils were extracted from WT and RGS5-/- mice blood, spleen, and bone marrow. The neutrophil labelled with Ly6G and cd11b antibodies were used to further cell count and receptor level analysis. Information about antibodies are listed in **Table 4**. For comparison and analysis, we included all single staining controls. Bone marrow isolation was performed as described the in neutrophil isolation section (1). Blood: 50 µl of whole blood was taken for each condition, followed by 20 mins incubation in 20 µl of antibody master mix at RT. After adding 2 ml freshly prepared FACS lysis solution for 10 mins, samples were centrifuged (300 g at RT for 7 mins). The cell pellet was washed twice with 2 ml of MACS buffer and centrifuged again. Spleen: The spleen single-cell suspension was prepared by cutting the tissue into small pieces and passing through a 100 µm cell strainer. The sample was collected and centrifuged (1100 rpm at 4°C for 7 mins). The cell pellet was haemolysed as described previously in the neutrophil isolation section to further obtain an erythrocyte-free cell pellet. The cells were counted on a Neubauer chamber using trypan blue dye. Unstained and stained cell samples were mixed with 200 µl of MACS buffer and stored at 4°C until measurements. For the receptor level analysis, purified bone marrow-derived neutrophils were either vehicle or CXCL1 (100 ng/ml) and CXCL12 (100 ng/ml; 250-20B, Pepprotech, Cranbury, NJ, USA) were treated for 5 and 15 mins. The immediately fixative solution was

added and transferred to ice. After centrifugation (8000 rpm at 4°C for 2 mins) cells were stained with Ly6G, Cd11b, CXCR2, and CXCR4 antibodies.

3.15 Hematoxylin and Eosin (H&E) staining

The lung tissues were deparaffined overnight at 60°C. The next day, tissues were rehydrated 2 times 10 mins incubation in xylol following 100%, 90%, 80%, 70%, 50% ethanol, and finally H_2O washings. Lung sections were dipped for 2 minutes in Mayer's hematoxylin solution (Gatt-Koller). Afterwards, running lukewarm water was for washing 3-5 minutes. The counterstaining was performed with eosin final staining solution (Gatt-Koller) for 1 minute and immediately rinsed for 5 minutes in distilled water. Dehydration steps were performed using 96%, 100% ethanol, and xylol. At last, slides were mounted using a mounting vector xylol-based medium.

3.16 Lung collagen analysis

Picrosirius red staining was used to lung tissue sections to analysis the collagen deposition in the mice lungs. For 4 minutes, 0.2 % Phosphomolybdic acid (freshly made) was applied to the tissues. The slides were incubated in Sirius red solution for 30-35 mins. The slides were washed with 0.5% acetic acid to remove excess staining for 2-3 mins. Dehydration steps were performed using 96%, 100% ethanol, and xylol. At last, slides were mounted using a mounting vector xylol-based medium.

3.17 Immunohistochemical stainings

Primary antibodies (RGS5 and Ly6G) were used to stain lung tissue slices from humans and mice as described previously(1). Information about primary and secondary antibodies are listed in **Table 4.** Each lung tissue section (2.5 µm) was deparaffined overnight at 60 °C and rehydrated the next day (2 times 10mins xylol following 100%, 90%, 80%, 70%, 50% ethanol and finally aqua dest). Tissue slides were incubated with Proteinase K (Peqlab, Erlangen, Germany) solution for 10 mins at RT. Then, antigen retrieval solution of PH=9 (DAKO, Glostrup, Denmark) for anti-RGS5 and PH=6 (DAKO, Santa Clara, CA, USA) for anti- Ly6G was used and slides were incubated for 30 min at 95 °C and later cooled down to RT before continuing with antibody staining. For neutrophil anti-RGS5 staining, cytospin slides were fixed with formalin for 15 mins at RT and subsequently, incubated for 10 mins with 0.2% triton x-100 (Sigma, Saint Louis, MO, USA) at RT. To prevent unspecific binding, samples

were incubated in MOM's kit (Vector Laboratories, Burlingame, CA, USA) blocking solution (only for RGS5 stainings on mouse samples) or 10%BSA in PBS for 1 hour at RT. Primary antibodies were incubated overnight at 4 °C; the following day washing steps were performed and secondary antibody labeled with peroxidase enzyme for 1 hour at RT. Stainings were developed using NOVA red and fast red (Vector Laboratories, Burlingame, CA and Abcam, Cambridge, UK). Nuclei staining was performed with haemalaun solution for 45 sec following dehydration steps (96%, 100% ethanol, and xylol) and slide mounting using mount media (Thermofischer, MI, USA). Negative controls were involved in every protocol. The primary antibodies were omitted while processing the negative controls.

3.18 Isolation of RNA and RT-qPCR

The peqGOLD Total RNA Kit was used to isolate total RNA from lung tissues according to the manufacturer's instructions (Peqlab, Erlangen, Germany) and as described previously (1). The specifics of primers are summarized in **Table 5**. The concentration and purity of isolated total RNA were measured at 260 nm and absorbance ratio at 280/260 nm respectively using the Nanodrop 2000c spectrophotometer (ThermoScientific, Wilmington, Delaware,USA). Total RNA was reverse transcribed to cDNA using iScript cDNA Synthesis kit (Bio-Rad, Hercules, CA, USA). Real-time RT-PCR reaction measured the expression of Genes using QuantiFast SYBR Green PCR kit (Qiagen, Hilden, Germany) on a Light cycler 480 System (Roche Applied Science, Vienna, Austria). RT-PCR reaction mixtures contained transcribed cDNA, SYBR Green master mix, forward and reverse primers. Each sample was measured in duplicates. Melting curves were analyzed after amplification to confirm the quality of the reaction. As ΔCT (targeted gene expression) adjusted to the level of the housekeeping gene beta-2 microglobulin (B2M), following formula was used ΔCT = CT (Housekeeping Gene) – CT (Gene of Interest). For ΔΔCT the following formula = ΔCT (test samples) – ΔCT (averaged controls).

3.19 Measurement of protein level and western blotting

Lung tissues and neutrophils were lysed in CHAPS (Tocris, UK) or RIPA (Sigma, USA) buffers containing EDTA and a protease inhibitor cocktail for protein extraction as described previously (1). The details of antibodies are in **Table 4**. Lung tissues were homogenized using ceramic beads with MagNA Lyser Rotor following supernatant collection and centrifugation (10,000 rpm at 4°C for 10 mins). Protein samples were separated by SDS-PAGE using 10-15% SDS gels (depending on protein-size of interest) and transferred to

0.45 µm nitrocellulose membrane (GE Healthcare, Buckinghamshire, UK). Blocking was performed with 5% milk or 10% BSA for 1 hour at RT, followed by primary antibodies overnight incubation at 4°C. Table 4 lists the antibodies utilized in this study along with their dilutions. The membranes were treated secondary antibodies (peroxidase-conjugated) for 1 hour at RT the next day. To detect the signal on membranes using a ChemiDoc Touch Imaging System (Bio-Rad, Hercules, CA, USA), ECL prime developing solution (GE Healthcare, Buckinghamshire, UK) was used. The pERK values were normalized to the tERK band and band intensity were calculated at control, 2, 5, 10, and 30 minutes. The area under the curve (AUC) was computed for quantifying pERK throughout the same time period (relative band intensities vs time). Total pERK can be quantified throughout the detection time using this representation of the data. Below is a diagram of the scheme.

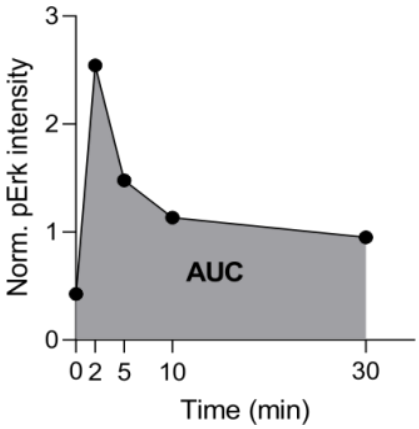

Figure 1: A representative scheme for quantifying total pERK during the course of the detection time.

3.20 Statistical analysis

GraphPad Prism 8 was used for the statistical analysis (GraphPad Software, CA). For the comparison of various groups, one-way analysis of variance (ANOVA) was used, along with Bonferroni's posthoc test to compare selected pairs of columns and unpaired two-tailed t-test. A p-value of less than 0.05 was considered significant. Box-and-whisker plots with interquartile range (min-max) and bar graphs with mean ± SEM are used to display the data. R (version 3.6) was used to make dendrograms and heatmaps (1,128). The dendrograms were clustered using the Lance-Williams dissimilarity update with complete linkage (R functions dist and hclust). The dendrograms were sorted (R function dendsort) at each merging point based on the average distance between subtrees, then shown on the heat maps (R function pheatmap).

4 Results

4.1 RGS5, the member of the R4 subfamily in the lung

4.1.1 Expression of R4 subfamily RGS in human lungs

Since our knowledge about the R4 subfamily in the lung is limited, first I examined the expression profile of the RGS R4 subfamily in human donor lungs. I used lung tissue from patients with interstitial lung diseases (ILD) as a comparison. **Table 1** lists the patient and donor population clinical parameters as well as how the samples were used in different experiments. RGS1, RGS3, RGS4, and RGS5 levels in ILD lung samples were substantially higher than in donor samples **(Figure 2A)**. RGS2, RGS8, RGS13, RGS16, and RGS18 expression remained unchanged between ILD and donor lungs. Based on these findings, I decided to determine the role of RGS5 in the progression of chronic fibrosing lung using lung injury animal models. Measurement of RGS5 expression and proteins levels in ILD and donor lung tissue homogenates showed increased RGS5 protein levels in ILD **(Figure 2B and C).**

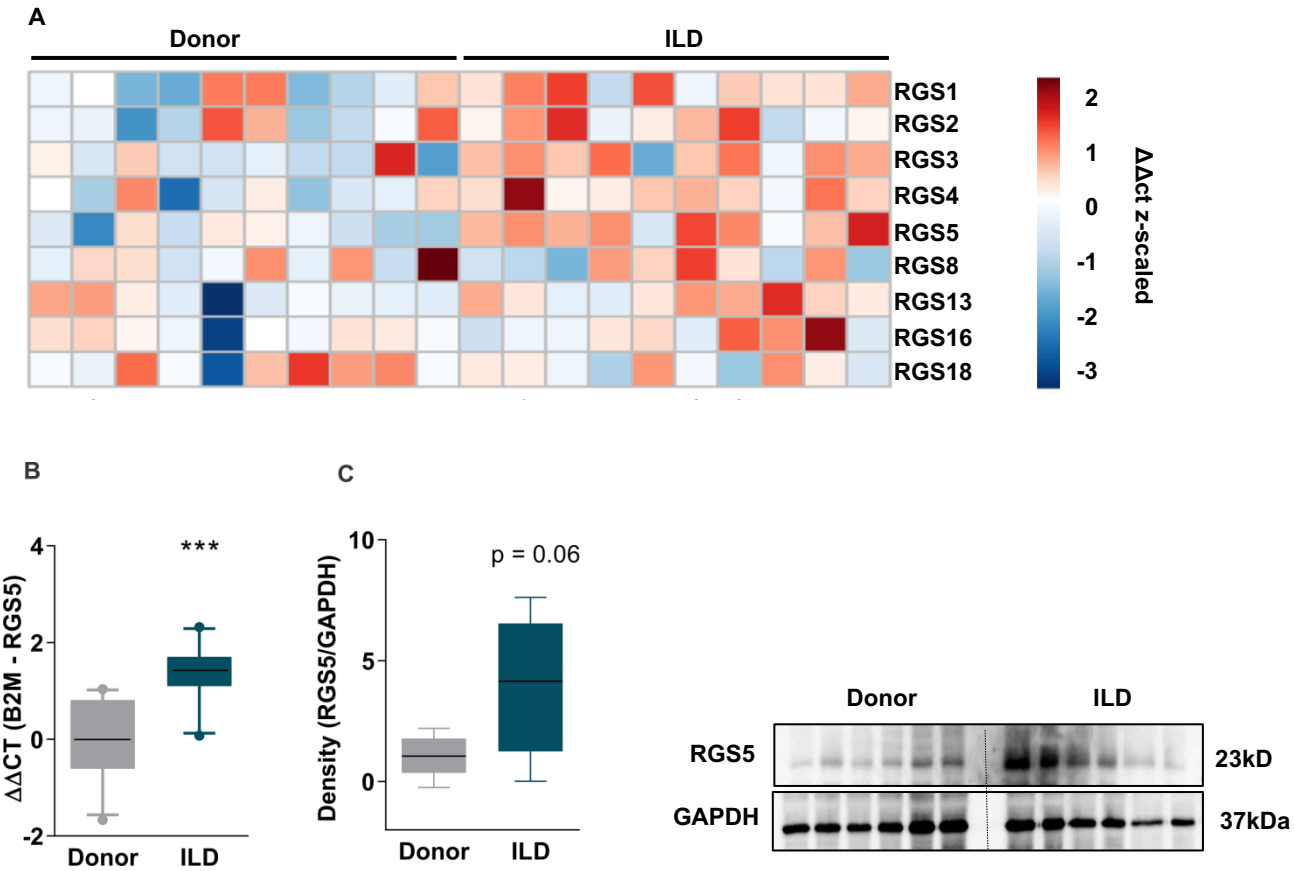

Figure 2: RGS5 expression in patients samples underwent lung transplantation. A) Gene expression (RT-qPCR) of the RGS subfamily members (RGS1, 2, 3, 4, 5, 8, 13, 16, 18) in donors (n=10) and ILD patient's lung tissue (n=10). **B)** RGS5 mRNA expression in the lungs of donors and ILD patients (n=10 each group). ΔΔCT values is obtained using formula ΔCT (target gene) – ΔCT (averaged controls). **C)** RGS5 protein levels compared *via* immune-blotting in donors and ILD patient's lung tissue (n=6 each group). As loading control, GAPDH was used. Box-and-whisker plots are used as graphical presentation and unpaired two-tailed t-test (** $p < 0.01$; *** $p < 0.001$) is used for analysis. (Reproduced from previously published study in MDPI (1) under CC BY 4.0 license).

4.1.2 Localization of RGS5 in human lungs

To determine RGS5 localization in lung tissue, next RGS5 immuno-histochemical (IHC) staining was performed on the lungs tissue sections obtained from the donor, ILD, and lung tissue collected from acute respiratory distress (ARDS) patients. We could show that RGS5 is present in airway smooth muscle cells; epithelium and pulmonary artery smooth muscle cells as well as inflammatory cells were also stained with RGS5 **(Figure 3A and B)**.

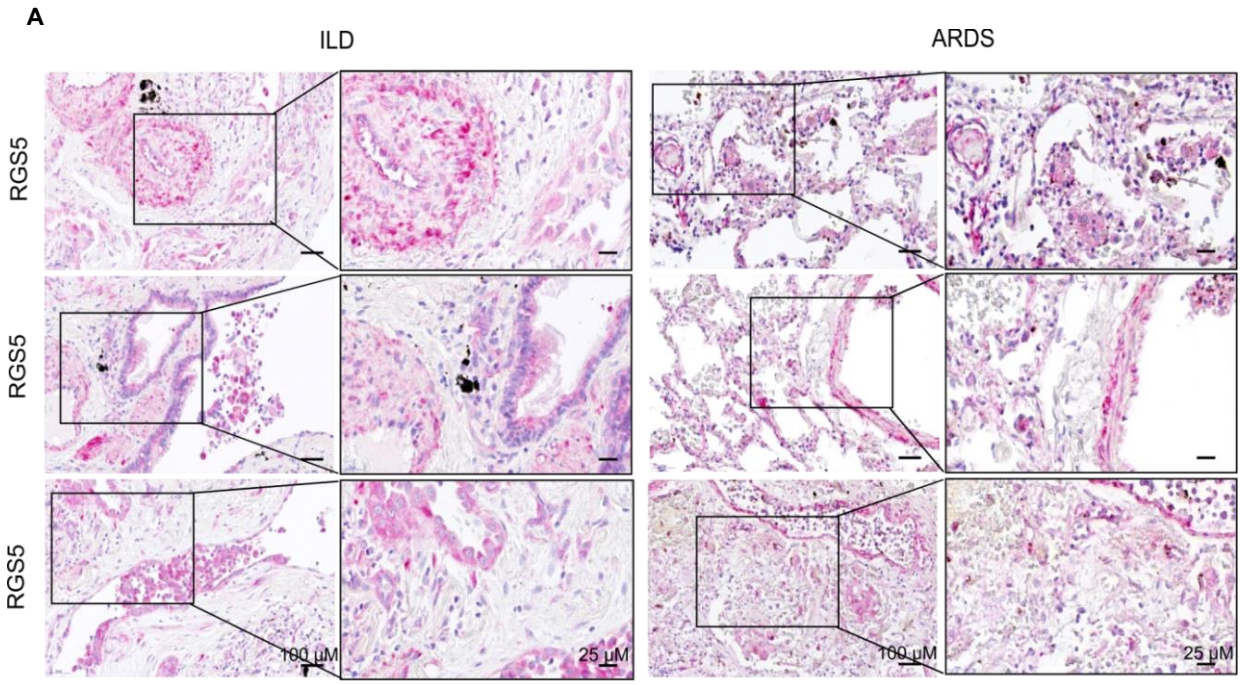

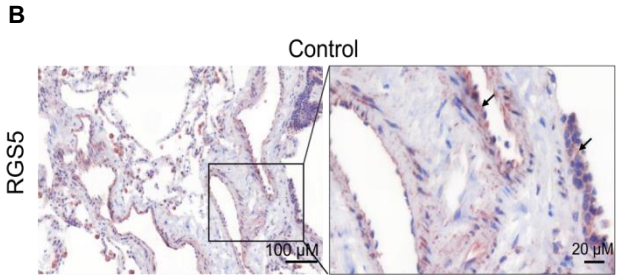

Figure 3: RGS5 localization in human lungs from IPF and donor. Lung tissue sections (n=3) **A)** RGS5 expression (dark pink) in ILD and ARDS lung sections shown by IHC staining. **B)** Donor lung tissues showing RGS5 expression (brown). Scale bar 100 µm, 25 µm, 20 µm. The staining was carried out with the help of Sabine Halsegger. (Reproduced from previously published study in MDPI (1) under CC BY 4.0 license).

4.1.3 RGS5 expression in lungs of pulmonary fibrosis mouse model

Based on expressional data from ILD, ARDS, and donor patients, next, I investigated longitudinal RGS5 mRNA and protein expression in a well-established bleomycin animal model for both acute inflammatory lung damage and lung fibrosis progression. Bleomycin sulfate or saline (control) were given intratracheally (i.t.) to mice and their lungs were collected at timepoint 3, 14, and 21 days to measure inflammation and fibrosis **(Figure 4A)**. In compared to saline-challenged lungs, I discovered that RGS5 mRNA levels and protein expression were considerably higher in lung homogenate of bleomycin-challenged lungs at 3, 14, and 21 days **(Figure 4B and C)**.

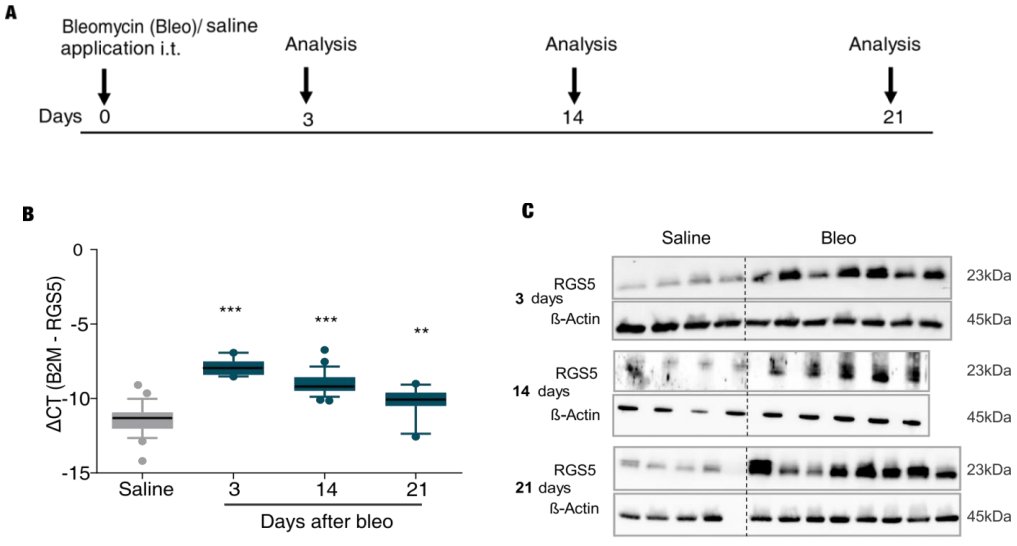

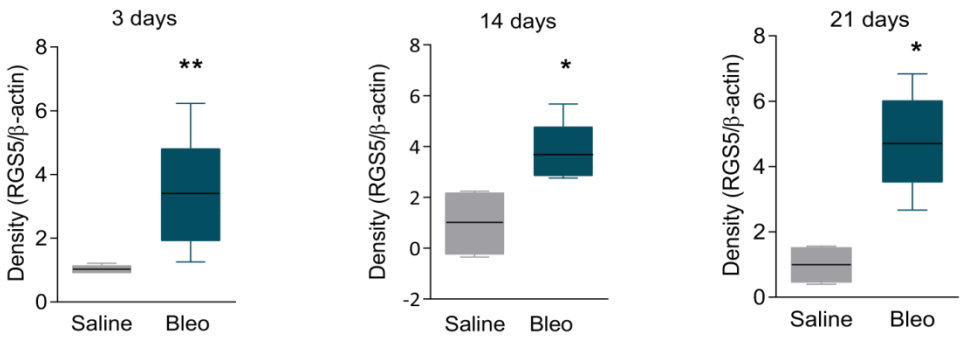

Figure 4: RGS5 expression in bleomycin treated mice lungs upon disease progression. A) Graphical diagram of saline and bleomycin treatment to mice at different timepoints. **B)** RGS5 gene expression (mRNA) in the lung upon bleomycin injury (minimum n = 10). ΔCT values are obtained using formula ΔCT = CT (reference gene) – CT (target gene). Box-and-whisker plots are used as graphical presentation and one-way ANOVA with Bonferroni's multiple comparison test (** $p < 0.01$, *** $p < 0.001$). **C)** RGS5 protein levels in lung homogenates are shown with their respective quantifications (n = 4 to 8). As loading control, β-actin was used. Box-and-whisker plots are used as graphical presentation and unpaired two-tailed t-test (* $p < 0.05$; ** $p < 0.01$) is used for analysis. (Reproduced from previously published study in MDPI (1) under CC BY 4.0 license).

4.1.4 Localization of RGS5 in lungs of pulmonary fibrosis mouse model

To assess the localization of RGS5 in lung tissues sections obtained from saline and bleomycin treated mice for different time-points, RGS5 IHC staining was performed.

In bleomycin-treated animals, RGS5 appeared stronger in the airway epithelium, smooth muscle cells, pulmonary vasculature, and inflammatory cells than in saline-treated mice. **(Figure 5)**.

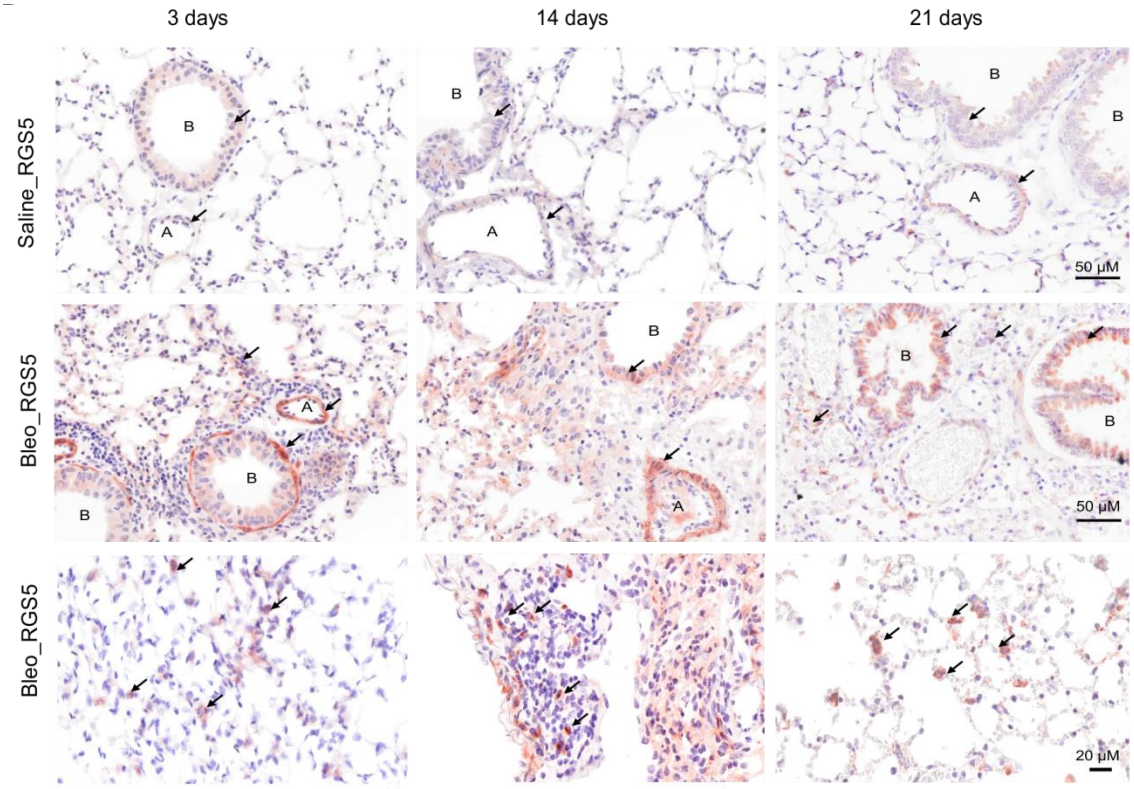

Figure 5: RGS5 expression RGS5 expression in lung tissue of mice given saline and bleomycin. Representative images (n = 3) of saline (upper panel) and bleomycin (middle and lower panel) treated mice lungs tissue section showing RGS5 expression (brown) in structural and inflammatory cells at different indicated time-points; arrows pointing RGS5 stained cells; A = pulmonary arteries, B = bronchioles. Scale bar: 20 or 50 µm. The staining was carried out with the help of Sabine Halsegger. (Reproduced from previously published study in MDPI (1) under CC BY 4.0 license).

4.2 Characterization of RGS5-/- mice

To elucidate the functional consequences of RGS5 loss, we decided to utilize RGS5-/- mice in our study. A comprehensive investigation including measuring of basal lung function parameters, hemodynamics, and R4 RGS family gene profiling in RGS5-/- mice was carried out. When compared to WT mice, RGS5 deletion had no effect on baseline lung function and it was similar for hemodynamic parameters. **(Figure 6A and B)**.

Furthermore, I found no compensatory up-regulation of other R4 family members in the lung of the mouse upon RGS5 loss. RGS3, RGS4, and RGS18 expression were down-regulated **(Figure 7)** which might be possible due to proximity of the gene location, interference of knockout strategy with intronic sequence, and tissue-dependent specific (90)(87)

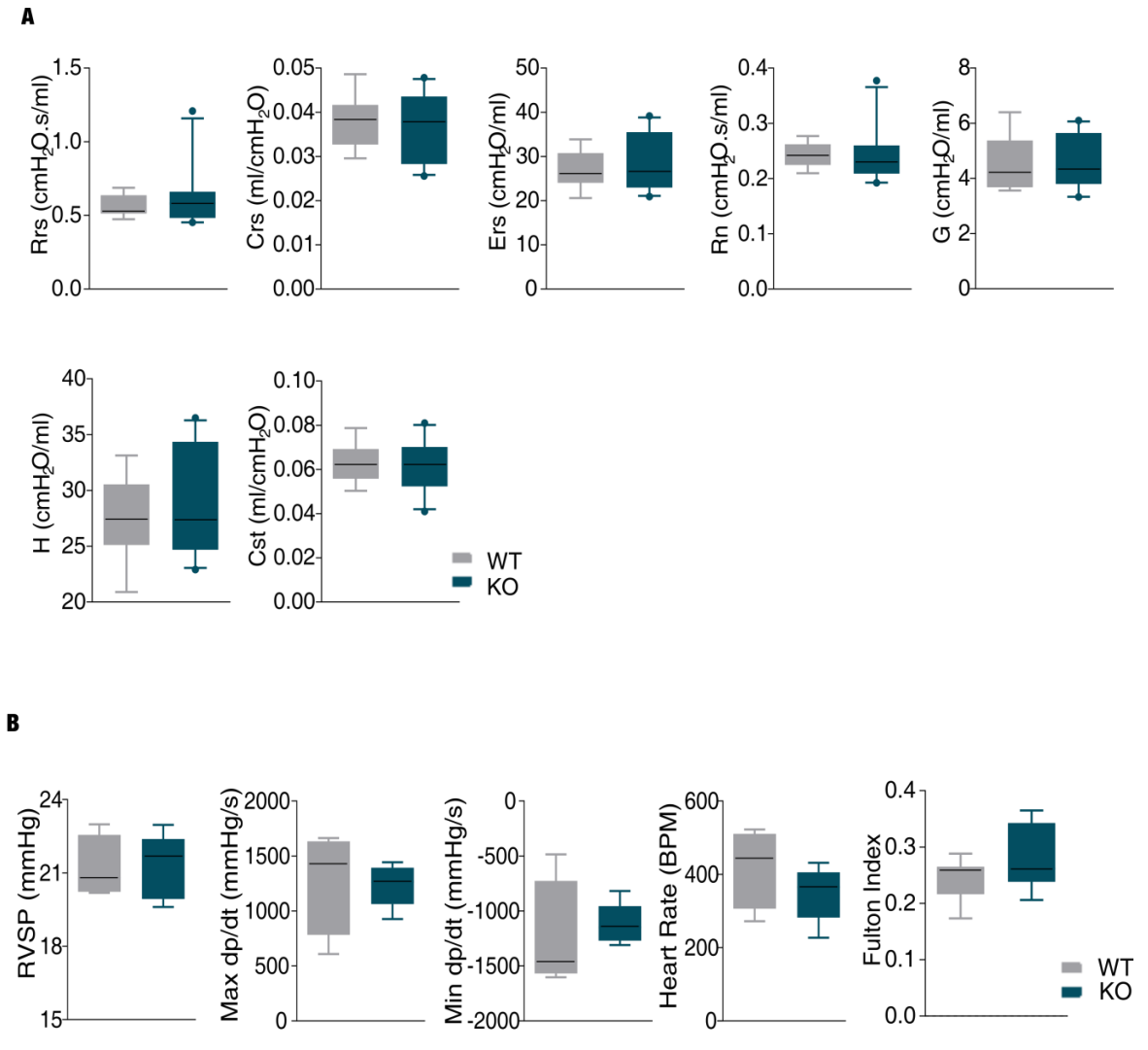

Figure 6: *in vivo* lung function and Hemodynamic characteristics of WT and RGS5-/- mice at baseline. **A)** Lung function measurements of WT and RGS5-/- mice; Rrs: resistance; Crs: compliance; Ers: Elastance; Rn: central airway resistance; G: tissue damping; H: tissue elastance; Cst: quasi-static compliance of the respiratory system. **B)** Hemodynamic measurements showing right ventricular systolic pressure (RVSP), max dp/dt, min dp/dt, heart rate (beats per minute), and Fulton index (RV/(LV+S) measurements in WT and RGS5-/- mice. Box-and-whisker plots are used as graphical presentation (n = 4-10) and

unpaired two-tailed t-test. The Hemodynamic measurements were carried out with the help of Bence M. Nagy and Chandran Nagaraj. (Reproduced from previously published study in MDPI (1) under CC BY 4.0 license).

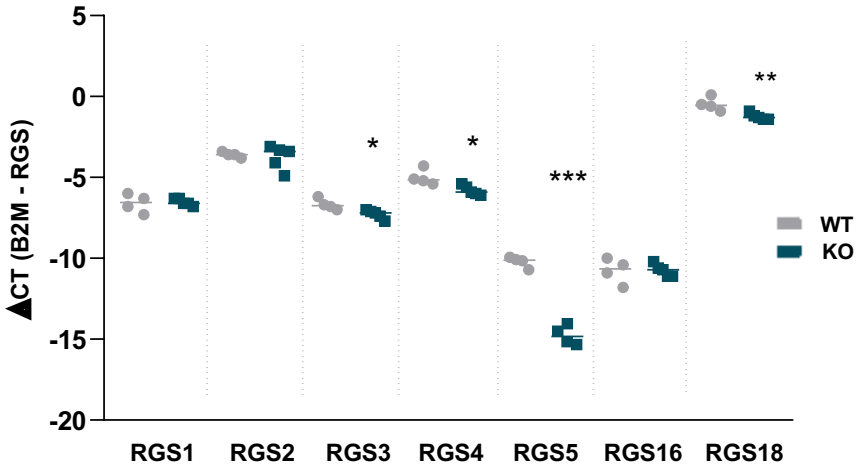

Figure 7: R4 RGS family gene expression in WT and RGS5-/- mice lung at baseline. Gene expression (RT-qPCR) of the RGS subfamily members (RGS1, 2, 3, 4, 5, 16, 18) in lungs from WT and RGS5-/- mice. ΔCT values, calculated by ΔCT = CT (reference gene) – CT (target gene). unpaired two-tailed t-test *p < 0.05, ** p < 0.01, *** p < 0.001.

4.3 RGS5 in acute pulmonary inflammation

4.3.1 Loss of RGS5 protects the lung from neutrophilic inflammation and lung damage

In two distinct animal models of acute pulmonary inflammation, the role of RGS5 was studied using RGS5-/- and WT mice at 12–16 weeks of age. In the first series of our investigation, mice were treated with saline and bleomycin (i.t.) and analyzed on day 3 **(Figure 8A)**. To assess the inflammation, hematoxylin, and eosin (H&E) staining were performed on the lung tissue sections. RGS5-/- animals had a higher immune cell count, recruited to bronchioles and pulmonary arteries in their lungs compared to WT mice **(Figure 8B)**. Heatmap represents specific inflammatory cell subpopulations in BALF, where a

significant attenuation of the total cell number in the BALF of RGS5-/- mice, predominantly made up of neutrophils **(Figure 8C and D)**.

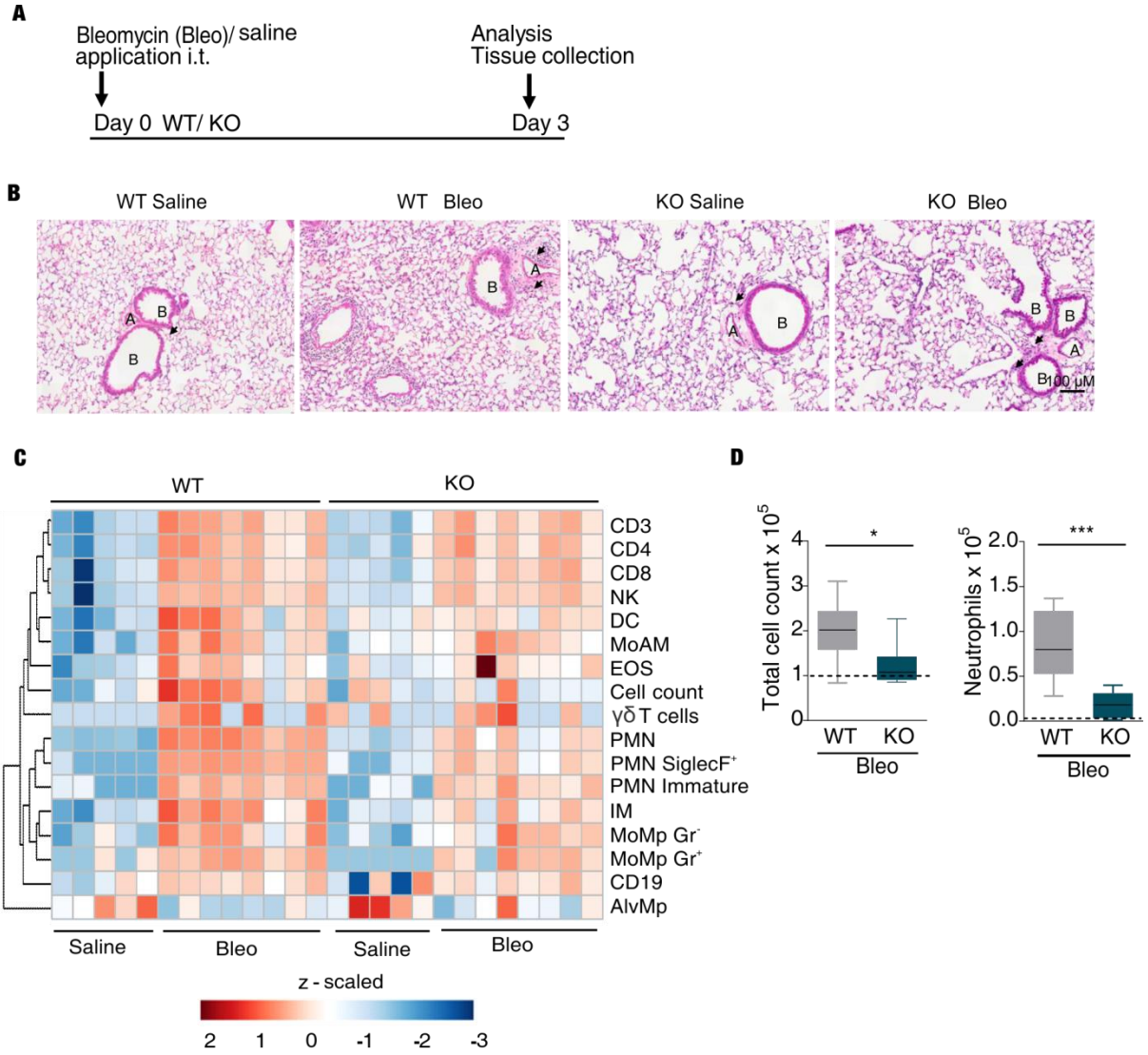

Figure 8: RGS5 deletion protects the lungs from lung damage induced *via* bleomycin. **A)** Graphical diagram of saline and bleomycin treatment to mice. *in vitro* and *in vivo* analyses carried out at the indicated time point. **B)** Hemotoxylin and Eosin (H&E) staining performed for the histological appearance of the lung tissue; arrows pointing inflammatory cells; A = pulmonary arteries, B = bronchioles; Scale bar 100 µM. **C)** Heatmap of flow cytometry BALF immune cell counts after Bleomycin-challenge at 3 days (log10(x+1) transformed, z-scaled

per cell type) are shown with average distance sorted dendrograms from hierarchical clustering analysis. **D)** Flow cytometry analysis of BALF total cells and total neutrophil count. WT and RGS5-/- saline-treated pooled together and presented as dotted lines as no differences were observed (n = 3-10). Box-and-whisker plots are used as graphical presentation and unpaired two-tailed t-test (* $p < 0.05$; *** $p < 0.001$) is used for analysis. (Reproduced from previously published study in MDPI (1) under CC BY 4.0 license).

I validated lower neutrophil counts in bleomycin-treated RGS5-/- animals compared to WT mice using anti-Ly6G IHC on lung tissue sections **(Figure 9A)**. Myeloperoxidase (MPO) enzymatic activity, a marker for neutrophilic inflammation, in lung tissue was significantly lowered in RGS5-/- compared to WT mice **(Figure 9B)**. When mice were given bleomycin, the BALF protein level, which represents alveolar leakage in the lungs, increased dramatically on day 3, and this reaction was likewise attenuated in RGS5-/- mice **(Figure 9C)**. Importantly, lung function testing showed that the airway resistance (Rrs) is increased and the reduction of lung compliance were prevented in RGS5-/-. RGS5-/- mice showed normal inspiration capacity (A) even upon lung injury **(Figure 9D)**.

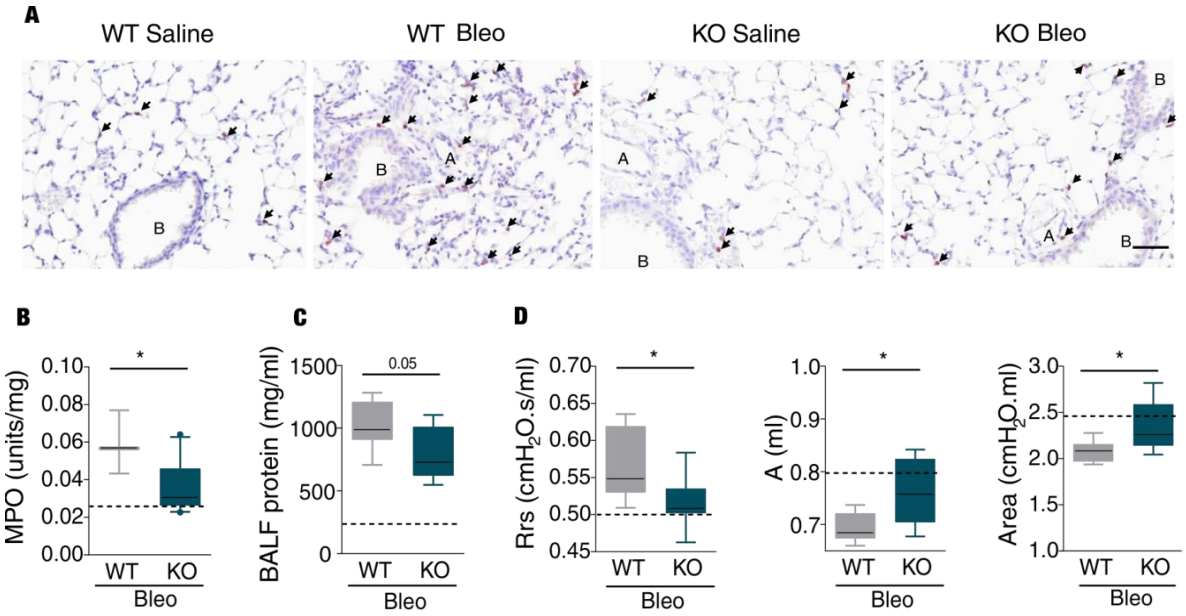

Figure 9: Loss of RGS5 protects the lungs from bleomycin-induced lung injury.

A) Anti-Ly6G IHC staining for neutrophils in lung tissue sections; arrows pointing inflammatory cells; A = pulmonary arteries, B = bronchioles; Scale bar 50 µM. **B)** MPO enzymatic activity in lung tissue per mg. **C)** BALF protein levels measured using BCA assay. **D)** Lung function measurements showing the estimation of resistance (left), inspiratory capacity (center), and the area enclosed under the P-V loop (right). WT and RGS5-/- saline-treated pooled together and presented as dotted lines as no differences were observed. Box-and-whisker plots are used as graphical presentation (n = 4-6) and unpaired two-tailed t-test (** $p < 0.01$) is used for analysis. (Reproduced from previously published study in MDPI (1) under CC BY 4.0 license).

Inflammatory cells analysis of lung tissue samples from WT and RGS5-/- was performed however we didn't see changes like BALF **(Figure 10A)**. Other lung function parameters e.g. Compliance, elastance, tissue damping, and tissue elastance remained unchanged between bleomycin treated WT and RGS5-/- mice **(Figure 10B)**.

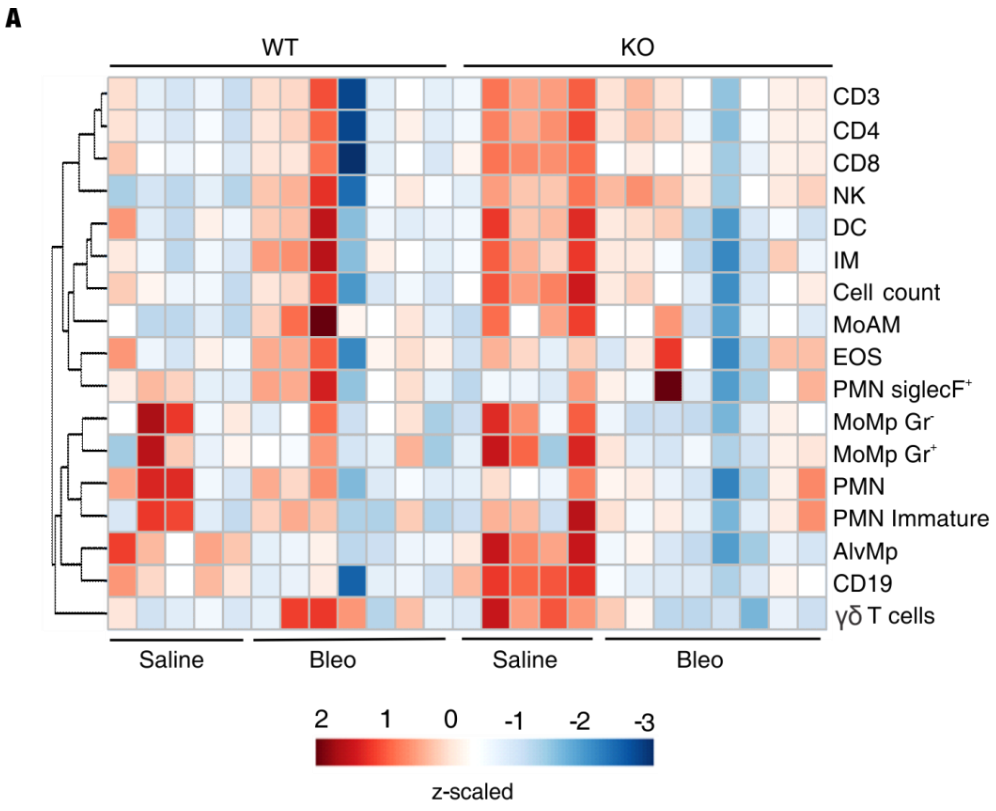

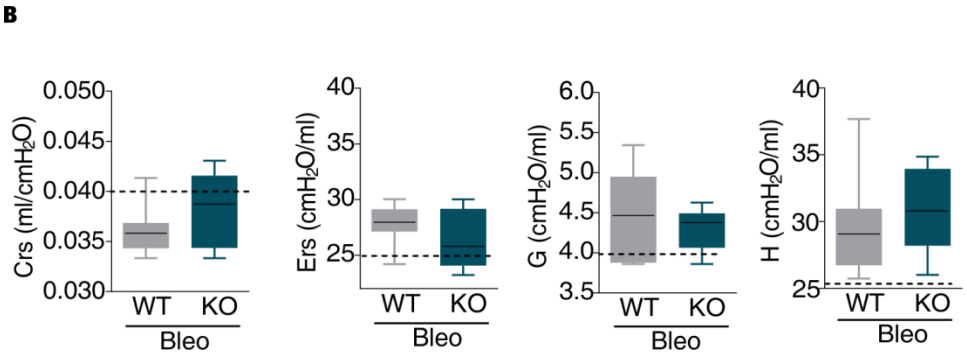

Figure 10: *in vivo* analysis of the lung after 3 days of bleomycin challenge.

A) Heatmap of flow-cytometry inflammatory cell counts in lung tissue 3 days after Bleomycin-challenge ($log_{10}(x+1)$ transformed, z-scaled per cell type) are shown with average distance sorted dendrograms from hierarchical clustering analysis. **B)** Lung function measurements of WT and RGS5-/- mice; Crs: compliance; Ers: Elastance; G: tissue damping; H: tissue elastance of the respiratory system. WT and RGS5-/- saline-treated pooled together and presented as dotted lines as no differences were observed. Box-and-whisker plots are used as graphical presentation (n = 3-10) and unpaired two-tailed t-test is used for analysis. (Reproduced from previously published study in MDPI (1) under CC BY 4.0 license).

4.3.2 RGS5 deficiency impairs neutrophil recruitment in LPS treated mice.

To further evaluate the impact of RGS5 loss in the acute inflammatory phase, in the second series of the investigations, the mice were challenged intranasal (i.n.) with saline and LPS for 24 hours. The schematic representation of the experiment is given in **(Figure 11A)**. H&E staining performed on lung tissue sections showed elevated infiltration of the inflammatory cells in the WT LPS-treated animals compared to saline control. Where RGS5-/- mice were protected from a massive influx of inflammatory cells compared to WT LPS-treated **(Figure 11B)**. Further investigation using flow cytometry of BALF and lung tissue revealed that total cell counts were significantly attenuated in RGS5-/- mice lungs which mainly contained neutrophils **(Figure 11C)**. These findings suggest that RGS5 intervenes with neutrophils recruitment in the lungs upon injury.

In the next steps, I could show less positivity for anti-Ly6G IHC staining's in RGS5-/- lung tissue sections, strongly supporting our findings of impaired neutrophil recruitment in RGS5-/- mice during the acute inflammatory phase **(Figure 12A)**. In line with this, I found significantly lower MPO activity in lungs of RGS5-/- animals treated with LPS, compared with WT animals **(Figure 12B)**, while BALF protein remained unchanged **(Figure 12C).**

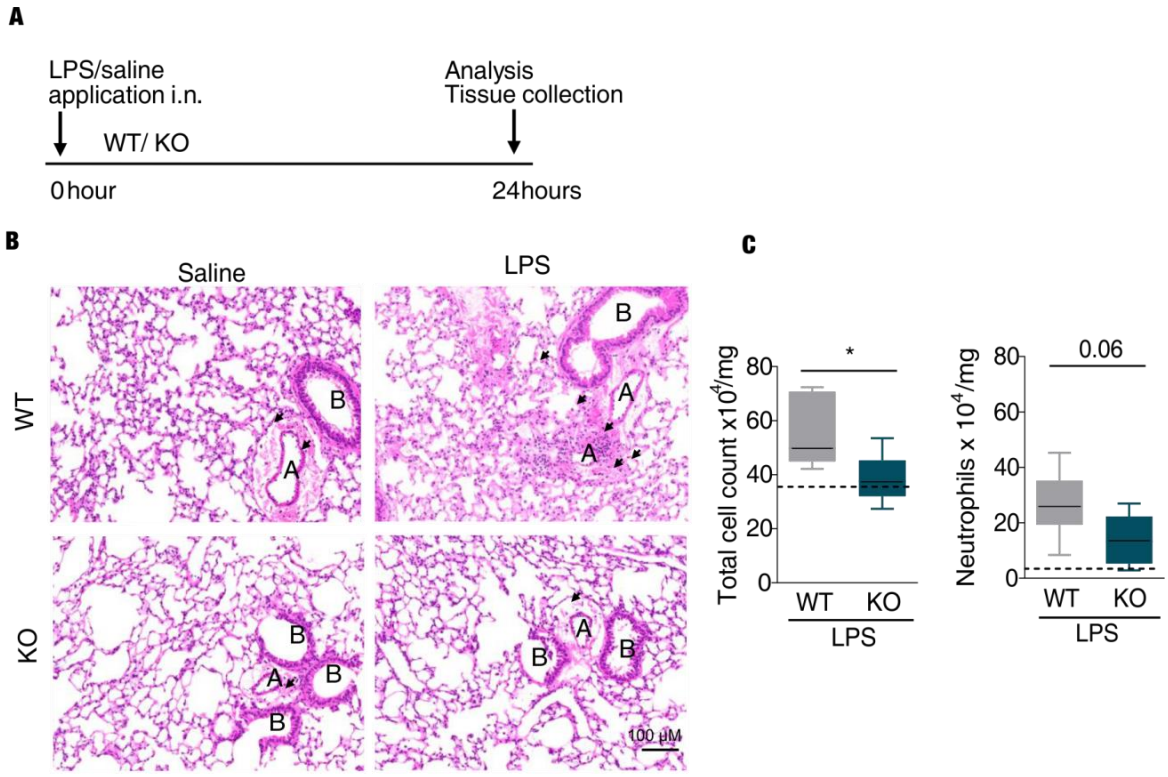

Figure 11: RGS5-/- mice protected from LPS induced lung injury. **A)** Graphical diagram of saline and LPS treatment to mice. *in vitro* and *in vivo* analyses carried out at the indicated time point. **B)** H&E staining performed for the histological appearance of the lung tissue; arrows pointing inflammatory cells; A = pulmonary arteries, B = bronchioles; Scale bar 100 µM. **C)** Flow cytometry analysis of lung tissue total cell and neutrophil count. WT and RGS5-/- saline-treated pooled together and presented as dotted lines as no differences were observed. Box-and-whisker plots are used as graphical presentation (n = 4-6) and unpaired two-tailed t-test (* $p < 0.05$) is used for analysis. (Reproduced from previously published study in MDPI (1) under CC BY 4.0 license).

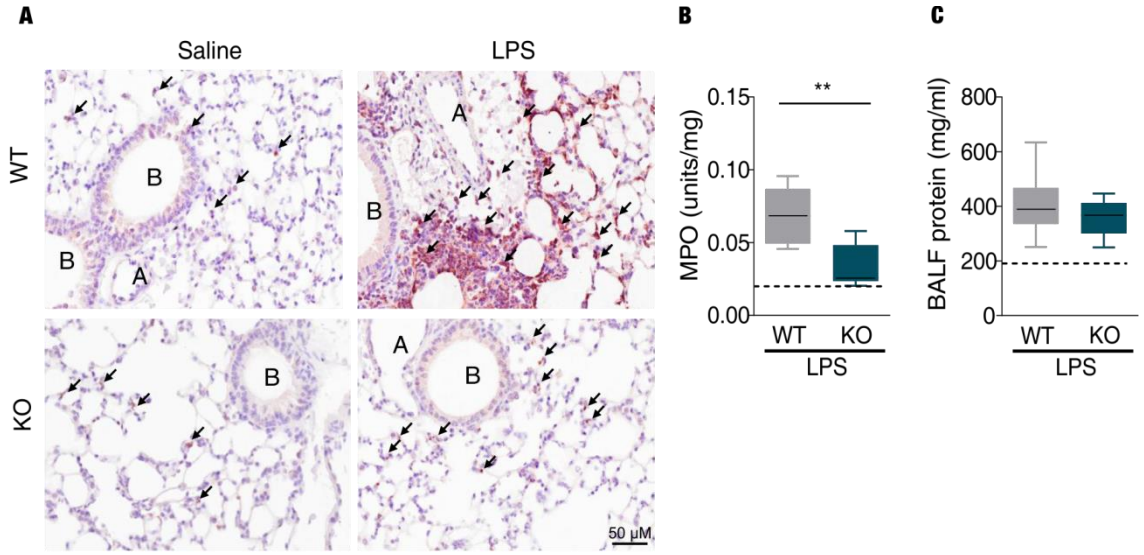

Figure 12: RGS5-/- mice protected from LPS induced lung injury. **A)** Anti-Ly6G IHC staining for neutrophils in lung tissue sections; arrows pointing inflammatory cells; A = pulmonary arteries, B = bronchioles; Scale bar 50 µM. **B)** MPO enzymatic activity in lung tissue per mg. **C)** BALF protein levels measured using BCA assay. WT and RGS5-/- saline-treated pooled together and presented as dotted lines as no differences were observed. Box-and-whisker plots are used as graphical presentation (n = 4-6) and unpaired two-tailed t-test (** $p < 0.01$) is used for analysis. (Reproduced from previously published study in MDPI (1) under CC BY 4.0 license).

4.4 The role of RGS5 in neutrophils

4.4.1 Characterization of RGS5 deficient neutrophils

According to our *in vivo* findings, RGS5 deletion reduces neutrophil recruitment in the lungs during the acute inflammatory phase. To further investigate, I studied lung chemokine levels, homeostatic neutrophil localization, and neutrophil migratory behavior isolated from WT and RGS5-/-animals in vitro. I found that CXCL1 and CXCL2 related chemokine mRNA levels were higher in bleomycin-treated mice the lung tissue, but that there were no obvious

changes between bleomycin-treated WT and RGS5-/- mice **(Figure 13A)**. After bleomycin treatment, CXCL1 protein levels in BALF decreased, whereas CXCL2 levels were considerably lower in RGS5-/- mice **(Figure 13B)**. In lung tissue, the amounts of CXCL1 and CXCL2 proteins were same **(Figure 13C)**.

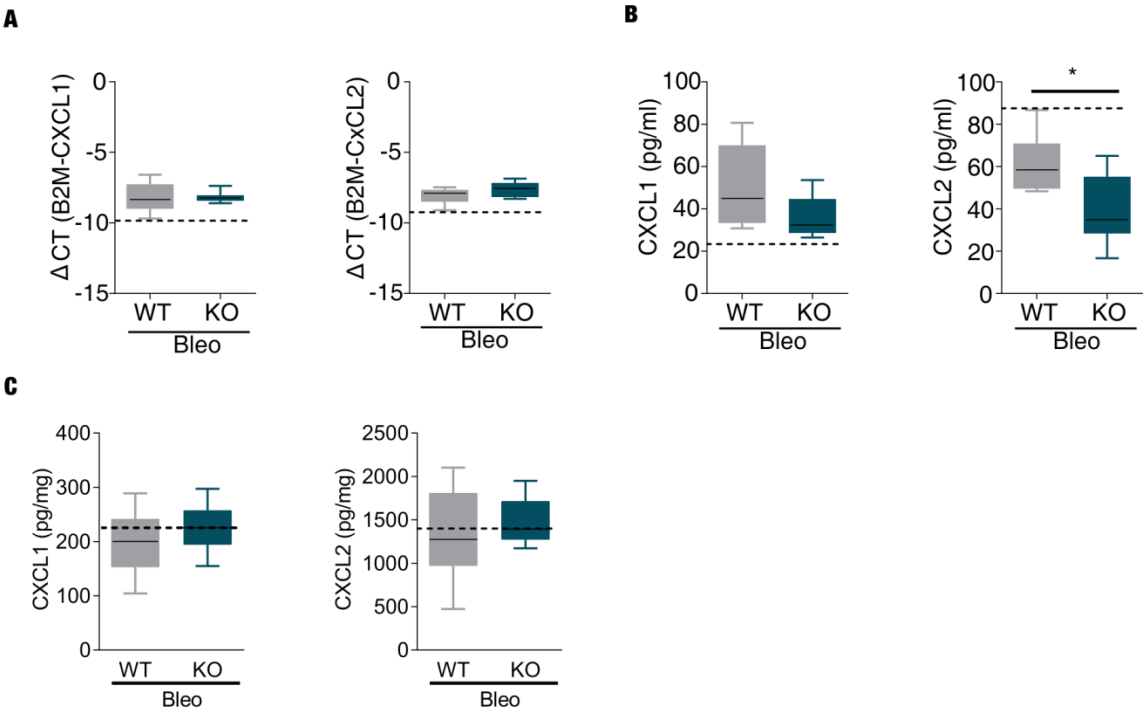

Figure 13: Chemokine measurements at bleomycin 3 day

A) CXCL1 and CXCL2 mRNA expression in lung tissue. The ΔCT values are normalized to β2M obtained *via* RT-qPCR. CXCL1 and CXCL2 protein levels in **B)** BALF **C)** Lung measured by ELISA. WT and RGS5-/- saline-treated pooled together and presented as dotted lines as no differences were observed. Box-and-whisker plots are used as graphical presentation ($n \geq 7$ mice) and unpaired two-tailed t-test ($^*p < 0.05$) is used for analysis. (Reproduced from previously published study in MDPI (1) under CC BY 4.0 license).

Similarly, CXCL1 and CXCL2 measurements in lung and BALF from LPS-treated WT and RGS-/- mice showed no differences between the groups **(Figure 14A – C)**.

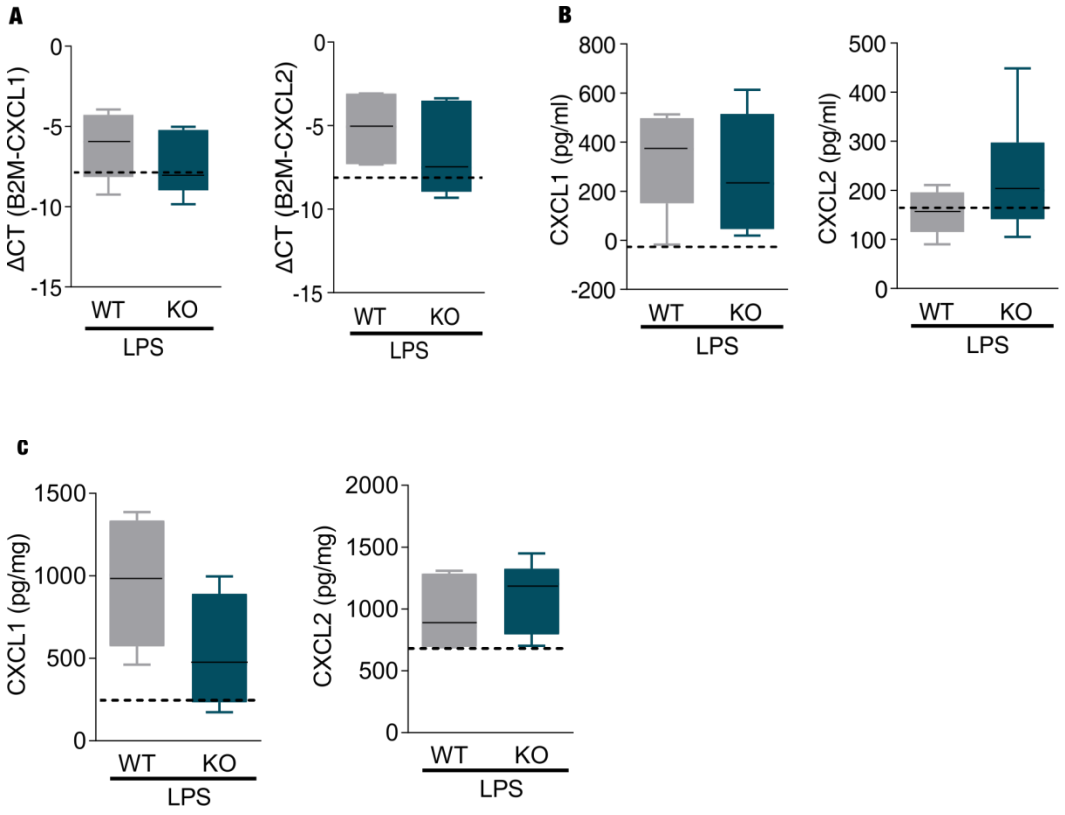

Figure 14: Chemokine measurements at LPS 24 hours. **A)** CXCL1 and CXCL2 mRNA expression in lung tissue. The ΔCT values are normalized to β2M obtained *via* RT-qPCR. CXCL1 and CXCL2 protein levels in **B)** BALF **C)** Lung measured by ELISA. WT and RGS5-/- saline-treated pooled together and presented as dotted lines as no differences were observed. Box-and-whisker plots are used as graphical presentation (n ≥ 7 mice) and unpaired two-tailed t-test is used for analysis. (Reproduced from previously published study in MDPI (1) under CC BY 4.0 license).

In addition, I measured inflammatory cytokines at mRNA levels in the lung tissue from both acute lung injury mouse models. At 3 day bleomycin, there was an increase in IL-6, TNF-α, and IL-33 in WT and RGS5-/- mice. TNF-α showed a significant increase in bleomycin treated RGS5-/- compared to WT **(Figure 15)**. Furthermore, at LPS 24h there was an increase in IL-1β and TNF-α in WT and RGS5-/- mice. IL-1β levels remained significantly lower in LPS treated RGS5-/- compared to WT mice **(Figure 16)**.

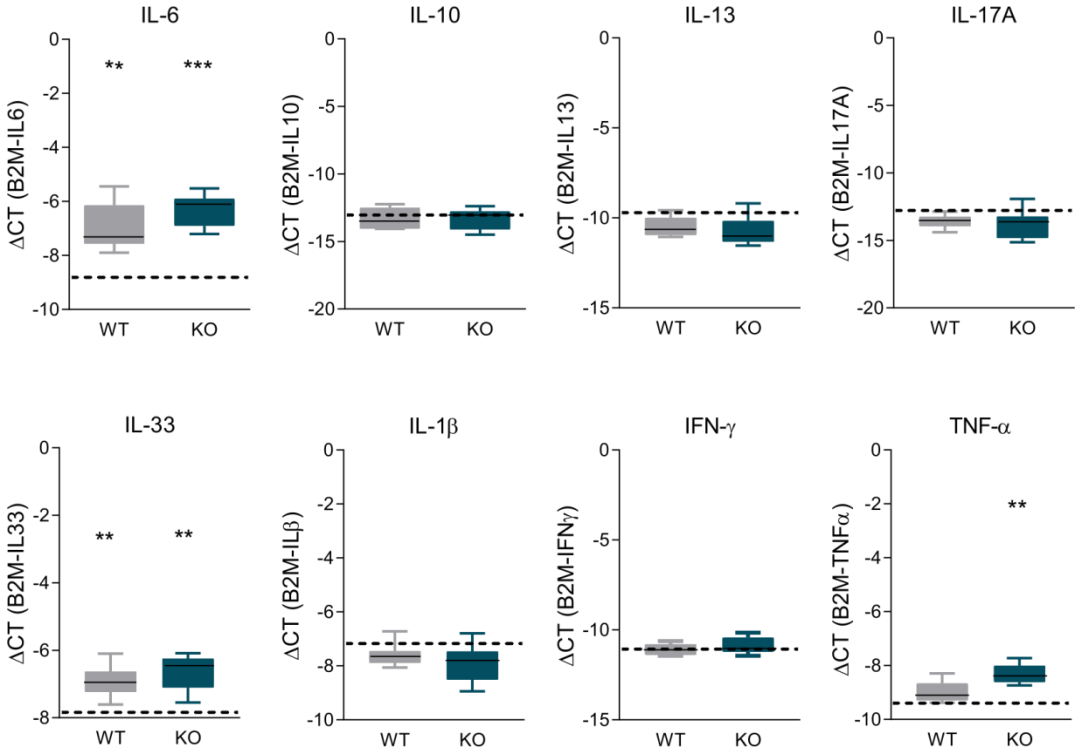

Figure 15: The inflammatory cytokine response in RGS5 mice in bleomycin 3days. mRNA expression in the lungs of WT and RGS5 mice upon saline and bleomycin treatment at day3 (n ≥ 7). ΔCT values, calculated by ΔCT = CT (reference gene) - CT (target gene). WT and RGS5-/- saline-treated pooled together and presented as dotted lines as no differences were observed. Box-and-whisker plots are used as graphical presentation (n ≥ 7 mice) and unpaired two-tailed t-test (* $p < 0.05$, ** $p < 0.01$) is used for analysis. (Reproduced from previously published study in MDPI (1) under CC BY 4.0 license).

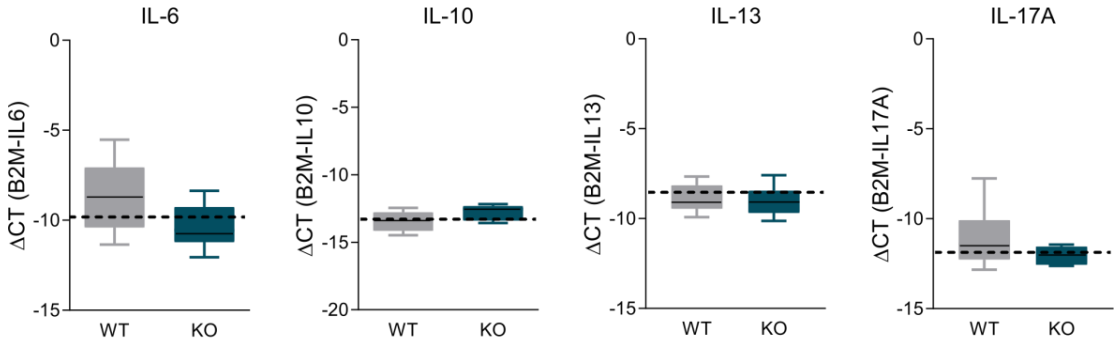

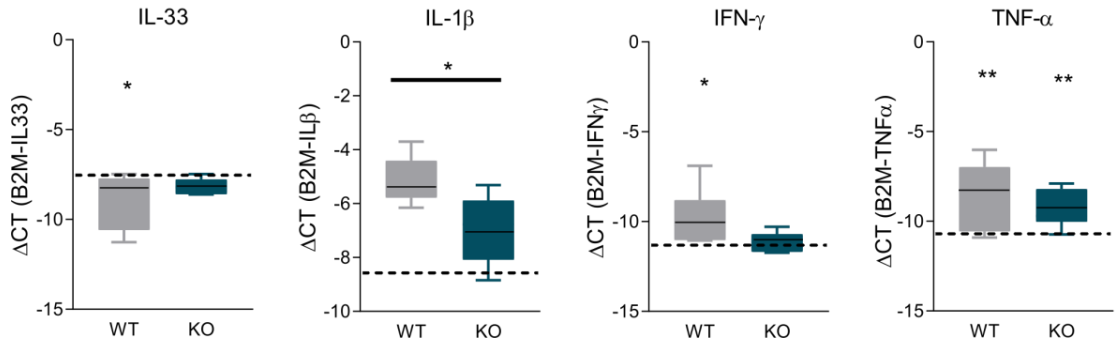

Figure 16: The inflammatory cytokine response in RGS5 mice in LPS 24 hours. mRNA expression in the lungs of WT and RGS5 mice treated with saline and LPS for 24 hours (n ≥ 5). ΔCT values, calculated by ΔCT = CT (reference gene) - CT (target gene). WT and RGS5-/- saline-treated pooled together and presented as dotted lines as no differences were observed. Box-and-whisker plots are used as graphical presentation (n ≥ 7 mice) and unpaired two-tailed t-test (* $p < 0.05$, ** $p < 0.01$ *** $p < 0.001$) is used for analysis. (Reproduced from previously published study in MDPI (1) under CC BY 4.0 license.

In our next step, I determined the expression of RGS5 in neutrophils isolated from WT mice bone marrow. The neutrophils were isolated using Ly6G positive bead selection and obtained a purity of 94% **(Figure 17A)**. We could also show that RGS5 is present in neutrophils **(Figure 17B).**

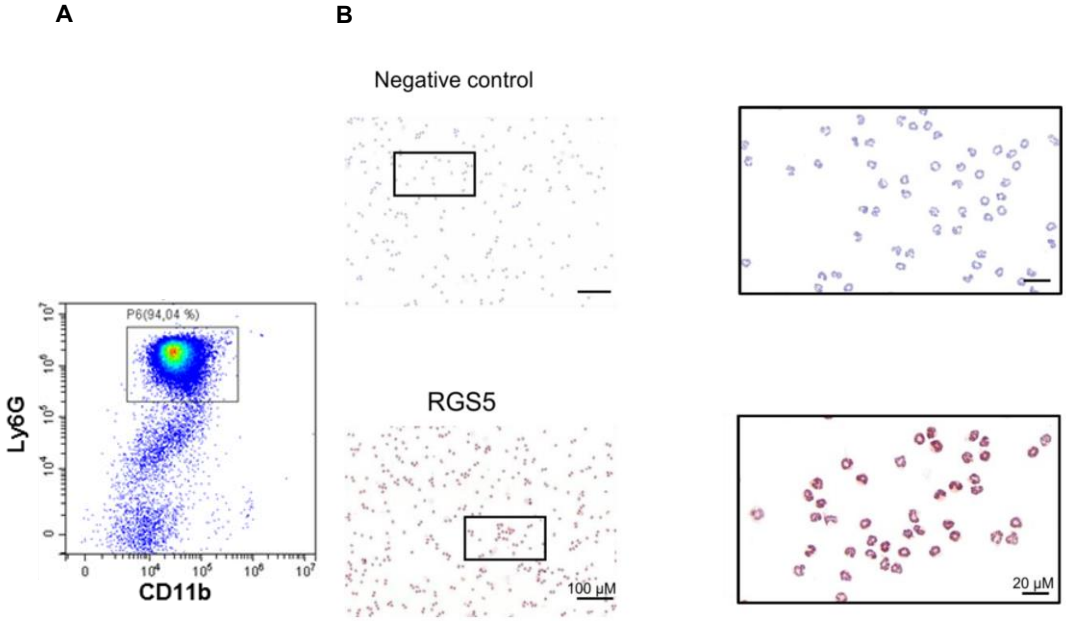

Figure 17: RGS5 expression in neutrophils. A) Flow cytometry measurements of Ly6G and CD11b positive neutrophils **B)** RGS5 IHC staining (brown) on the neutrophils isolated from WT mice with negative control. Scale bar 100 µM and 20 µM. (Reproduced from previously published study in MDPI (1) under CC BY 4.0 license).

Based on these observations, I suspected that RGS5 loss might affect homeostatic neutrophil localization and lead to neutropenia in the mice. To address this question, I performed flow cytometry analysis neutrophil numbers in WT and RGS5-/- mice blood, spleen, and bone marrow under naive conditions **(Figure 18)**. I found no difference between the two genotypes.

Surface receptor expressions on neutrophils for chemoattractants are essential for their migratory function. To examine the impact of RGS5 deficiency, I measured CXCR2 and CXCR4 receptors levels employing flow cytometry in neutrophils. I found that the receptor levels remained equal between WT and RGS5-/-. After treatment with receptor ligands CXCL1 and CXCL12 for 5 mins and 15 mins, there was no difference in CXCR2 and CXCR4 receptor levels **(Figure 19)**.

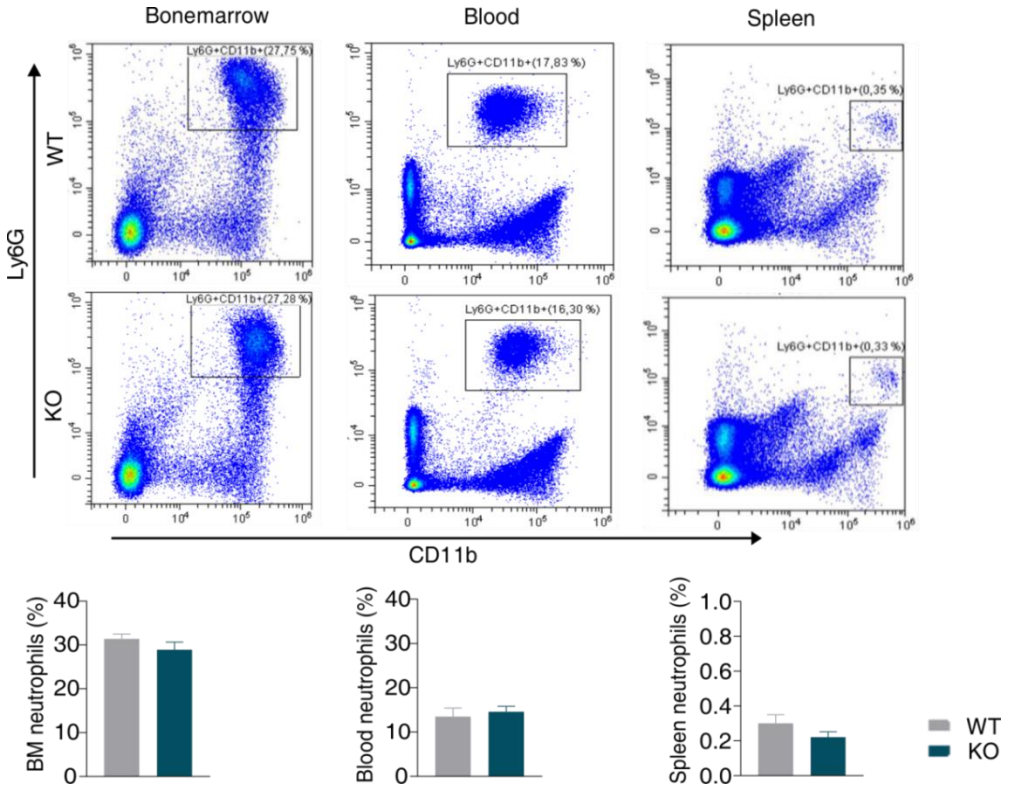

Figure 18: Neutrophils count in WT and RGS5-/- mice. Representative Ly6G and cd11b positive gated cell population from flow-cytometry for neutrophils count from bone marrow, blood, and spleen and graphical presentation with quantification. 2–3 mice pooled per genotype for each experiment and Four experiments were performed independent. bar plots as mean ± SEM are used as graphical presentation and unpaired two-tailed t-test is used for analysis. (Reproduced from previously published study in MDPI (1) under CC BY 4.0 license).

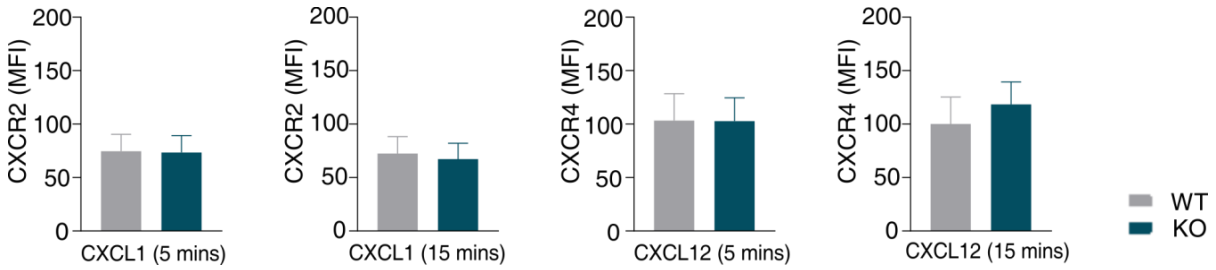

Figure 19: Surface receptor expression on RGS5-/- neutrophils. CXCR2 and CXCR4 expression level measured *via* flow-cytometry on the neutrophils treated with CXCL1 and CXCL12 for 5 and 15 minutes after extracting from WT and RGS5-/-. 2–3 mice pooled per genotype for each experiment and Four experiments were performed independent. bar plots as mean ± SEM are used as graphical presentation and unpaired two-tailed t-test is used for analysis. (Reproduced from previously published study in MDPI (1) under CC BY 4.0 license).

The neutrophil migration towards a high gradient of chemokine upon tissue injury is a multistep process. Since limited recruitment of neutrophils in the lungs of RGS5-/- mice upon bleomycin as well as LPS challenges were observed, next, the migratory response of neutrophils from RGS5-/- mice was investigated. Consistent with the *in vivo* finding, markedly diminished chemotaxis response in RGS5-/- neutrophils compared to neutrophils from WT mice was seen using the chemotaxis trans-well assay toward fMLP, CXCL1, and CXCL2. The response was independent of the type of chemoattractant **(Figure 20)**.

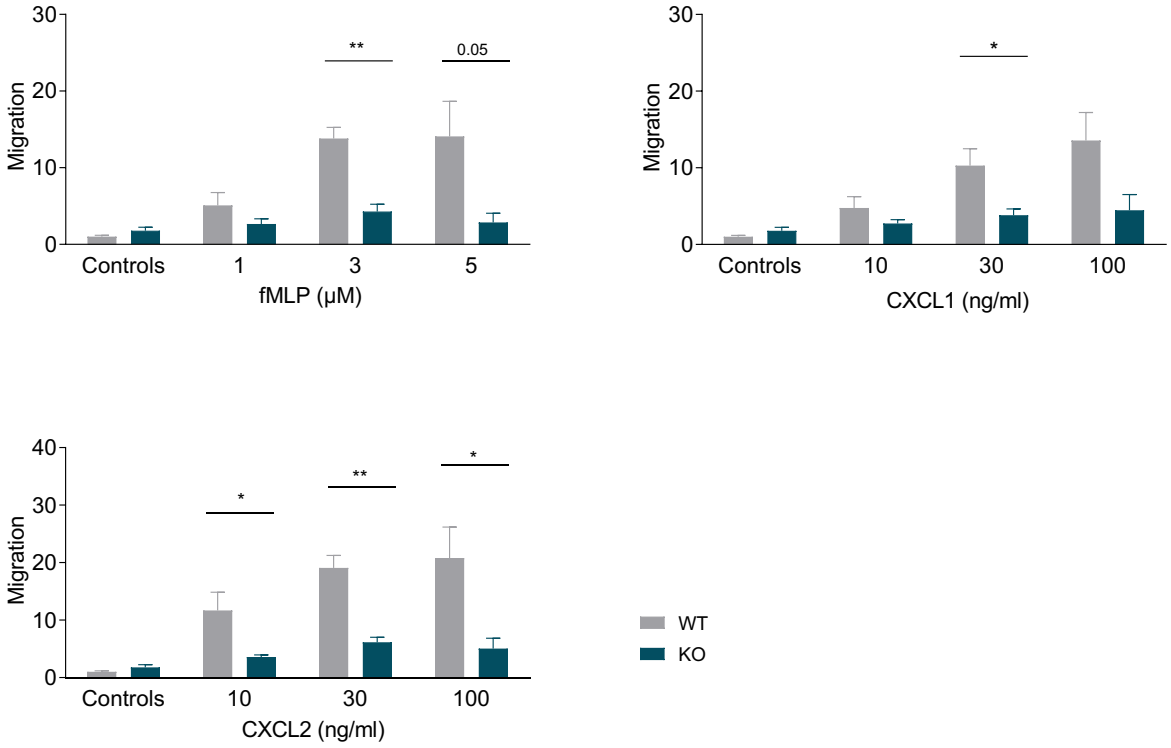

Figure 20: Impaired chemotaxis capabilities of RGS5-deficient neutrophils.
Chemotaxis of neutrophils were assessed by corning trans-well assays using fMLP, CXCL1, CXCL2. 2–3 mice pooled per genotype for each experiment and four experiments were performed independent. bar plots as mean ± SEM are used as graphical presentation and unpaired two-tailed t-test (* $p < 0.05$, ** $p < 0.01$) is used for analysis. The investigations were performed with the help of Iris Red. (Reproduced from previously published study in MDPI (1) under CC BY 4.0 license).

4.4.2 RGS5-/- neutrophils downstream signaling

In neutrophils, the classical signaling upon GPCRs activation entails the mobilization of free calcium (Ca^{2+}) levels in cytoplasm. When neutrophils were activated with fMLP, CXCL1, or CXCL2, their Ca^{2+} levels peaked. RGS5-deficient neutrophils had intracellular calcium levels that peaked same as WT neutrophils and thereafter dropped **(Figure 21)**. These data suggest that calcium signaling is intact in neutrophils even after RGS5 deletion.

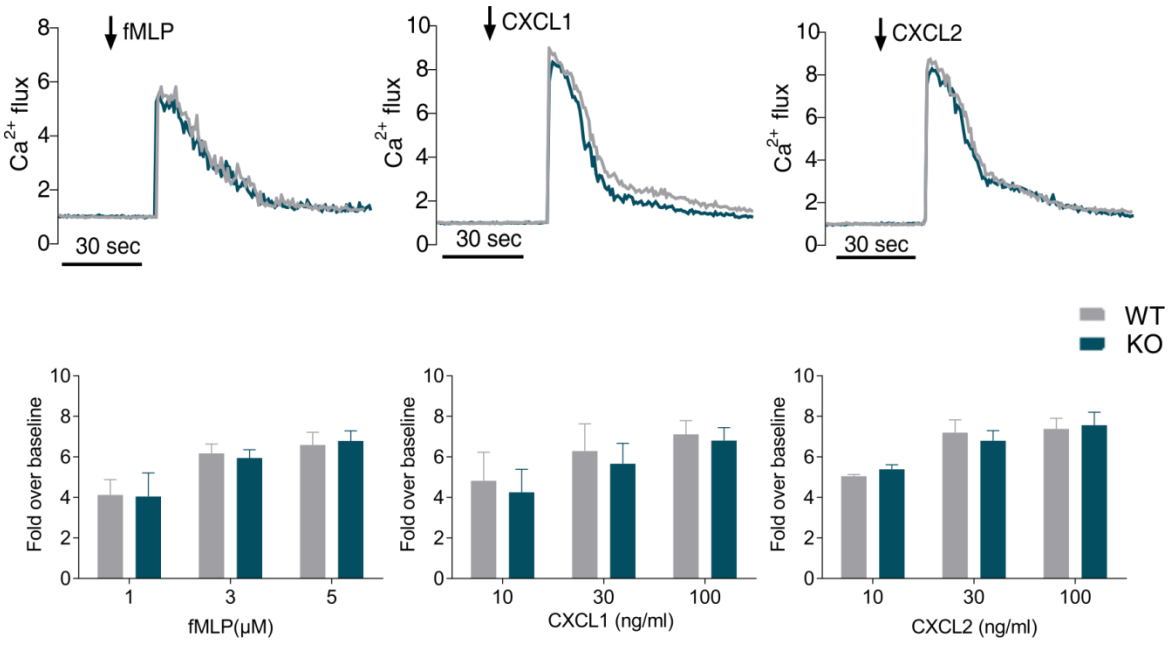

Figure 21: Intracellular Ca^{2+} flux in RGS5-deficient neutrophils. Peak intracellular calcium response upon fMLP, CXCL1, and CXCL2 calculated fold change over baseline with representative histogram measured in the neutrophils isolated from WT and RGS5-/- mice. 2–3 mice pooled per genotype for each experiment and four experiments were performed independent. bar plots as mean ± SEM are used as graphical presentation and unpaired two-tailed t-test is used for analysis. The investigations were performed with the help of Iris Red. (Reproduced from previously published study in MDPI (1) under CC BY 4.0 license).

Further investigation of signaling pathway analysis revealed that ERK activation was more sustained in RGS5-/- mice than in WT mice. Upon stimulation, I found that ERK activity peaked early in WT and RGS5-/- neutrophils. However, in WT neutrophils, a subsequent reduction was seen back to baseline after 30 minutes. In contrast, neutrophils from RGS5-/- mice demonstrated delayed dephosphorylation (inactivation) of ERK **(Figure 22A)**.

To determine whether key cytoskeleton regulators of neutrophils were involved in the migratory response; I examined RhoA, the main Rho isoform in neutrophils as well as Cdc42. At baseline, the RhoA activity was unchanged between the genotypes. However, under-stimulation, RGS5-/- neutrophils showed a significantly stronger RhoA increase **(Figure 22B)**. The Cdc42 activity remained unchanged between the genotypes under chemokine stimulation **(Figure 22B)**.

A

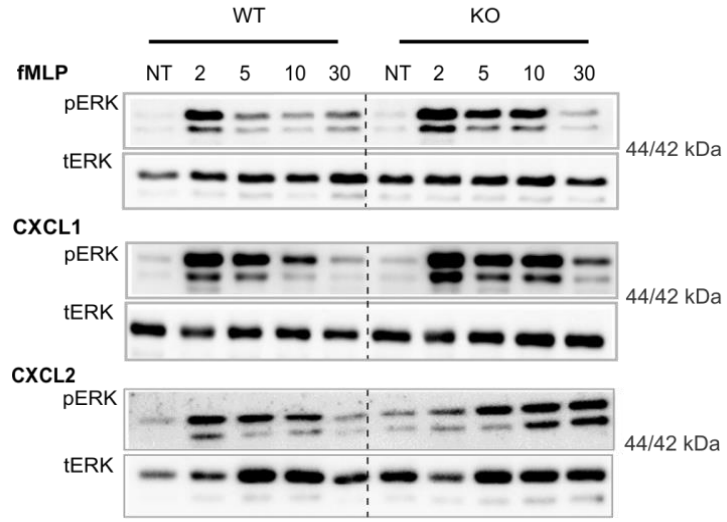

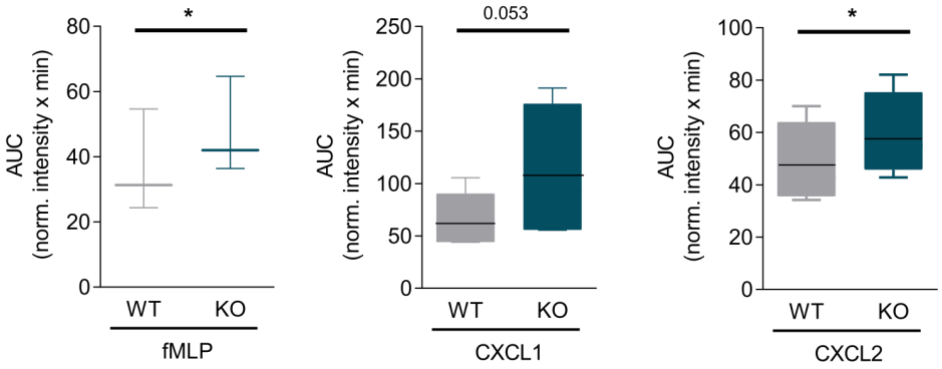

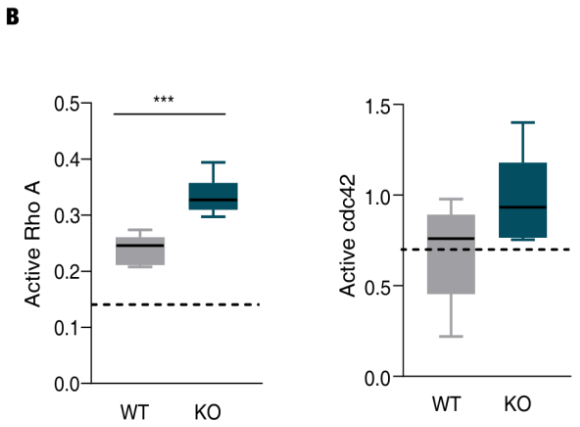

Figure 22: ERK and small GTPase in RGS5-deficient neutrophils. **A)** Representative western blots indicating the phosphorylation of ERK in neutrophils isolated from WT and RGS5-/- mice with their total ERK levels. fMLP, CXCL1and CXCL2 were used for neutrophil treatment for indicated time points. NT= non-treated. AUC values are presented for all chemoattractants per genotype. Values represent normalized intensity x mins. The representative blots are from n=2-3 (each n WT = 3 and RGS5-/- = 3). **B)** Active RhoA and Cdc42 in neutrophils treated for 5 mins with fMLP, CXCL1and CXCL2. Neutrophils pooled from each genotype (WT n = 6, RGS5-/- n = 6 mice). WT and RGS5-/- saline-treated pooled together and presented as dotted lines as no differences were observed. Box-and-whisker plots are used as graphical presentation and unpaired two-tailed t-test (* $p < 0.05$, *** $p < 0.001$) is used for analysis. (Reproduced from previously published study in MDPI (1) under CC BY 4.0 license). The investigations were performed with the help of Elisabeth Blanz and Sabine Halsegger.

4.5 Role of RGS5 in lung fibrosis

4.5.1 Absence of RGS5 failed to prevent bleomycin-induced injury on day 21

Encouraging findings from acute inflammatory phase of pulmonary fibrosis led us to further investigate the impact of RGS5 loss in the chronic phase of the disease. At day 0, WT and RGS5-/- mice were treated with bleomycin intratracheal (i.t.) and analyzed at 21 days as presented in the scheme **(Figure 23A)**. H&E staining on lung tissue sections showed

distortions in lung normal appearance between saline and bleomycin treated mice whereas we observed no differences for lung structural changes and inflammatory cells infiltration between bleomycin treated WT and RGS5-/- mice **(Figure 23B)**.

Heat maps depict flow cytometry analysis of inflammatory cells in BALF and lung tissue. The total cell count and neutrophil recruitment were considerably increased in BALF after bleomycin treatment in BALF and lung tissue of both genotypes. However, there were no differences between WT and RGS5-/- animals **(Figure 23C, D, and Figure 25A)**.

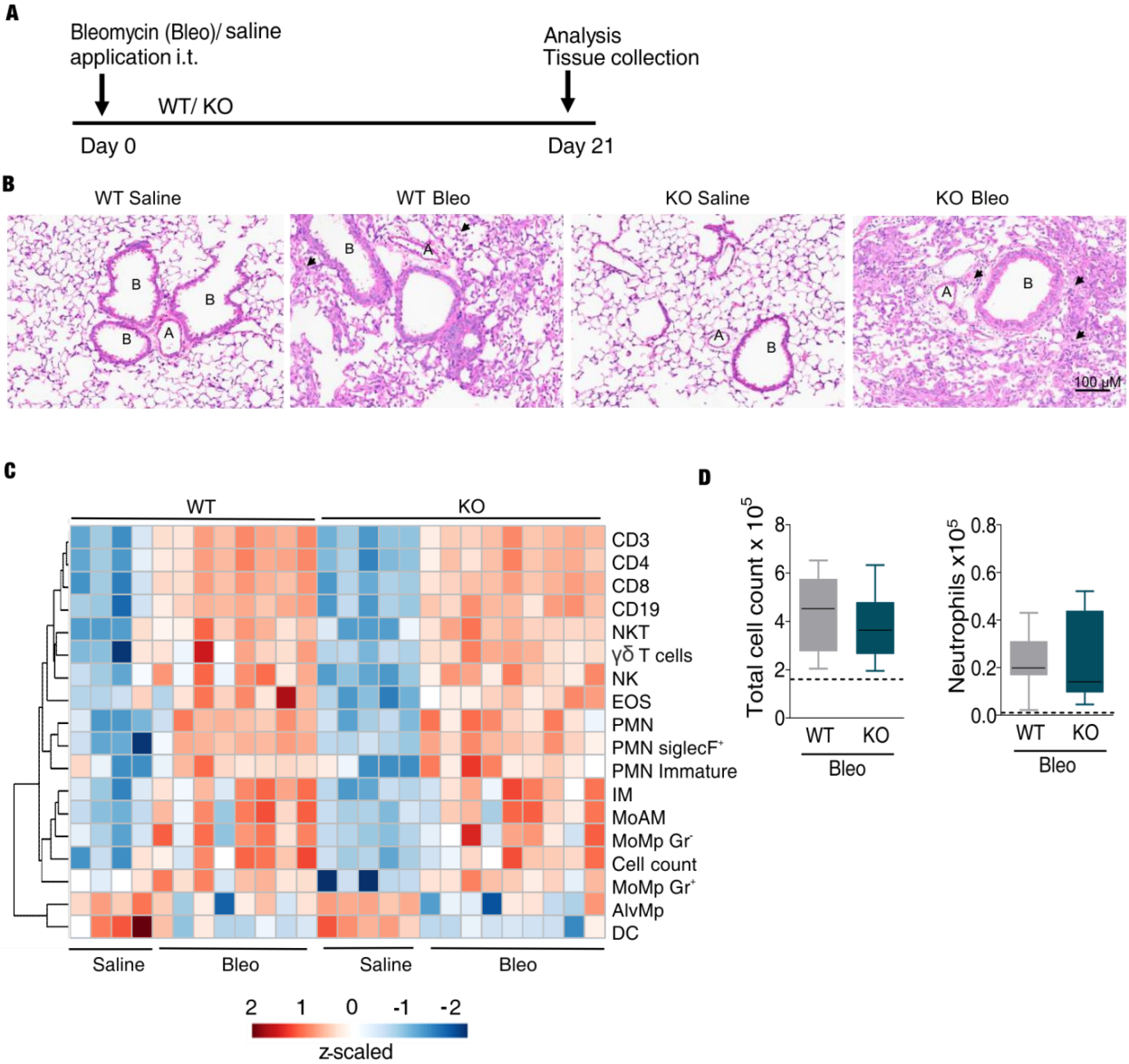

Figure 23: RGS5 deletion does not prevent from lung damage induced by bleomycin treatment at day 21. A) Graphical diagram of saline and bleomycin treatment to mice. *in vitro* and *in vivo* analyses carried out at the indicated time point. **B)** H&E staining for the histological appearance of the lung tissue; arrows pointing inflammatory cells; A = pulmonary arteries, B = bronchioles; Scale bar 100μM (10X). **C)** Heatmap of flow cytometric inflammatory cell counts in BALF 21 days after Bleomycin-challenge (log10(x+1) transformed, z-scaled per cell type) are shown with average distance sorted dendrograms from hierarchical clustering analysis. **D)** Flow cytometry analysis of lung tissue total cell and neutrophil count. WT and RGS5-/- saline-treated pooled together and presented as dotted lines as no differences were observed. Box-and-whisker plots are used as graphical presentation (n = 3-10) and unpaired two-tailed t-test is used for analysis. (Reproduced from previously published study in MDPI (1) under CC BY 4.0 license).

Next, I performed Ly6G staining on lung tissues and found no differences in the neutrophil infiltrations in the lung tissue **(Figure 24A)**. The levels of MPO in lung tissue did not change between the WT and RGS5-/- bleomycin treated groups **(Figure 24B)**. I found increased BALF protein levels at day 21, however, they showed no difference between WT and RGS5-/- bleomycin treated groups **(Figure 24C)**. Lung function measurements revealed worsening of resistance estimated inspiratory capacity and no changes in the area in WT and RGS5-/- mice treated with bleomycin. Other lung parameters such as compliance, elastance, tissue damping, and tissue elastance showed similar development **(Figure 24D** and **Figure 25B)**.

Finally, the collagen content in the lungs using Picrosirius red staining was analyzed to determine whether the lack of RGS5 would affect collagen production. In both WT and RGS5-/- mice, the histologic study of fibrosis revealed significantly altered lung tissue with enhanced Picrosirius red staining. However no differences were observed between WT and RGS5-/- bleomycin treated mice **(Figure 26)**.

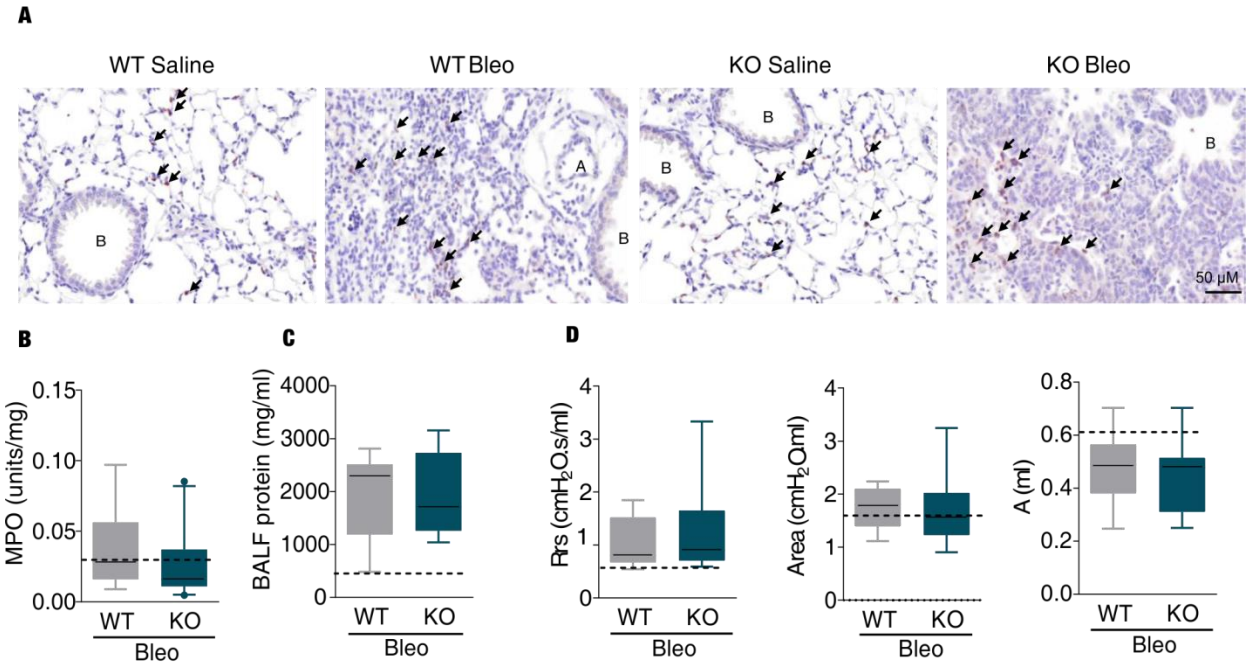

Figure 24: RGS5 deletion does not prevent from lung damage induced by bleomycin treatment at day 21. A) Anti-Ly6G IHC staining for neutrophils in lung tissue sections; Scale bar 50 µM **B)** MPO enzymatic activity in lung tissue per mg. **C)** BALF protein levels measured using BCA assay. **D)** Lung function measurements showing the airway resistance (Rrs), estimation of inspiratory capacity (A), and area (enclosed under P-V loop). WT and RGS5-/- saline-treated pooled together and presented as dotted lines as no differences were observed. Box-and-whisker plots are used as graphical presentation (n = 3-10 mice) and unpaired two-tailed t-test is used for analysis. (Reproduced from previously published study in MDPI (1) under CC BY 4.0 license). The lung function measurements were carried out with the help of Thomas Fuchs.

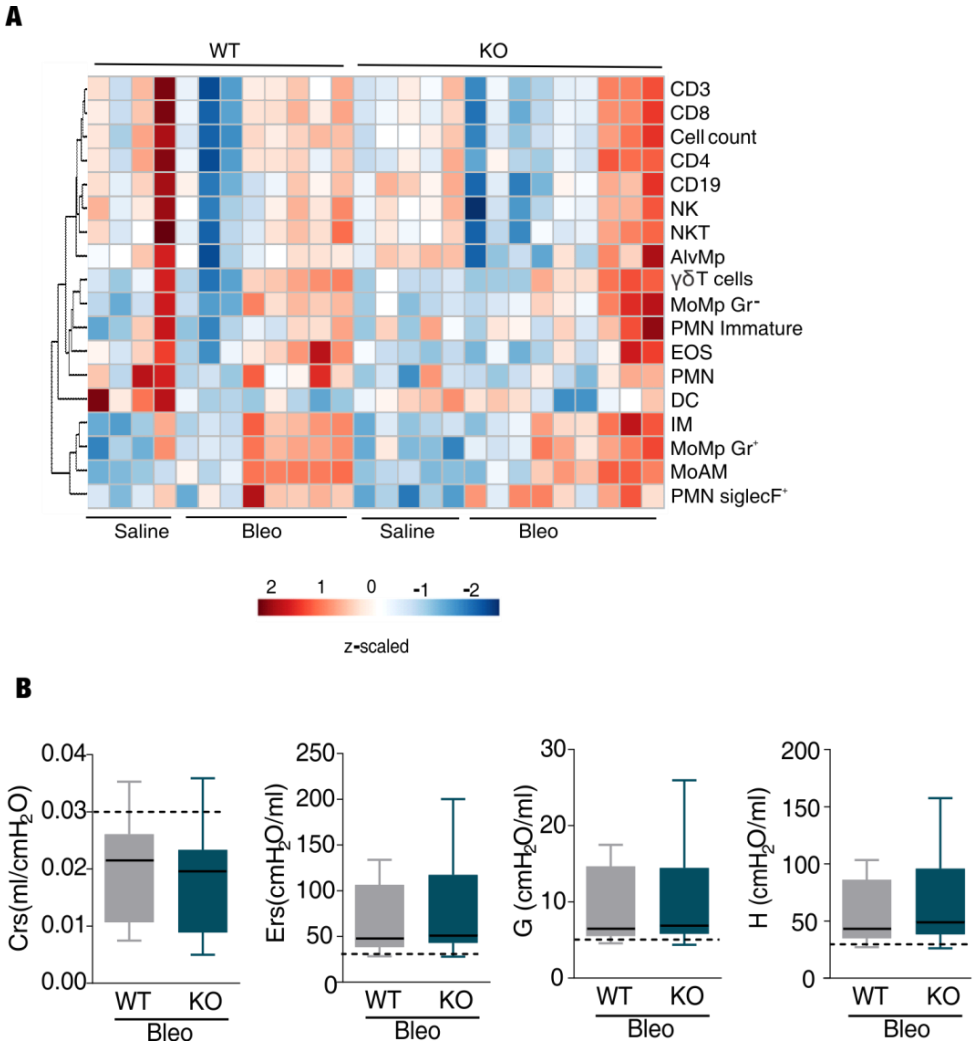

Figure 25: *in vivo* analysis of the lung after 21 days of bleomycin injury. **A)** Heatmap presenting the inflammatory profile of the lung tissue ($log_{10}(x+1)$ transformed, z-scaled per cell type) are shown with average distance sorted dendrograms from hierarchical clustering analysis at 21 days obtained from the flow-cytometry analysis. **B)** Lung function measurements; Crs: compliance; Ers: Elastance; G: tissue damping; H: tissue elastance of the respiratory system. WT and RGS5-/- saline-treated pooled together and presented as dotted lines as no differences were observed. Box-and-whisker plots are used as graphical presentation (n = 3-10 mice) and unpaired two-tailed t-test is used for analysis. (Reproduced from previously published study in MDPI (1) under CC BY 4.0 license). The lung function measurements were carried out with the help of Thomas Fuchs.

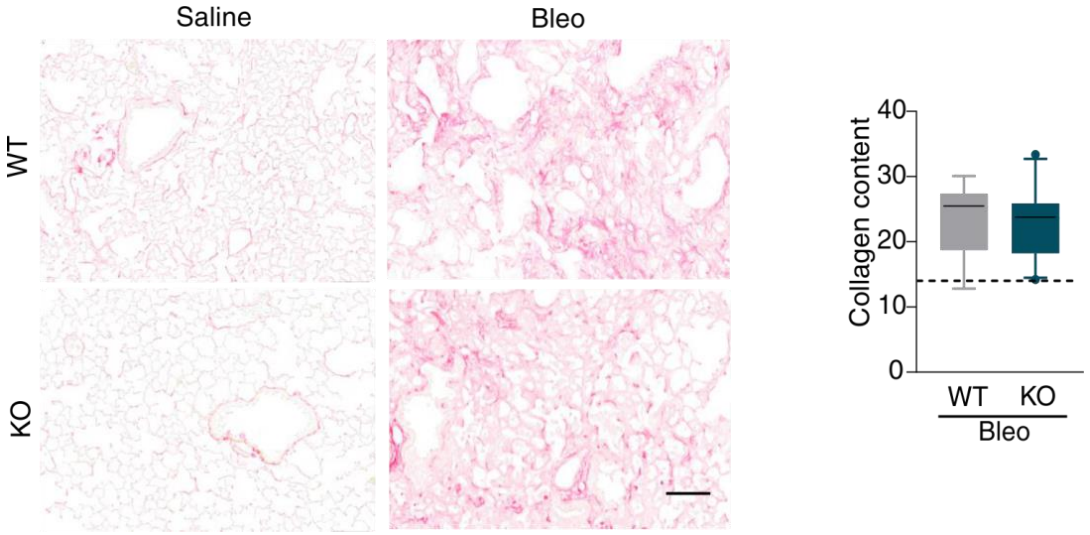

Figure 26: Lack of RGS5 does not change collagen deposition in lungs. Sirius red staining showing lung collagen in lungs with respective quantification. Scale bar 50 µM. WT and RGS5-/- saline-treated pooled together and presented as dotted lines as no differences were observed. Box-and-whisker plots are used as graphical presentation (n = 8 mice) and unpaired two-tailed t-test is used for analysis. (Reproduced from previously published study in MDPI (1) under CC BY 4.0 license).

4.6 Role of RGS5 in the pulmonary vasculature

The expression of RGS5 is primarily shown to be restricted to pericytes and vascular smooth muscle cells (129). In the current study, the mRNA expression of RGS5 was elevated in laser micro-dissected materials from pulmonary arteries (PA) of donor and IPF patient lungs **(Figure 27)**. Using mice lung tissue sections, I confirmed the presence of RGS5 in pulmonary arteries, expressed in smooth muscle cells **(Figure 28)**.

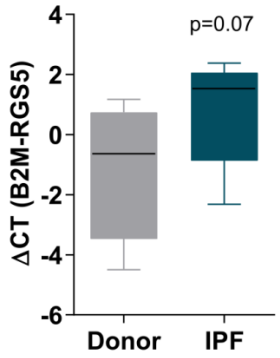

Figure 27: RGS5 expression human pulmonary vasculature. mRNA expression of RGS5 in the pulmonary arteries from donor and IPF patients. ΔCT values, calculated by ΔCT = CT (reference gene) – CT (target gene). Box-and-whisker plots are used as graphical presentation (n = 8 mice) and unpaired two-tailed t-test (*p < 0.05) is used for analysis.

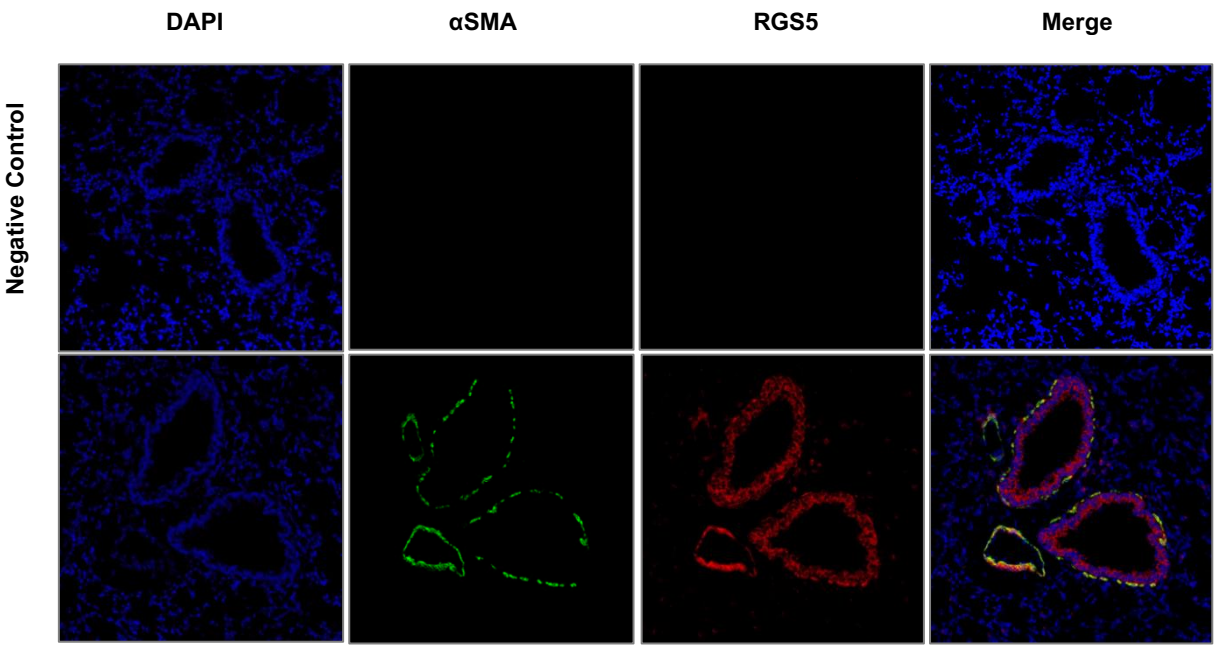

Figure 28: RGS5 localization in WT mice pulmonary arteries. DAPI (blue), α-Smooth muscle Actin (αSMA; green), and RGS5 (red).

To understand the impact of RGS5 loss on pulmonary vasoreactivity, I determined the basal vascular response in WT and RGS5-/- mice using a wiremyograph. In intact intrapulmonary arteries isolated from WT and RGS5-/- mice lungs, I used vasoactive compounds for dose-dependent vasoconstriction. RGS5-/- PA revealed attenuated vasoconstrictory response upon high potassium chloride (KCl) at concentration 120mM and similarly 5-hydroxytryptamine or serotonin (5-HT) at 3 μM **(Figure 29A and B)**. However, I did not observe any differences between WT and RGS5-/- upon other vasoconstrictors e.g. stable synthetic thromboxane A2 receptor agonist (U44619) and phenylephrine (PE) **(Figure 29C and D)**.

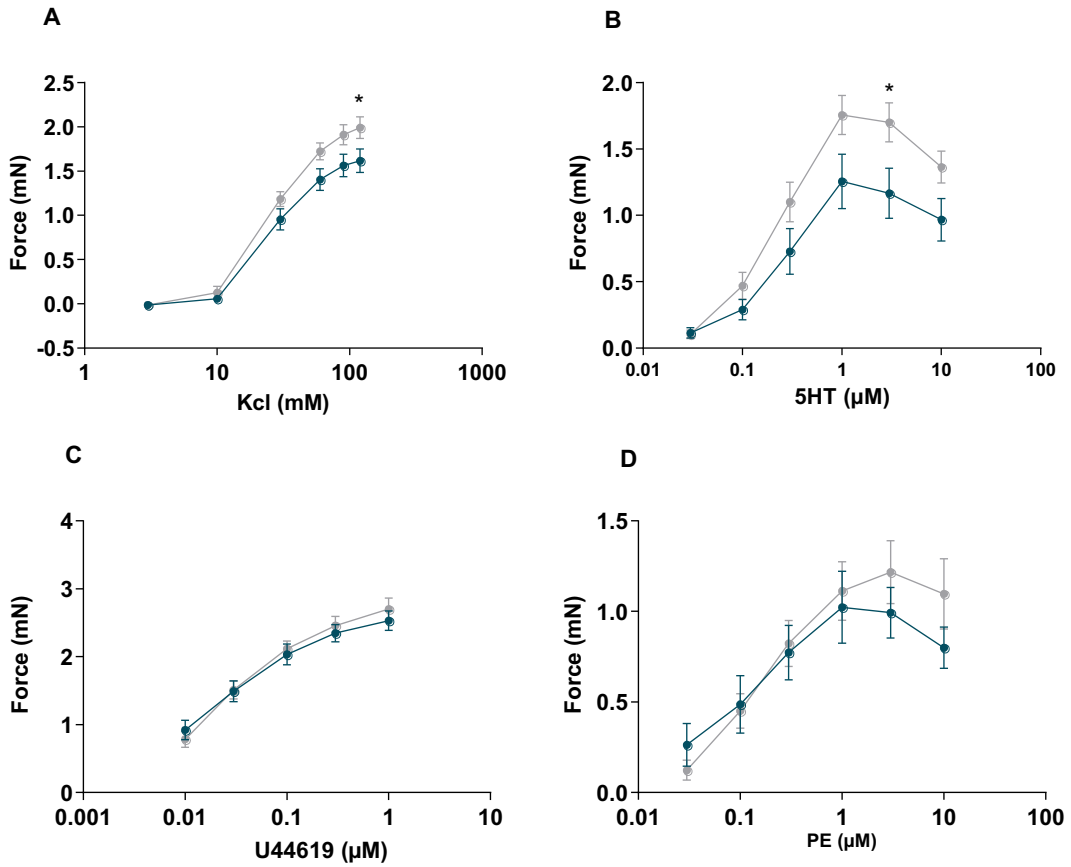

Figure 29: RGS5-/- mice have altered vasoconstrictory responses.

Dose-dependent vasoconstrictive response of intrapulmonary arteries isolated from WT and RGS5-/- mice in response to **A)** potassium chloride (KCl) **B)** 5-hydroxytryptamine (5HT) **C)** thromboxane A2 receptor agonist (U44619) and **D)** phenylephrine (PE). Data are expressed

as means +SEM, mice per group n = 5, pulmonary arteries per group n = 18-12; Two-way ANOVA, Tukey's post-test *P<0.05.

Based on our finding from *ex vivo* pulmonary vasoconstriction, we further measured the right ventricular systolic pressure (RVSP) in bleomycin-treated mice at day 21. There was an increase in RVSP upon bleomycin treatment in both the genotypes compared to saline groups, however, there was no protective phenotype observed in RGS5-/- mice **(Figure 30A)**. In addition, we did not observe any changes in right ventricle size measured by the Fulton index **(Figure 30B)**.

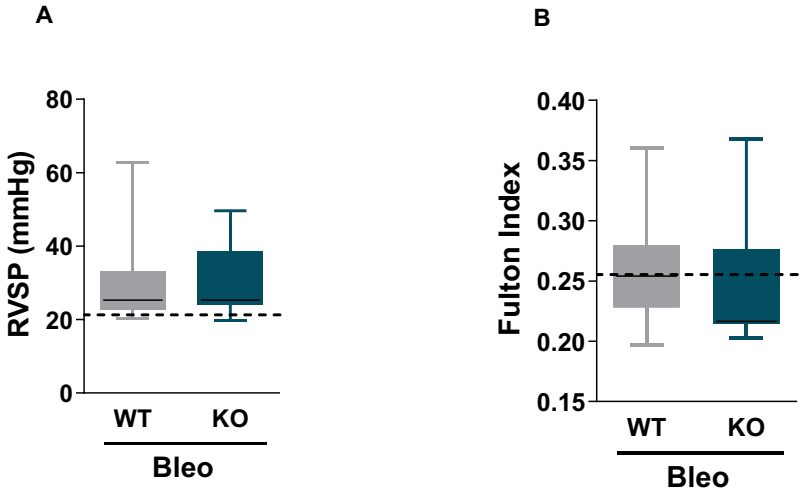

Figure 30: Hemodynamic measurements at day 21 after bleomycin challenge.
A) Right ventricular systolic pressure (RVSP). **B)** Fulton index (right ventricular weight/weight of left ventricle plus inter-ventricular septum). WT and RGS5-/- saline-treated pooled together and presented as dotted lines as no differences were observed. Box-and-whisker plots are used as graphical presentation (n = 8-9 mice) and unpaired two-tailed t-test is used for analysis. (Reproduced from previously published study in MDPI (1) under CC BY 4.0 license). The Hemodynamic measurements were carried out with the help of Bence M. Nagy and Chandran Nagaraj.

5 Discussion

The regulators of G-protein signaling (RGS) are becoming targets for novel treatments considering their involvement in GPCR signaling and cell specific function. Anti-inflammatory drugs tuning neutrophil recruitment in the lungs is a key factor for modulation of the exaggerated innate immune response (1). In my study, the contribution of RGS5, the member of the R4 RGS subfamily was investigated in acute pulmonary inflammation as well as in chronic lung fibrosis development. I applied two independent lung injury mouse models, the bleomycin and LPS-induced acute lung injury model and the bleomycin-induced chronic lung fibrosis model (4–7).

The current work demonstrates the complex relationship between RGS5 and neutrophil inflammation, with surprising results. During the acute phase of lung injury in mice (bleomycin and LPS-induced mouse models), the lack of RGS5 resulted in reduced loss of lung function and a suppressed inflammatory response. This was related to a reduction in neutrophil recruitment to the lungs. In addition, upon chemokine stimulation, RGS5-/- neutrophils had significantly enhanced RhoA levels and delayed ERK dephosphorylation. In contrast, this protective phenotype is abolished in the absence of RGS5 in the chronic lung fibrosis model (1).

5.1 Acute lung injury and Fibrosing interstitial lung diseases

ALI or ARDS is characterized by an uncontrollable inflammatory response upon direct or indirect injury to the lungs. This leads to activation of leukocytes—alveolar macrophages and sequestered neutrophils—and damage to the lungs (36,38,39). BALF and lung biopsy samples from ALI patients revealed the accumulation of neutrophils within the airspaces, and, indeed, the degree of neutrophilic influx correlates with mortality in ALI (130–132). Using different animal models, it has been shown that depletion of neutrophils protects from acute inflammatory damage to the lungs (43). However, completely blocking neutrophil recruitment in the lungs can strongly weaken the primary defense against infections. Therefore, specific therapeutic targets are much needed to manipulate neutrophil migration and recruitment without compromising anti-infection response. IPF is one of the most common fibrosing interstitial lung diseases with complex pathophysiology involving multiple lung structural and inflammatory cells, with poor prognosis and limited therapeutic options

(11). Inflammation is an important pathological mechanism during fibrosis development (10,12).

Increased chemokines and inflammatory cells have been seen in the BALF of IPF patients in recent studies (22,133,134). However, the involvement of inflammation has been debated in the development of fibrosing lung diseases in the past due to a lack of understanding of the inflammatory components. Prednisolone and interferon-gamma have not been successful to treat the chronic progression of IPF (15,135). However, an important feature of IPF is an exacerbation, affecting between 4–15% of individuals with IPF per year, and representing an important cause of IPF-related mortality (136,137). Therefore, the acute inflammatory response may play a major role in the deterioration of IPF patients and RGS5 might play an important role in this context.

5.2 R4 subfamily in lung diseases

RGS proteins have the main function of diminishing signaling output following GPCR activationNot many studies have been directly linked to any of the RGS family members to be either causative or consequential targets for pulmonary fibrosis. To our knowledge, this is the first study to indicate that the R4 subfamily is regulated differently in human fibrosing lung disease (1).
In the animal model, RGS2-/- mice showed enhanced acute inflammation in response to HDM and LPS inoculations(55,56,82). RGS2 has been investigated in the bleomycin lung fibrosis model, showing exaggerated fibrosis with impaired lung function. Upregulation of RGS2 expression has been suggested as a partial mechanism for pirfenidone treatment action specific to fibroblasts (82). In a previous study, increased expression of RGS4 in smooth muscle cells in human bronchi induced significant airway blockage. RGS4-/- mice showed reduced allergen sensitivity which was linked to altered PGE2 secretion upon allergen stimulation (59,61). These findings indicate that RGS proteins play substantially varied in the signaling pathways and biological functions (1).

5.3 RGS5 in lung diseases

Previous studies have shown that global loss of RGS5 in the lung led to increased basal AHR and contraction without inflammation in mice (2). More importantly, a recent study has shown that loss of RGS5 increased neutrophil recruitment in the airway of mice upon

pneumonia virus of mice (PVM) challenge (138). We and others show that RGS5 is present in the lungs specific to smooth muscle cells and airway epithelium (73,74). Gene expression of RGS5 was increased in the lung of IPF patients and localized in airway epithelial and smooth muscle cells, pulmonary vasculature, and inflammatory cells as well as in ALI patients. In addition, RGS1, RGS3, and RGS4 also showed increased expression in IPF lungs. We determined the RGS5 expression in the lungs of bleomycin treated mice, a mouse model of pulmonary fibrosis with systematic development of fibrosis, for different time points. Similar to the findings in human samples, RGS5 expression was increased in bleomycin-treated lungs with its stronger appearance in smooth muscle cells, epithelium, and inflammatory cells.

In *in vitro* assay, airway smooth muscle cells showed reduced contraction upon RGS5 overexpression. *in vivo* study, RGS5 deletion caused AHR (spontaneous) or airway neutrophil inflammation following viral infection (73,74,138). In our *in vivo* experiments, we show that RGS5 deletion attenuates lung function worsening in the acute inflammatory phase. Furthermore, the inflammatory cell inflow in the lungs was limited in bleomycin and LPS animal models (1). The inflammatory cells in the lungs were mainly containing neutrophils and significant reductions in neutrophil counts in the lung and BALF of bleomycin and LPS-induced lung damage. In connection to neutrophil's number, we found that MPO enzymatic activity was also significantly reduced in the lungs RGS5-/- mice treated with Bleomycin (1).

In our study, neutrophils from RGS5-/- showed reduced migration toward chemoattractant stimulation, indicating an essential role of RGS5 in neutrophil migration in the lung. RGS5 function and molecular mechanism were investigated using both *in vitro* and *in vivo* experimental methods, therefore improving our understanding of RGS5 protein in lungs injury (1,51). Neutrophils release proteases, oxidants, and chemokine which act as a potential source for alveolar epithelial injury during the acute inflammatory phase (43,139). We can speculate that lack of RGS5 in neutrophil affect their recruitment in the BALF causing less damage to the alveolar sac which might ultimately help to preserve the lung function parameters related to alveolar structure and ability to maintain oxygenation.

5.4 Neutrophils are key mediators in acute lung injury

Neutrophils are critical mediators of host protection responses on the preliminary tiers of injury. Upon tissue infection and damage, neutrophils quickly pass across tissues to reach harmed tissue sites. Increased neutrophil counts, as well as the chemotactic factors that

promote neutrophil recruitment, are linked to a worsening of the disease and greater fatality rates in acute lung injury. Hence studies of neutrophil responses in inflammatory lung disorders have piqued attention in withinside the current decade(140). Over the last decade, there has been a surge of interest in studies of neutrophil responses in fibrotic lung disorders. Studies have shown an elevated number of neutrophils in IPF patients' BALF and also chemotactic factors responsible for neutrophil recruitment in tissue, which was linked to an increased risk of patient death (23). Moreover, studies revealed that NE promotes pulmonary fibrosis by stimulating fibroblasts to myofibroblasts and boosting collagen buildup during lung fibrosis progression (26–28). As a result, fine-tuned neutrophil recruitment to inflammatory and damaged areas could be a useful tool for therapeutic development (1).

Despite finding higher RGS5 expression in chronic fibrotic lungs from mice and human ILD lungs, our chronic animal investigation had no effect on inflammatory cell recruitment, lung function, or fibrotic lung development in WT and RGS5-/- mice. Unlike the chronic phase, RGS5 appears to oversee inflammatory cell migration during the acute phase. From our RGS5 staining's in human lung sections, we found that RGS5 was present in lung structural cells. However, we must keep in mind that human ILD lungs are end-stage disease lungs without acute inflammation. Due to the participation of several lung structural and inflammatory cell types in fibrosis development, RGS5 may play diverse functions at different phases of the disease (1).

The migration and recruitment of neutrophils to the site of injury is a multistep process involving a cascade of chemo-attractant release (99,141,142). RGS protein has been shown to modulate the different functions of inflammatory cells including modulating the release of chemokine and chemotaxis response (50). In line with the *in vivo* findings, I found that RGS5 deficient neutrophils showed restricted migration toward different chemoattractants fMLP, CXCL1, and CXCL2 during *in vitro* trans-well chemotaxis assay. This shows that RGS5 is necessary for proper neutrophil migration in the lungs (1).These findings are in contrast with previously published data where increased RGS5-/- neutrophil migration. In these studies neutrophils from RGS5/- mice showed increased migration toward chemoattractant (138). The strongest chemotaxis response was seen toward CXCL1. The two studies have substantial discrepancies, such as distinct RGS5-/- lines and assays. Chan et al. used the RGS5-/- mouse model which was created by replacing exon 1 and intron 1 of the RGS5 gene with a dual cassette carrying lacZ. Mice from Chan et al. study had significantly fewer lymphocytes, which could be due to lymphocyte trafficking problems. Furthermore, these

animals had an abnormally high level of phosphorylation of ERK both at rest and when stimulated in vascular cells(91). Before performing the experiments, Chan et al. treated the isolated neutrophils overnight with granulocyte/macrophage colony-stimulating factor (GM-CSF). RGS5-/- mouse model used in our study was created by specifically deleting the complete RGS domain of RGS5 (90) and and the neutrophils were not stimulated with GM-CSF overnight used for *in vitro* experiments. Therefore, these differences might explain the different outcomes of the studies (1).

Prerequisites for neutrophil activation and migration are to convert the external response from chemoattractants to internal release and mobilization of secondary messenger like Ca^{2+}. RGS regulates the internal Ca^{2+} homeostasis and hyperactivity of the cells *via* regulating the activation of GPCR. In previous studies, RGS5 deficiency leads to a dramatic increase in cytosolic Ca^{2+} upon receptor activation compared to their controls (73,87,138). Surprisingly, I observed activation of neutrophils with different chemoattractants rapidly increased the cytosolic Ca2+ in RGS5-/- and WT mice but with no differences between both the genotypes. This indicates that even upon receptor activation, calcium cytosolic concentration in RGS5-/- neutrophils were unaffected (1).

Previously, deletion of RGS2 has been shown to regulate the inositol 1,4,5-trisphosphate (IP3) receptor levels on endoplasmic reticulum (ER) and reduce the response of the cells to changes in the ER Ca^{2+} load and an increase in extracellular Ca^{2+} (143). Likely, RGS5 deficient neutrophils are still able to buffer the overloaded amount of Ca^{2+} *via* limiting the release from internal stores and regulating the Ca^{2+} transport through the plasma membrane. Thus, the Ca^{2+} response from RGS5-/- mice do not explain the restricted migration of neutrophils. Calcium signaling plays an important central role in various cellular processes. Therefore, manipulating expression RGS5 could be a very selective method to alter the acute neutrophil inflammation without changing intracellular calcium levels (1).

Neutrophil migration, cytokine release, neutrophil extracellular traps (NETs), and apoptosis have all been linked to ERK signaling(144–147). ERK has been shown to regulate the migration of neutrophils using different chemoattractants and acute injury models (103,104,148). I checked the levels of ERK phosphorylation in WT and RGS5-/- neutrophils upon different chemoattractants to learn more about how ERK is regulated at different time points. I found more pERK in neutrophils from RGS5-/- mice upon different chemoattractants compared to WT, which could indicate that ERK dephosphorylation (inactivation) is delayed

in neutrophils from RGS5-/- mice (1). Although the role of ERK in neutrophil chemotaxis has been debated. The current research from Liu and co-workers backs up our theory. The inhibition of ERK increased neutrophil chemotaxis *in vitro*, according to Liu and colleagues. This study used the HL-60 cell line to investigate that p38 and ERK and proved that they are regulators of neutrophil migration with opposing effects. HL-60 cell line treatment with fMLP at concentrations more than 500 nM resulted in a considerable reduction in cell migration, whereas rising fMLP doses resulted in an ERK activation plateau. Furthermore, cell movement was restored after treatment with an ERK inhibitor or ERK RNAi towards chemoattractant (1,103).

In addition, RGS5 deficiency has been shown to increase phosphorylation of ERK in vascular smooth muscle cells (92). In contrast, *in vitro* study using human neutrophil and *in vivo* mouse model of intestine inflammation, ERK activation led to increased migration of the neutrophil (149,150). Although it is difficult to link ERK activation to RGS5-/- neutrophil migration at this time, we might infer that ERK activation triggers a negative feedback loop that restricts RGS5-/- neutrophil migration in the presence of continuous GPCR receptor signals. To fully comprehend the significance of ERK activation in this circumstance, more research utilizing particular ERK inhibitors will be required (1).

Neutrophils promote tissue damage as well as vascular permeability and endothelial damage in acute and chronic inflammatory diseases. Neutrophils rolling, firm attachment, intravascular crawling, and diapedesis are spatially and temporally regulated by multiple factors including GTPases (142). The trans-endothelial migration is well coordinated by Rho GTPase, also so-called cytoskeleton regulators, where RhoA is important for the formation of myosin filaments at the rear end and Rac and Cdc42 regulates the directionality and polarity of the neutrophils at the front end (111,151). I examined the effect of RGS5 deficiency on activation levels of RhoA and Cdc42 in neutrophils from WT and RGS5-/- mice. I detected increased levels of RhoA in RGS5-/- neutrophils compared to WT upon activation with a different chemoattractant. This suggests the loss of RGS5 leads to a significant increase in RhoA activity levels which might further suppress neutrophil migration toward chemoattractant gradients.

A recent study has indicated that RhoA maintains neutrophil quiescence, controls priming responses, and discriminates between chemotactic stimuli, acting as a negative regulator of β2-independent neutrophil motility. RhoA as a predominant negative regulator of neutrophil

migration where neutrophil migration in response to CXCL1, thioglycollate, zymosan particles, E Coli, and influenza A virus (IAV) was strikingly augmented in the absence of Rho proteins (110). In addition, RhoA and Rac mutual inhibition are required for the directional migration of neutrophils. It has been shown that RhoA can inhibit Rac GTPase at the front end of neutrophils *via* activating ROCK and filamin A which can suppress leading edge protrusion and actin remodeling (120). This suggests another possibility where increased RhoA levels in neutrophils upon RGS5 loss can cause dysfunction front end, *via* inhibiting Rac and accumulation of actin polymers. However, these are only speculations that would further need separate studies to understand this complex and delicate balance of cytoskeleton regulators in absence of RGS5.

Different studies have shown that Cdc42, Rac, and RhoA can be activated and inactivated by positive feedback, suggesting that their potential to be the elusive chemotactic compass (40, 42, and 43). Cdc42 deletion and over-activation led to impaired location and stability of the leading edge and directed migration in neutrophils (111,117). I also investigated the activity of Cdc42 and found that Cdc42 remained intact in RGS5 deficient neutrophils upon chemokine activation. A previous study showed overexpression of RGS5 reduced protein levels of Cdc42 in human lung cancer cell lines as a marker for cell migration and adhesion (75).

Recently Cdc42 has been shown to locally inactivate RhoA and myosin-mediated contraction in neutrophils using knockdown and constitutively active Cdc42 indicates a tight regulation between Cdc42 and RhoA activities (118). We can speculate that increased activation of RhoA in RGS5 deficient neutrophils can negatively regulate the migration by preventing the proper functioning of the front end. The conserved activity of Cdc42 of neutrophils from RGS5-/- mice might accentuate the specificity of RGS5 loss on RhoA RGS5-/- neutrophils. The delicate balance of Rho GTPase activation and deactivation is very important for unconstrained neutrophil migration. However, further studies using RhoA-specific inhibitors are required to fully understand its function upon RGS5 deficiency.

5.5 RGS5 in the pulmonary vasculature

Initially, RGS5 was identified as a marker for pericytes. Further, it has been also investigated in smooth muscle cells in systemic vasculature (88,129,152). RGS5-/- mice claimed to be

hypotensive and hypertensive in different studies. Further, it was confirmed that contradictory findings, due to differences in the genetic background and also technical differences between blood pressure measurements (88,89,91). A recent study showed that RGS5-/- mice, treated with DOCA salt to induce experimental hypertension, have only a slight increase in systemic pressure compared to controls. RGS5-/- mice neither showed vascular structural remodeling or thickening with conserved contractile/quiescent phenotype of vascular smooth muscle cells. RGS5 expression may attenuate extensive arterial constriction while promoting adaptive arterial remodeling (92). However, no studies are linking RGS5 and its impact on the pulmonary vasculature.

We detected increased expression of RGS5 in pulmonary arteries from IPF patients and localized RGS5 in pulmonary artery smooth muscle cells in human as well as mouse lung tissue. I showed that KCl and 5-HT dependent vasoconstriction is compromised in pulmonary arteries from RGS5 deficient mice. These findings indicate that RGS5 might play a specific role in the regulation of potassium and serotonin response and hence modulating the pulmonary vascular response during increased pulmonary vascular resistance. Our results indicate that lack of RGS5 can be protective against increased pulmonary arterial pressure in lung diseases. Therefore, we employed the bleomycin mouse model to confirm our *ex vivo* findings. We found that RGS5-/- mice were not protected from the increased pulmonary artery pressure in the fibrosis model. These findings suggest that RGS5 might not participate in maintaining pulmonary arterial pressure in a bleomycin-induced increase in pulmonary pressure. However, further studies are required to confirm the role of RGS5 in pulmonary vascular remodeling and vasculature dysfunction using different animal models. Hypoxia or blocking VEGF to induce an increase in pulmonary pressure might represent a better tool to answer the relevance of RGS5 in the pulmonary vascular hemostasis.

5.6 Limitations of the study

In our study, we investigated RGS5 expression in human lung tissue samples from individuals with end-stage lung diseases. As a result, more research is needed to determine the involvement of RGS5 in interstitial lung disease development. Furthermore, RGS5 role in the occurrence of spontaneous or infection-induced flare-ups require more studies. The use of mouse models of acute lung injury is another disadvantage (1). Intra tracheal bleomycin mouse model is well acknowledged in the pulmonary fibrosis field due to its systematic

behavior for the development of pulmonary fibrosis. This makes it simpler to understand the pathophysiology and relevance of the targeted gene in a phase-dependent manner, quantified at three well-defined stages (3day (initial inflammation), 14day (profibrotic), and 21day (fibrotic)) during the disease development. Although, these models can be criticized as induced by non-physiological stimuli and not completely replicating the pathophysiological environment of diseased human lungs. However, they are still regarded as a gold standard in the scientific field and provide the backbone for the majority of preclinical studies of interstitial lung diseases.

The relevance of RGS5 deficient neutrophils in the chronic phase of fibrosis development remained unclear which requires further investigations using neutrophil-specific RGS5 depletion. Finally, more research is needed in the clinical setting to understand the role of RGS5 in acute pulmonary inflammation and lung injury. Despite the drawbacks, we provide enough evidence using two different lung injury animal models and *in vitro* assays to conclude RGS5 as an important target in the development of fibrosing lung diseases (1).

6 Conclusion

Finally, the findings in this thesis show that RGS5 is associated with retained lung function and reduced neutrophilic inflammation using two independent animal models of acute lung injury, bleomycin and LPS as well as *in vitro* neutrophil experiments.The delayed ERK dephosphorylation and activation of RhoA in RGS5-/- neutrophils might act as a negative regulator of their chemotaxis capabilities leading to reduced inflammation during early inflammatory responses. Given the involvement of RGS5 in neutrophil migration behavior, Lack of RGS5 could offer a unique therapeutic approach for exacerbations in inflammatory pulmonary disease without jeopardizing anti-infection defense mechanisms.

7 Bibliography

1. Sharma N, Nagaraj C, Nagy BM, Marsh LM, Bordag N, Zabini D, et al. RGS5 Determines Neutrophil Migration in the Acute Inflammatory Phase of Bleomycin-Induced Lung Injury. Int J Mol Sci. 2021;(22):9342.
2. Interstitial lung diseases. ERS Eur Lung Whiteb. 2015;22.
3. Naghavi M, Wang H, Lozano R, Davis A, Liang X, Zhou M, et al. Global, regional, and national age–sex specific all-cause and cause-specific mortality for 240 causes of death, 1990–2013: a systematic analysis for the Global Burden of Disease Study 2013. Lancet. 2015;385(9963):117–71.
4. Marshall DC, Salciccioli JD, Shea BS, Akuthota P. Trends in mortality from idiopathic pulmonary fibrosis in the European Union: an observational study of the WHO mortality database from 2001–2013. Eur Respir J. 2018;5(1):1701603.
5. Ley B, Collard HR, King TE. Clinical Course and Prediction of Survival in Idiopathic Pulmonary Fibrosis. Am J Respir Crit Care Med. 2011;183(4):431–40.
6. Raghu G, Collard HR, Egan JJ, Martinez FJ, Behr J, Brown KK, et al. An Official ATS/ERS/JRS/ALAT Statement: Idiopathic Pulmonary Fibrosis: Evidence-based Guidelines for Diagnosis and Management. Am J Respir Crit Care Med. 2011;183(6):788–824.
7. Kolb M, Vašáková M. The natural history of progressive fibrosing interstitial lung diseases. Respir Res. 2019;20(1):57.
8. Wolters PJ, Collard HR, Jones KD. Pathogenesis of Idiopathic Pulmonary Fibrosis. Annu Rev Pathol Mech Dis. 2014;9(1):157–79.
9. Ryu JH, Moua T, Daniels CE, Hartman TE, Yi ES, Utz JP, et al. Idiopathic Pulmonary Fibrosis: Evolving Concepts. Mayo Clin Proc. 2014;89(8):1130–42.
10. Heukels P, Moor CC, von der Thüsen JH, Wijsenbeek MS, Kool M. Inflammation and immunity in IPF pathogenesis and treatment. Respir Med. 2019;147:79–91.
11. Richeldi L, Collard HR, Jones MG. Idiopathic pulmonary fibrosis. Lancet. 2017;389(10082):1941–52.
12. Balestro E, Calabrese F, Turato G, Lunardi F, Bazzan E, Marulli G, et al. Immune Inflammation and Disease Progression in Idiopathic Pulmonary Fibrosis. PLoS One. 2016;11(5):e0154516.
13. Raghu G, Brown KK, Collard HR, Cottin V, Gibson KF, Kaner RJ, et al. Efficacy of simtuzumab versus placebo in patients with idiopathic pulmonary fibrosis: a randomised, double-blind, controlled, phase 2 trial. Lancet Respir Med. 2017;5(1):22–

32.
14. Richeldi L, Davies HRHR, Spagnolo P, Luppi F. Corticosteroids for idiopathic pulmonary fibrosis. Cochrane Database Syst Rev. 2003;
15. Martinez FJ, Raghu G, Schwarz M, Toews GB HG. Prednisone, Azathioprine, and N - Acetylcysteine for Pulmonary Fibrosis. N Engl J Med. 2012 May 24;366(21):1968–77.
16. Raghu G, Brown KK, Bradford WZ, Starko K, Noble PW, Schwartz DA, et al. A Placebo-Controlled Trial of Interferon Gamma-1b in Patients with Idiopathic Pulmonary Fibrosis. N Engl J Med. 2004;350(2):125–33.
17. Agostini C, Gurrieri C. Chemokine/cytokine cocktail in idiopathic pulmonary fibrosis. Proc Am Thorac Soc. 2006;3(4):357-363.
18. Hunninghake GW, Gadek JE, Lawley TJ, Crystal RG. Mechanisms of neutrophil accumulation in the lungs of patients with idiopathic pulmonary fibrosis. J Clin Invest. 1981;68(1):259–69.
19. Obayashi Y, Yamadori I, Fujita J, Yoshinouchi T, Ueda N, Takahara J. The role of neutrophils in the pathogenesis of idiopathic pulmonary fibrosis. Chest. 1997;112(5):1338–43.
20. Lynch JP, Standiford TJ, Rolfe MW, Kunkel SL, Strieter RM. Neutrophilic alveolitis in idiopathic pulmonary fibrosis. The role of interleukin-8. Am Rev Respir Dis. 1992;145(6):1433–9.
21. Beeh KM, Beier J, Kornmann O, Buhl R. Neutrophilic inflammation in induced sputum of patients with idiopathic pulmonary fibrosis. Sarcoidosis Vasc Diffus Lung Dis. 2003;20(2):138–43.
22. Guiot J, Henket M, Corhay JL, Moermans C, Louis R. Sputum biomarkers in IPF: Evidence for raised gene expression and protein level of IGFBP-2, IL-8 and MMP-7. PLoS One. 2017;12(2):e0171344.
23. Kinder BW, Brown KK, Schwarz MI, Ix JH, Kervitsky A, King TE. Baseline BAL Neutrophilia Predicts Early Mortality in Idiopathic Pulmonary Fibrosis. Chest. 2008;133(1):226–32.
24. Paplińska-Goryca M, Goryca K, Misiukiewicz-Stępień P, Nejman-Gryz P, Proboszcz M, Górska K, et al. mRNA expression profile of bronchoalveolar lavage fluid cells from patients with idiopathic pulmonary fibrosis and sarcoidosis. Eur J Clin Invest. 2019;49(9).
25. Song H, Sun D, Ban C, Liu Y, Zhu M, Ye Q, et al. Independent clinical factors relevant to prognosis of patients with idiopathic pulmonary fibrosis. Med Sci Monit. 2019;25:4193–201.

26. Chua F, Dunsmore SE, Clingen PH, Mutsaers SE, Shapiro SD, Segal AW, et al. Mice Lacking Neutrophil Elastase Are Resistant to Bleomycin-Induced Pulmonary Fibrosis. Am J Pathol. 2007;170(1):65–74.
27. Takemasa A, Ishii Y, Fukuda T. A neutrophil elastase inhibitor prevents bleomycin-induced pulmonary fibrosis in mice. Eur Respir J. 2012;40(6):1475–82.
28. Gregory AD, Kliment CR, Metz HE, Kim K-H, Kargl J, Agostini BA, et al. Neutrophil elastase promotes myofibroblast differentiation in lung fibrosis. J Leukoc Biol. 2015;98(2):143–52.
29. Schupp JC, Binder H, Jäger B, Cillis G, Zissel G, Müller-Quernheim J, et al. Macrophage Activation in Acute Exacerbation of Idiopathic Pulmonary Fibrosis. PLoS One. 2015;10(1):e0116775.
30. Flaherty KR, Toews GB, Lynch JP, Kazerooni EA, Gross BH, Strawderman RL, et al. Steroids in idiopathic pulmonary fibrosis: A prospective assessment of adverse reactions, response to therapy, and survival. Am J Med. 2001;110(4):278–82.
31. Davies HRHR, Richeldi L, Walters EH. Immunomodulatory agents for idiopathic pulmonary fibrosis. Cochrane Database Syst Rev. 2003;3:CD003134.
32. Raghu G. Pharmacotherapy for idiopathic pulmonary fibrosis: Current landscape and future potential. Eur Respir Rev. 2017;26(145):170071.
33. Lunardi F, Pezzuto F, Vuljan SE, Calabrese F. Idiopathic pulmonary fibrosis and antifibrotic treatments focus on experimental studies. Arch Pathol Lab Med. 2018;142(9):1090–7.
34. Wollin L, Distler JHW, Redente EF, Riches DWH, Stowasser S, Schlenker-Herceg R, et al. Potential of nintedanib in treatment of progressive fibrosing interstitial lung diseases. Eur Respir J. 2019;54(3):1900161.
35. Rubenfeld GD, Caldwell E, Peabody E, Weaver J, Martin DP, Neff M, et al. Incidence and Outcomes of Acute Lung Injury. N Engl J Med. 2005;353(16):1685–93.
36. Tsushima K, King LS, Aggarwal NR, De Gorordo A, D'Alessio FR, Kubo K. Acute lung injury review. Intern Med. 2009;48(9):621–30.
37. Wheeler AP, Bernard GR. Acute lung injury and the acute respiratory distress syndrome: a clinical review. Lancet. 2007;369(9572):1553–64.
38. Matthay MA, Zemans RL, Zimmerman GA, Arabi YM, Beitler JR, Mercat A, et al. Acute respiratory distress syndrome. Nat Rev Dis Prim. 2019;5:18.
39. Grommes J, Soehnlein O. Contribution of neutrophils to acute lung injury. Mol Med. 2011;17((3-4)):293–307.
40. Han S, Mallampalli RK. The Acute Respiratory Distress Syndrome: From Mechanism

to Translation. J Immunol. 2015;194(3):855–60.
41. Johnson ER, Matthay MA. Acute Lung Injury: Epidemiology, Pathogenesis, and Treatment. J Aerosol Med Pulm Drug Deliv. 2010;23(4):243–52.
42. Matute-Bello G, Frevert CW, Martin TR. Animal models of acute lung injury. Am J Physiol Cell Mol Physiol. 2008;295(3):L379–99.
43. Potey PMD, Rossi AG, Lucas CD, Dorward DA. Neutrophils in the initiation and resolution of acute pulmonary inflammation: understanding biological function and therapeutic potential. J Pathol. 2019;247:672–85.
44. O'Brien JB, Wilkinson JC, Roman DL. Regulator of G-protein signaling (RGS) proteins as drug targets: Progress and future potentials. J Biol Chem. 2019;294(49):18571–85.
45. Bansal G, Druey KM, Xie Z. R4 RGS proteins: Regulation of G-protein signaling and beyond. Pharmacol Ther. 2007;116(3):473–95.
46. DiBello PR, Garrison TR, Apanovitch DM, Hoffman G, Shuey DJ, Mason K, et al. Selective uncoupling of RGS action by a single point mutation in the G protein α-subunit. J Biol Chem. 1998;273(10):5780–4.
47. Sethakorn N, Yau DM, Dulin NO. Non-canonical functions of RGS proteins. Cell Signal. 2010;22:1274–81.
48. Sjögren B, Neubig RR. Thinking outside of the "RGS Box": New approaches to therapeutic targeting of regulators of G protein signaling. Mol Pharmacol. 2010;78(4):550–7.
49. Roy AA, Baragli A, Bernstein LS, Hepler JR, Hébert TE, Chidiac P. RGS2 interacts with Gs and adenylyl cyclase in living cells. Cell Signal. 2006;18(3):336–48.
50. Xie Z, Chan EC, Druey KM. R4 Regulator of G Protein Signaling (RGS) Proteins in Inflammation and Immunity. AAPS J. 2016;18(2):294–304.
51. Druey KM. Regulators of G protein signalling: potential targets for treatment of allergic inflammatory diseases such as asthma. Expert Opin Ther Targets. 2003;7(4):475–84.
52. Moratz C, Hayman JR, Gu H, Kehrl JH. Abnormal B-Cell Responses to Chemokines, Disturbed Plasma Cell Localization, and Distorted Immune Tissue Architecture in Rgs1−/− Mice. Mol Cell Biol. 2004;24(13):5767–75.
53. Larminie C, Murdock P, Walhin JP, Duckworth M, Blumer KJ, Scheideler MA, et al. Selective expression of regulators of G-protein signaling (RGS) in the human central nervous system. Mol Brain Res. 2004;122(1):24–34.
54. Xie Y, Jiang H, Nguyen H, Jia S, Berro A, Panettieri RA, et al. Regulator of G protein signaling 2 is a key modulator of airway hyperresponsiveness. J Allergy Clin Immunol. 2012;130(4):968-976.e3.

55. George T, Chakraborty M, Giembycz MA, Newton R. A bronchoprotective role for Rgs2 in a murine model of lipopolysaccharide-induced airways inflammation. Allergy, Asthma Clin Immunol. 2018;14(1):40.
56. George T, Bell M, Chakraborty M, Siderovski DP, Giembycz MA, Newton R. Protective Roles for RGS2 in a Mouse Model of House Dust Mite-Induced Airway Inflammation. PLoS One. 2017;12(1):e0170269.
57. Williams JW, Yau D, Sethakorn N, Kach J, Reed EB, Moore T V., et al. RGS3 controls T lymphocyte migration in a model of Th2-mediated airway inflammation. Am J Physiol Cell Mol Physiol. 2013;305(10):L693–701.
58. Song KS, Choi YH, Kim JM, Lee H, Lee TJ, Yoon JH. Suppression of prostaglandin E2-induced MUC5AC overproduction by RGS4 in the airway. Am J Physiol - Lung Cell Mol Physiol. 2009;296(4):L684-92.
59. Damera G, Druey KM, Cooper PR, Krymskaya VP, Soberman RJ, Amrani Y, et al. An RGS4-Mediated Phenotypic Switch of Bronchial Smooth Muscle Cells Promotes Fixed Airway Obstruction in Asthma. PLoS One. 2012;7(1):e28504.
60. Madigan LA, Wong GS, Gordon EM, Chen W-S, Balenga N, Koziol-White CJ, et al. RGS4 Overexpression in Lung Attenuates Airway Hyperresponsiveness in Mice. Am J Respir Cell Mol Biol. 2018;58(1):89–98.
61. Wong GS, Redes JL, Balenga N, McCullough M, Fuentes N, Gokhale A, et al. RGS4 promotes allergen- and aspirin-associated airway hyperresponsiveness by inhibiting PGE2 biosynthesis. J Allergy Clin Immunol. 2020;146:1152–1164.e13.
62. Shi G-X, Harrison K, Wilson GL, Moratz C, Kehrl JH. RGS13 Regulates Germinal Center B Lymphocytes Responsiveness to CXC Chemokine Ligand (CXCL)12 and CXCL13. J Immunol. 2002;169(5):2507–15.
63. Bansal G, DiVietro JA, Kuehn HS, Rao S, Nocka KH, Gilfillan AM, et al. RGS13 Controls G Protein-Coupled Receptor-Evoked Responses of Human Mast Cells. J Immunol. 2008;181(11):7882–90.
64. Raedler D, Ballenberger N, Klucker E, Böck A, Otto R, Prazeres Da Costa O, et al. Identification of novel immune phenotypes for allergic and nonallergic childhood asthma. J Allergy Clin Immunol. 2015;135(1):81–91.
65. Hwang IY, Hwang KS, Park C, Harrison KA, Kehrl JH. Rgs13 Constrains Early B Cell Responses and Limits Germinal Center Sizes. PLoS One. 2013;8(3):e60139.
66. Lippert E, Yowe DL, Gonzalo J-A, Justice JP, Webster JM, Fedyk ER, et al. Role of Regulator of G Protein Signaling 16 in Inflammation- Induced T Lymphocyte Migration and Activation. J Immunol. 2003;171(3):1542–55.

67. Shankar SP, Wilson MS, DiVietro JA, Mentink-Kane MM, Xie Z, Wynn TA, et al. RGS16 Attenuates Pulmonary Th2/Th17 Inflammatory Responses. J Immunol. 2012;188(12):6347–56.
68. Delesque-Touchard N, Pendaries C, Volle-Challier C, Millet L, Salel V, Hervé C, et al. Regulator of G-protein signaling 18 controls both platelet generation and function. PLoS One. 2014;9(11):e113215.
69. Alshbool FZ, Karim ZA, Vemana HP, Conlon C, Lin OA, Khasawneh FT. The regulator of G-protein signaling 18 regulates platelet aggregation, hemostasis and thrombosis. Biochem Biophys Res Commun. 2015;462(4):378–82.
70. Cohen SP, Buckley BK, Kosloffs M, Garland AL, Bosch DE, Cheng G, et al. Regulator of G-protein signaling-21 (RGS21) is an inhibitor of bitter gustatory signaling found in lingual and airway epithelia. J Biol Chem. 2012;287(50):41706–19.
71. Seki N, Sugano S, Suzuki Y, Nakagawara A, Ohira M, Muramatsu MA, et al. Isolation, tissue expression, and chromosomal assignment of human RGS5, a novel G-protein signaling regulator gene. J Hum Genet. 1998;43(3):202–5.
72. Yang Z, Cooper PR, Damera G, Mukhopadhyay I, Cho H, Kehrl JH, et al. β-agonist-associated reduction in RGS5 expression promotes airway smooth muscle hyper-responsiveness. J Biol Chem. 2011;286(13):11444–55.
73. Balenga NA, Jester W, Jiang M, Panettieri RA, Druey KM. Loss of regulator of G protein signaling 5 promotes airway hyperresponsiveness in the absence of allergic inflammation. J Allergy Clin Immunol. 2014;134(2):451-459.e11.
74. Yang Z, Balenga N, Cooper PR, Damera G, Edwards R, Brightling CE, et al. Regulator of G-Protein Signaling–5 Inhibits Bronchial Smooth Muscle Contraction in Severe Asthma. Am J Respir Cell Mol Biol. 2012;46(6):823–32.
75. Xu Z, Zuo Y, Wang J, Yu Z, Peng F, Chen Y, et al. Overexpression of the regulator of G-protein signaling 5 reduces the survival rate and enhances the radiation response of human lung cancer cells. Oncol Rep. 2015;33(6):2899–907.
76. Chan EC, Ren C, Xie Z, Jude J, Barker T, Koziol-White CA, et al. Regulator of G protein signaling 5 restricts neutrophil chemotaxis and trafficking. J Biol Chem. 2018;293(33):12690–702.
77. Cheng WL, Wang PX, Wang T, Zhang Y, Du C, Li H, et al. Regulator of G-protein signalling 5 protects against atherosclerosis in apolipoprotein E-deficient mice. Br J Pharmacol. 2015;172(23):5676–89.
78. Ceolotto G, Papparella I, Sticca A, Bova S, Cavalli M, Cargnelli G, et al. An abnormal gene expression of the β-adrenergic system contributes to the pathogenesis of

cardiomyopathy in cirrhotic rats. Hepatology. 2008;48(6):1913–23.

79. Zhang P, Su J, King ME, Maldonado AE, Park C, Mende U. Regulator of G protein signaling 2 is a functionally important negative regulator of angiotensin II-induced cardiac fibroblast responses. Am J Physiol - Hear Circ Physiol. 2011;301(1):H147-56.
80. Jang HS, Kim JI, Noh M, Rhee MH, Park KM. Regulator of G protein signaling 2 (RGS2) deficiency accelerates the progression of kidney fibrosis. Biochim Biophys Acta - Mol Basis Dis. 2014;1842(9):1733–41.
81. Jiang H, Xie Y, Abel PW, Wolff DW, Toews ML, Panettieri RA, et al. Regulator of G-protein signaling 2 repression exacerbates airway hyper-responsiveness and remodeling in asthma. Am J Respir Cell Mol Biol. 2015;53(1):42–9.
82. Xie Y, Jiang H, Zhang Q, Mehrotra S, Abel PW, Toews ML, et al. Upregulation of RGS2: a new mechanism for pirfenidone amelioration of pulmonary fibrosis. Respir Res. 2016;17(1):103.
83. Liu Y, Huang H, Zhang Y, Zhu XY, Zhang R, Guan LH, et al. Regulator of G protein signaling 3 protects against cardiac hypertrophy in mice. J Cell Biochem. 2014;115(5):977–86.
84. Li H, He C, Feng J, Zhang Y, Tang Q, Bian Z, et al. Regulator of G protein signaling 5 protects against cardiac hypertrophy and fibrosis during biomechanical stress of pressure overload. Proc Natl Acad Sci U S A. 2010;107(31):13818–23.
85. Bahrami AJ, Gunaje JJ, Hayes BJ, Riehle KJ, Kenerson HL, Yeung RS, et al. Regulator of G-protein signaling-5 is a marker of hepatic stellate cells and expression mediates response to liver injury. PLoS One. 2014;9(10):e108505.
86. Ganss R. Keeping the Balance Right: Regulator of G Protein Signaling 5 in Vascular Physiology and Pathology. Prog Mol Biol Transl Sci. 2015;133:93–121.
87. Arnold C, Feldner A, Pfisterer L, Hödebeck M, Troidl K, Genové G, et al. RGS 5 promotes arterial growth during arteriogenesis. EMBO Mol Med. 2014;6(8):1075–89.
88. Holobotovskyy V, Manzur M, Tare M, Burchell J, Bolitho E, Viola H, et al. Regulator of G-protein signaling 5 controls blood pressure homeostasis and vessel wall remodeling. Circ Res. 2013;112(5):781–91.
89. Holobotovskyy V, Chong YS, Burchell J, He B, Phillips M, Leader L, et al. Regulator of G protein signaling 5 is a determinant of gestational hypertension and preeclampsia. Sci Transl Med. 2015;7(290):290ra88.
90. Nisancioglu MH, Mahoney WM, Kimmel DD, Schwartz SM, Betsholtz C, Genové G. Generation and Characterization of rgs5 Mutant Mice. Mol Cell Biol. 2008;28(7):2324–31.

91. Cho H, Park C, Hwang I-Y, Han S-B, Schimel D, Despres D, et al. Rgs5 Targeting Leads to Chronic Low Blood Pressure and a Lean Body Habitus. Mol Cell Biol. 2008;28:2590–2597.
92. Arnold C, Demirel E, Feldner A, Genové G, Zhang H, Sticht C, et al. Hypertension-evoked RhoA activity in vascular smooth muscle cells requires RGS5. FASEB J. 2018;32(4):2021–35.
93. Seeger W, Adir Y, Barberà JA, Champion H, Coghlan JG, Cottin V, et al. Pulmonary Hypertension in Chronic Lung Diseases. J Am Coll Cardiol. 2013;62(25):D109–16.
94. Lawrence SM, Corriden R, Nizet V. How Neutrophils Meet Their End. Trends Immunol. 2020;41(6):531–44.
95. Hidalgo A, Chilvers ER, Summers C, Koenderman L. The Neutrophil Life Cycle. Trends Immunol. 2019;40(7):584–97.
96. Maas SL, Soehnlein O, Viola JR. Organ-specific mechanisms of transendothelial neutrophil migration in the lung, liver, kidney, and aorta. Front Immunol. 2018;27(9):2739.
97. Casanova-Acebes M, Nicolás-Ávila JA, Yao Li JL, García-Silva S, Balachander A, Rubio-Ponce A, et al. Neutrophils instruct homeostatic and pathological states in naive tissues. J Exp Med. 2018;215(11):2778–95.
98. Manley HR, Keightley MC, Lieschke GJ. The Neutrophil Nucleus: An Important Influence on Neutrophil Migration and Function. Front Immunol. 2018;4(9):2867.
99. Futosi K, Fodor S, Mócsai A. Neutrophil cell surface receptors and their intracellular signal transduction pathways. Int Immunopharmacol. 2013;17(3):638–50.
100. Mócsai A, Walzog B, Lowell CA. Intracellular signalling during neutrophil recruitment. Cardiovasc Res. 2015;107(3):373–85.
101. Immler R, Simon SI, Sperandio M. Calcium signalling and related ion channels in neutrophil recruitment and function. Eur J Clin Invest. 2018;48:e12964.
102. Zhou J, Moroi K, Nishiyama M, Usui H, Seki N, Ishida J, et al. Characterization of RGS5 in regulation of G protein-coupled receptor signaling. Life Sci. 2001;68(13):1457–69.
103. Liu X, Ma B, Malik AB, Tang H, Yang T, Sun B, et al. Bidirectional regulation of neutrophil migration by mitogen-activated protein kinases. Nat Immunol. 2012;13(5):457–64.
104. Mizuno R, Kamioka Y, Kabashima K, Imajo M, Sumiyama K, Nakasho E, et al. In vivo imaging reveals PKA regulation of ERK activity during neutrophil recruitment to inflamed intestines. J Exp Med. 2014;211(6):1123–36.

105. McCormick B, Chu JY, Vermeren S. Cross-talk between Rho GTPases and PI3K in the neutrophil. Small GTPases. 2019;10(3):187–95.
106. Bros, Haas, Moll, Grabbe. RhoA as a Key Regulator of Innate and Adaptive Immunity. Cells. 2019;8(7):733.
107. Wong K, Pertz O, Hahn K, Bourne H. Neutrophil polarization: Spatiotemporal dynamics of RhoA activity support a self-organizing mechanism. Proc Natl Acad Sci U S A. 2006;103(10):3639–44.
108. Thumkeo D, Watanabe S, Narumiya S. Physiological roles of rho and rho effectors in mammals. Eur J Cell Biol. 2013;92((10-11)):303–15.
109. Pedersen E, Brakebusch C. Rho GTPase function in development: How in vivo models change our view. Exp Cell Res. 2012;318(14):1779–87.
110. Jennings RT, Strengert M, Hayes P, El-Benna J, Brakebusch C, Kubica M, et al. RhoA determines disease progression by controlling neutrophil motility and restricting hyperresponsiveness. Blood. 2014;123(23):3635–45.
111. Srinivasan S, Wang F, Glavas S, Ott A, Hofmann F, Aktories K, et al. Rac and Cdc42 play distinct roles in regulating PI(3,4,5)P3 and polarity during neutrophil chemotaxis. J Cell Biol. 2003;160(3):375–85.
112. Glogauer M, Marchal CC, Zhu F, Worku A, Clausen BE, Foerster I, et al. Rac1 Deletion in Mouse Neutrophils Has Selective Effects on Neutrophil Functions. J Immunol. 2003;170(11):5652–7.
113. Li S, Yamauchi A, Marchal CC, Molitoris JK, Quilliam LA, Dinauer MC. Chemoattractant-Stimulated Rac Activation in Wild-Type and Rac2-Deficient Murine Neutrophils: Preferential Activation of Rac2 and Rac2 Gene Dosage Effect on Neutrophil Functions. J Immunol. 2002;169(9):5043–51.
114. Weiner OD, Neilsen PO, Prestwich GD, Kirschner MW, Cantley LC, Bourne HR. A PtdInsP3- and Rho GTPase-mediated positive feedback loop regulates neutrophil polarity. Nat Cell Biol. 2002;4(7):509–13.
115. Wang F, Herzmark P, Weiner OD, Srinivasan S, Servant G, Bourne HR. Lipid products of PI(3)Ks maintain persistent cell polarity and directed motility in neutrophils. Nat Cell Biol. 2002;4(7):513–8.
116. Xu J, Wang F, Van Keymeulen A, Herzmark P, Straight A, Kelly K, et al. Divergent signals and cytoskeletal assemblies regulate self-organizing polarity in neutrophils. Cell. 2003;114(2):201–14.
117. Szczur K, Xu H, Atkinson S, Zheng Y, Filippi MD. Rho GTPase CDC42 regulates directionality and random movement via distinct MAPK pathways in neutrophils.

Blood. 2006;108:4205–13.
118. Yang HW, Collins SR, Meyer T. Locally excitable Cdc42 signals steer cells during chemotaxis. Nat Cell Biol. 2016;18(2):191–201.
119. Kumar S, Xu J, Perkins C, Guo F, Snapper S, Finkelman FD, et al. Cdc42 regulates neutrophil migration via crosstalk between WASp, CD11b, and microtubules. Blood. 2012;120(17):3563–74.
120. Ohta Y, Hartwig JH, Stossel TP. FilGAP, a Rho- and ROCK-regulated GAP for Rac binds filamin A to control actin remodelling. Nat Cell Biol. 2006;8(8):803–14.
121. Li Z, Dong X, Wang Z, Liu W, Deng N, Ding Y, et al. Regulation of PTEN by Rho small GTPases. Nat Cell Biol. 2005;7(4):399–404.
122. Biasin V, Crnkovic S, Sahu-Osen A, Birnhuber A, El Agha E, Sinn K, et al. PDGFRα and αSMA mark two distinct mesenchymal cell populations involved in parenchymal and vascular remodeling in pulmonary fibrosis. Am J Physiol Cell Mol Physiol. 2020;318(4):L684–97.
123. Biasin V, Wygrecka M, Marsh LM, Becker-Pauly C, Brcic L, Ghanim B, et al. Meprin β contributes to collagen deposition in lung fibrosis. Sci Rep. 2017;7(1):39969.
124. Nagaraj C, Haitchi HM, Heinemann A, Howarth PH, Olschewski A, Marsh LM. Increased Expression of p22phox Mediates Airway Hyperresponsiveness in an Experimental Model of Asthma. Antioxid Redox Signal. 2017;27(18):1460–72.
125. Gungl A, Biasin V, Wilhelm J, Olschewski A, Kwapiszewska G, Marsh LM. Fra2 Overexpression in Mice Leads to Non-allergic Asthma Development in an IL-13 Dependent Manner. Front Immunol. 2018;9.
126. Bordag N, Biasin V, Schnoegl D, Valzano F, Jandl K, Nagy BM, et al. Machine Learning Analysis of the Bleomycin Mouse Model Reveals the Compartmental and Temporal Inflammatory Pulmonary Fingerprint. iScience. 2020;23:101819.
127. Jandl K, Stacher E, Bálint Z, Sturm EM, Maric J, Peinhaupt M, et al. Activated prostaglandin D2 receptors on macrophages enhance neutrophil recruitment into the lung. J Allergy Clin Immunol. 2016;137(3):833–43.
128. R Core Development Team. R: A language and environment for statistical computing. R Foundation for Statistical Computing, Vienna, Austria.;
129. Adams LD, Geary RL, McManus B, Schwartz SM. A comparison of aorta and vena cava medial message expression by cDNA array analysis identifies a set of 68 consistently differentially expressed genes, all in aortic media. Circ Res. 2000;87(7):623–31.
130. Matthay MA, Eschenbacher WL, Goetzl EJ. Elevated concentrations of leukotriene D4

in pulmonary edema fluid of patients with the adult respiratory distress syndrome. J Clin Immunol. 1984;4(6)(6):479–88.

131. Miller EJ, Cohen AB, Nagao S, Griffith D, Maunder RJ, Martin TR, et al. Elevated levels of NAP-1/interleukin-8 are present in the airspaces of patients with the adult respiratory distress syndrome and are associated with increased mortality. Am Rev Respir Dis. 1992;146(2):427–32.
132. Parsons PE, Fowler AA, Hyers TM, Henson PM. Chemotactic activity in bronchoalveolar lavage fluid from patients with adult respiratory distress syndrome. Am Rev Respir Dis. 1985;132(3):490–3.
133. Car BD, Meloni F, Luisetti M, Semenzato G, Gialdroni-Grassi G, Walz A. Elevated IL-8 and MCP-1 in the bronchoalveolar lavage fluid of patients with idiopathic pulmonary fibrosis and pulmonary sarcoidosis. Am J Respir Crit Care Med. 1994;149(3):655–9.
134. Xaubet A, Agustí C, Luburich P, Barberá JA, Carrión M, Ayuso MC, et al. Interleukin-8 expression in bronchoalveolar lavage cells in the evaluation of alveolitis in idiopathic pulmonary fibrosis. Respir Med. 1998;92(2):338–44.
135. Ziesche R, Hofbauer E, Wittmann K, Petkov V, Block L-H. A Preliminary Study of Long-Term Treatment with Interferon Gamma-1b and Low-Dose Prednisolone in Patients with Idiopathic Pulmonary Fibrosis. N Engl J Med. 1999;341(17):1264–9.
136. Judge EP, Fabre A, Adamali HI, Egan JJ. Acute exacerbations and pulmonary hypertension in advanced idiopathic pulmonary fibrosis. Eur Respir J. 2012;40(1):93–100.
137. Mura M, Porretta MA, Bargagli E, Sergiacomi G, Zompatori M, Sverzellati N, et al. Predicting survival in newly diagnosed idiopathic pulmonary fibrosis: a 3-year prospective study. Eur Respir J. 2012;40(1):101–9.
138. Chan EC, Ren C, Xie Z, Jude J, Barker T, Koziol-White CA, et al. Regulator of G protein signaling 5 restricts neutrophil chemotaxis and trafficking. J Biol Chem. 2018;293(33):12690–702.
139. Grommes J, Soehnlein O. Contribution of Neutrophils to Acute Lung Injury. Mol Med. 2011;17(3–4):293–307.
140. Bhatia M, Zemans RL, Jeyaseelan S. Role of chemokines in the pathogenesis of acute lung injury. Am J Respir Cell Mol Biol. 2012;46(5):566–72.
141. Mayadas TN, Cullere X, Lowell CA. The Multifaceted Functions of Neutrophils. Annu Rev Pathol Mech Dis. 2014;9(1):181–218.
142. Sadik CD, Kim ND, Luster AD. Neutrophils cascading their way to inflammation. Trends Immunol. 2011;32(10):452–60.

143. Wang X, Huang G, Luo X, Penninger JM, Muallem S. Role of regulator of G protein signaling 2 (RGS2) in Ca2+ oscillations and adaptation of Ca2+ signaling to reduce excitability of RGS2-/- cells. J Biol Chem. 2004;279(40):41642–9.
144. Tanimura S, Takeda K. ERK signalling as a regulator of cell motility. J Biochem. 2017;162(3):145–7.
145. Hakkim A, Fuchs TA, Martinez NE, Hess S, Prinz H, Zychlinsky A, et al. Activation of the Raf-MEK-ERK pathway is required for neutrophil extracellular trap formation. Nat Chem Biol. 2011;7(2):75–7.
146. Mansfield PJ, Shayman JA, Boxer LA. Regulation of polymorphonuclear leukocyte phagocytosis by myosin light chain kinase after activation of mitogen-activated protein kinase. Blood. 2000;95(7):2407–12.
147. Simard FA, Cloutier A, Ear T, Vardhan H, McDonald PP. MEK-independent ERK activation in human neutrophils and its impact on functional responses. J Leukoc Biol. 2015;98(4):565–73.
148. Zhang ER, Liu S, Wu LF, Altschuler SJ, Cobb MH. Chemoattractant concentration-dependent tuning of ERK signaling dynamics in migrating neutrophils. Sci Signal. 2016;9(458):ra1.
149. Hirata E, Kiyokawa E. ERK activity imaging during migration of living cells in vitro and in vivo. Int J Mol Sci. 2019;20(3):679.
150. Mizuno R, Kamioka Y, Kabashima K, Imajo M, Sumiyama K, Nakasho E, et al. In vivo imaging reveals PKA regulation of ERK activity during neutrophil recruitment to inflamed intestines. J Cell Biol. 2014;211(6):1123–36.
151. Tapon N. Rho, Rac and Cdc42 GTPases regulate the organization of the actin cytoskeleton. Curr Opin Cell Biol. 1997;9(1):86–92.
152. Manzur M, Ganss R. Regulator of G Protein Signaling 5: A New Player in Vascular Remodeling. Trends Cardiovasc Med. 2009;19(1):26–3.

8 Tables

Table 1: Clinical characteristics of patients with interstitial lung disease (ILD) and donors with detailed use of material

Lung ID/Diagnosis	Age	Sex	BMI	FEV1(%)	FVC(%)	FEV1/ FVC(%)	LTOT	Material used
Control 1	43	Female	22.43	NA	NA	NA	no	Lung tissue, RNA
Control 2	40	Female	20.76	NA	NA	NA	no	Lung tissue, RNA
Control 3	17	Male	17.96	NA	NA	NA	no	Lung tissue, RNA
Control 4	62	Male	23.12	NA	NA	NA	no	Lung tissue, RNA
Control 5	59	Male	26.3	NA	NA	NA	no	Lung tissue, RNA
Control 6	70	Female	22.04	NA	NA	NA	no	Lung tissue, RNA
Control 7	58	Female	22.86	NA	NA	NA	no	Lung tissue, RNA
Control 8	42	Female	NA	NA	NA	NA	no	Lung tissue, RNA, protein
Control 9	24	Female	21.7	NA	NA	NA	no	Lung tissue, RNA
Control 10	71	Female	NA	NA	NA	NA	no	Lung tissue, RNA
Control 11	53	Female	31.11	NA	NA	NA	no	Protein
Control 12	39	Female	24.22	NA	NA	NA	no	Protein
Control 13	52	Male	NA	NA	NA	NA	no	Protein
Control 14	19	Male	NA	NA	NA	NA	no	Protein
Control 15	73	Female	NA	NA	NA	NA	no	Protein
ILD 1/HP	66.5	Female	26.93	49	47	104	yes	Lung tissue, RNA, protein
ILD 2/HP	64.2	Male	28.09	67	NA	NA	no	Lung tissue, RNA, protein
ILD 3/CTD	58.2	Female	17.31	30	31	97	yes	Lung tissue, RNA, protein
ILD 4/IPF	54	Male	24.15	40	34.9	115	yes	Lung tissue, protein
ILD 5/IPF	60	Male	21.88	34	36.2	94	yes	Lung tissue, RNA
ILD 6/IPF	72.3	Male	24.3	41	35	117	yes	Lung tissue, RNA, Protein
ILD 7/NSIP	48.4	Female	21.5	40	40	100	yes	Lung tissue, RNA, Protein
ILD 8/IPF	63.7	Male	23.03	47.5	40	119	yes	Lung tissue, RNA
ILD 9/HP	54.7	Male	32.05	31	27.5	113	yes	Lung tissue, RNA
ILD 10/IPF	58.2	Male	17.92	41	NA	NA	yes	Lung tissue, RNA
ILD 11/HP	68	Male	18.83	46.2	37.2	124	yes	Lung tissue, RNA
ILD 12/HP	67.5	Male	33.25	59.4	53.1	112	yes	Lung tissue
ILD 13/IPF	56	Male	NA	NA	NA	76	NA	Lung tissue
ILD 14/IPF	63	Male	NA	NA	NA	93	NA	Lung tissue
ILD 15/IPF	66	Female	NA	NA	NA	89	NA	Lung tissue

BMI: Body mass index (Kg/m2); FEV1: Forced expiratory volume in 1 s; FVC: Forced vital capacity; LTOT: Long-term oxygen therapy; CTD: Connective tissue diseases; HP: Hypersensitivity pneumonitis; IPF: Idiopathic pulmonary fibrosis; NSIP: Nonspecific interstitial pneumonia; NA: Not available.

Table 2: Clinical characteristics of patients with acute respiratory distress syndrome (ARDS) with detailed use of material

Lung ID	Age	Sex	Background	Modified APACHE II	PaO_2/FiO_2 (mmHg)	Material used
ARDS 1	40	Female	Pneumonia	11	83	Lung tissue
ARDS 2	51	Female	Trauma	6	181.5	Lung tissue
ARDS 3	67	Male	Sepsis	20	109	Lung tissue

FiO2: Fraction of inspired oxygen PaO2: Partial pressure of oxygen .

Table 3: Antibodies for flow-cytometry analysis of immune cells from BALF and lung tissue

Antigen	Label	company	Clone	isotype	dilution
CD45	PerCP-Cy5.5	eBioscience	30-F11	Rat IgG2b. κ	1:200
CD45	FITC	Thermo Fisher	30-F11	Rat IgG2b. κ	1:200
CD11b	ef506	Thermo Fisher	M1/70	Rat IgG2b. κ	1:50
CD11c	ef450	Thermo Fisher	N418	Hamster IgG	1:50
Gr-1(Ly6G/Ly6C)	PE-Cy7	Biolegend	RB6-8C5	Rat IgG2b. κ	1:800
CD64	AF647	BD Bioscience	X54-5/7.1	Mouse IgG1. κ	1:20
Siglec-F	PE	BD Bioscience	E50-2240	Rat IgG2a. κ	1:20
MHC-II	APC-Cy7	Biolegend	M5/114.15.2	Rat IgG2b. κ	1:400
CD3	AF700	Thermo Fisher	eBio500A2	Hamster IgG	1:50
CD4	APC	Biolegend	GK 1.5	Rat IgG2b. κ	1:100
CD8	PE	Biolegend	53-6.7	Rat IgG2a. κ	1:100
CD19	BB515	BD Bioscience	1D3	Rat IgG2a. κ	1:50
NK1.1	SB600	eBioscience	PK136	Mouse / IgG2a. κ	1:20
γδTCR	ef450	Thermofischer	eBiogL3	Hamster IgG	1:50

Table 4: Antibodies for western blots and staining

Antibodies	Company/cataloge number	Experiments	Sample/Dilution
RGS5	Santa cruz/(B-4) sc514184	IHC (mouse and human)	Lung tissue/1:250
		western blot	Protein/1:1000
	Abcam/196799	IHC	Neutrophils/1:100
Ly6G	Biolegend/12706	IHC	Lung tissue/ 1:200
	Biolegend/127618	FACS	Bone marrow. blood.spleen/1:800
		FACS	Neutrophils/1:800
Cd11b	Invitrogen/69011282	FACS	Neutrophils/1:50
CXCR2	Biolegend/149312	FACS	Neutrophils/1:40
CXCR4	Biolegend/146505	FACS	Neutrophils/1:40
Erk	Cell signaling/9102S	Western blot	Protein/ 1:1000
pERK	Cell signaling/9101S	Western blot	Protein/ 1:1000
GAPDH	Santa cruz/(FL-335) sc25778	Western blot	Protein/ 1:1000
ß-actin	Santa cruz/(C-4) sc47778	Western blot	Protein/ 1:1000

Table 5: Primers sequences for human and mouse

Primers	Species	Forward (5'-3')	Reverse (5'-3')
RGS1	Human	TTGAGTTCTGGCTGGCTTGTG	GCAGCATCTGAATGCACAAATG
RGS2	Human	TTCTGGCTGGCCTGTGAAG	GCAGTTGTAAAGCAGCCACTTG
RGS3	Human	GCACACCAAGGACAACCTGC	ACGGAGAAAGCGAGGGTACG
RGS4	Human	ACCAGGGAAGAGACAAGCCG	ACTTGAGGAAGCGGCGGTAG
RGS5	Human	ACCTGGTGGAACCTTCCCTG	AACTCAGAGCGCACAAAGCG
RGS8	Human	CTGCATTCCGTGCCTTCTTG	TTTACCTCCCGTGGAGCCTG
RGS13	Human	CGGTGGAGCAGAATTTCTAGGG	TGTTTCAGTGGGTTCCTGAATG
RGS16	Human	AACCTGCAGACTGCCACAGC	CGGTAAGCAGGCGACTTCAG
RGS18	Human	CAAGGGACCTCAACAAATTCACC	TGGAGGGTAGGTTGAGTGATGC
β2M	Human	CCTGGAGGCTATCCAGCGTACTCC	TGTCGGATGGATGAAACCCAGACA
CXCL1	Mouse	CCTTGACCCTGAAGCTCCCT	CGGTGCCATCAGAGCAGTCT
CXCL2	Mouse	ACATCCAGAGCTTGAGTGTGA	TTCAGGGTCAAGGCAAACTT
β2M	Mouse	CGGCCTGTATGCTATCCAGAAAACC	TGTGAGGCGGGTGGAACTGTG
IL-1β	Mouse	GCCACCTTTTGACAGTGATGAG	GACAGCCCAGGTCAAAGGTT
IL-6	Mouse	ACAACCACGGCCTTCCCTACTT	CACGATTTCCCAGAGAACATGTG
IL-10	Mouse	ATAACTGCACCCACTTCCCA	TCATTTCCGATAAGGCTTGG
IL-13	Mouse	GCCAAGATCTGTGTCTCTCCC	CCAGGTCCACACTCCATACC
IL-17	Mouse	AGGACGCGCAAACATGAGTC	GGACACGCTGAGCTTTGAGG
IL-33	Mouse	ACCATGAGACCTAGAATGAAGTAT	TTAGATTTTCGAGAGCTTAAAC
IFN-γ	Mouse	CAGCAACAGCAAGGCGAAAAAGG	TTTCCGCTTCCTGAGGCTGGAT
TNF-α	Mouse	CATCTTCTCAAAATTCGAGTGACAA	TGGGAGTAGACAAGGTACAACCC

Table 6: Details of reagents

Reagent	Company	Catalogue number
DMSO	AppliChem	A3672,0250
FCS	Biowest, France	S1810-500
384 Well PCR Platte	Biozym, Germany	711225X
Blue S'Green qPCR Kit	Biozym, Germany	331416XL
CaCl2	Carl-Roth, Germany	5239.2
NaCl	Carl-Roth, Germany	3957.2
HEPES	Carl-Roth, Germany	HN78.2
Dako Target Retrieval Solution	Dako, Denmark	S236784
Dako Fluorescent mounting medium	Dako, Denmark	S3023
Formaldehyde	Donauchem, Austria	A191483
U-44619	Enzo Life Sciences, USA	BML-PG023-0001
ECL Start Western Blotting Detection Reagent	GE Healthcare, USA	RPN3243
ECL Prime Western Blotting Detection Reagent	GE Healthcare, USA	RPN2232
DPBS	Pan Biotech, Germany	P04-36500
KCl	Sigma-Aldrich, Germany	P9333
NaH2PO4	Sigma-Aldrich, Germany	S3139-250G
D-(+)-glucose	Sigma-Aldrich, Germany	G8270-1KG
NaHCO3	Sigma-Aldrich, Germany	S5761-1KG
Acetylcholine	Sigma-Aldrich, Germany	A6625.25G
Western blotting membranes, nitrocellulose, pore size 0.45 µm	Sigma-Aldrich, Germany	GE10600008

TEMED	Sigma-Aldrich, Germany	T9281
Ammonium persulfate (APS)	Sigma-Aldrich, Germany	A3678-25G
Tween 20	Sigma-Aldrich, Germany	P7949
Pierce protease inhibitor tablets	ThermoFisher Scientific, USA	A32953
Pierce phosphatase inhibitor tablets	ThermoFisher Scientific, USA	A32957
SuperSignal West Femto Chemiluminescent Substrate	ThermoFisher Scientific, USA	34095
Restore Plus Western Blot Stripping Buffer	ThermoFisher Scientific, USA	A323654

Table 7: Details of solutions

Solutions	Ingredients (mM)	Supplement	Used
Physiological salt solution (PSS)	KCl (5.5), NaCl (140.5), $CaCl_2$ (1.5), $MgCl_2$ (1), Glucose (10), HEPES (10), Na_2HPO_4 (0.5), KH_2PO_4 (0.5)	pH adjusted to 7.4 using NaOH	Wire Myography, Ca2+ imaging
Physiological salt solution with isotonic replacement of NaCl by KCl (KPSS)	KCl (120), NaCl (120), $CaCl_2$ (1.5), $MgCl_2$ (1), Glucose (10), HEPES (10), Na_2HPO_4 (0.5), KH_2PO_4 (0.5)	pH adjusted to 7.4 using NaOH	Wire Myography
Lysis buffer CHAPS[2]	NaCl (500), Tris-Hcl pH 7.5 (50), 5 % glycerol, 2 % CHAPS, 2 % sodium deoxycholate, 1 % sodium dodecyl sulfate	Supplemented with protease- and phosphatase inhibitors	Protein collection
TBS-T	Tris-HCl (5), NaCl (150), 0.4 % Tween 20	pH adjusted to 7.5	Western blot